INVESTIGATION OF THE MECHANO-ELECTROCHEMICAL COUPLING OF SOLID POLYETHYLENE OXIDE AND STRETCHABLE LITHIUM ION BATTERIES

A Dissertation

Presented to

the Faculty of the Department of Materials Science and Engineering

University of Houston

In Partial Fulfillment

of the Requirements for the Degree

Doctor of Philosophy

in Materials Science and Engineering

by

Taylor Hidemi Kelly

December 2016

INVESTIGATION OF THE MECHANO-ELECTROCHEMICAL COUPLING OF SOLID POLYETHYLENE OXIDE AND STRETCHABLE LITHIUM ION BATTERIES

Taylor Hidemi Kelly

Approved:

Chair of the Committee
Haleh Ardebili, Associate Professor,
Mechanical Engineering

Committee Members:

Kenneth White, Professor,
Mechanical Engineering

Li Sun, Professor,
Mechanical Engineering

Yashashree Kulkarni, Associate Professor,
Mechanical Engineering

Jae-Hyun Ryou, Assistant Professor,
Mechanical Engineering

Suresh K. Khator, Associate Dean,
Cullen College of Engineering

Pradeep Sharma, Director of the Materials Science and Engineering Program

Acknowledgements

I would like to dedicate this Doctoral degree to several important people in my life. First, I dedicate this degree to my parents. I am grateful for your constant love, continuous support, and never-ending belief that I can achieve more. Words cannot express my eternal gratitude for everything you've done and sacrificed for me. Second, I dedicate this degree to my husband. Thank you for your love, support, and selflessness. I appreciate that you continue to be my cheerleader through the good times and hold my hand through the bad. Third, I dedicate this degree to my Grandma Ruth Dizon. Thank you for being such a wonderful role model. I admire that you are a strong woman who worked hard so that her children and grandchildren might have a better life. I've promised you time and time again that I would finish my education, and here I am! Finally, I would also like to thank all of my family and friends for their love and support through past, present, and future adventures.

From the bottom of my heart, I would like to thank my advisor and mentor, Dr. Haleh Ardebili. I am grateful for your support, guidance, and patience. You took a chance on me and hired me after a ten-minute meeting in your office. Your enthusiasm and love for research has been encouraging throughout my time here. I am eternally grateful for the freedom and resources you have given me to explore my curiosities and grow into the scientist and engineer I am today. I would also like to thank all of my colleagues and collaborators: Mejdi Kammoun, Mengying Yuan, Bahar Ghadi, William Walker, and Sean Berg. Thank you for your friendship,

company, help, guidance, and discussions. In addition, I want to thank my undergraduate assistant, Julie Rogers, for your help and company.

I would also like to thank Dr. Pradeep Sharma, Dr. Fritz Claydon, Dr. Hanadi Rifai, and Dr. Eugene Chiappetta for the opportunity to be a NSF GK12 Fellow. It was a wonderful learning and growing experience that took me to places I never thought I would go. Finally, I would like to thank Dr. Robert Pardue for your mentorship, company, and discussions.

Thank you to NSF for the financial support for this research.

INVESTIGATION OF THE MECHANO-ELECTROCHEMICAL COUPLING OF SOLID POLYETHYLENE OXIDE AND STRETCHABLE LITHIUM ION BATTERIES

An Abstract

of a

Dissertation

Presented to

the Faculty of the Department of Materials Science and Engineering

University of Houston

In Partial Fulfillment

of the Requirements for the Degree

Doctor of Philosophy

In Materials Science and Engineering

by

Taylor Kelly

December 2016

Abstract

It is necessary to develop deformable energy storage devices that are compatible with the next generation flexible and stretchable electronics such as medical implants and wearable devices. Lithium ion batteries are a popular energy storage method for modern technology that provides high energy density and efficiency. However, the electrochemical instability of the organic liquid electrolytes poses a real hazard to using conventional lithium ion batteries in deformable electronics. Replacing the liquid electrolyte with a solid polymer reduces the risk of the battery setting aflame among many other benefits. Solid polymer electrolytes are of particular interest to battery scientists because they allow for the development of safe and deformable batteries. On the other hand, solid polymer electrolytes are also disadvantaged because of their poor ion transport properties. There has been extensive research in improving the ion conductivity of solid polymer electrolytes, but the best achievable conductivities are still two orders of magnitude less than that of liquid electrolytes.

The present study investigates the feasibility of using solid polymer electrolytes (i.e. polyethylene oxide) in stretchable lithium ion batteries. The ion conductivity of a solid polymer electrolyte film is demonstrated to increase with tensile strain and this research delves into the mechanisms behind this conductivity improvement. The coefficients of ion conductivity enhancement are found to be similar in both in-plane and out-of-plane directions. Furthermore, molecular weight blending (i.e. 100k and 600k Mw) is used to enhance the electrochemical properties

of the solid polymer electrolyte while minimally affecting the polymer's mechanical stability. The relatively optimized stretchable polymer electrolyte is tested inside a sliding electrode battery and the effect of tensile strain on overall battery performance is investigated.

Table of Contents

Acknowledgements v

Abstract viii

Table of Contents x

List of Figures xiv

List of Tables xviii

Chapter 1: Introduction 1

1.1 Energy Crisis 1

1.2 Lithium Ion Batteries 2

1.2.1 Material Selection 4

1.2.2 Safety 9

1.3 Battery Electrolytes 10

1.3.1 Characterization 10

1.3.2 Liquid 13

1.3.3 Hard Solid 14

1.3.4 Polymer 14

1.4 Next Generation Batteries 16

1.4.1 Flexible Batteries 16

1.4.2 Stretchable Batteries 19

1.5 Overview of this Dissertation 22

Chapter 2: *In Situ* Study of Strain-Dependent Ion Conductivity of Stretchable Polyethylene Oxide Electrolyte . 24

2.1 Overview 24

2.2 Introduction 24
2.3 Methods 26
2.3.1 Polymer Electrolyte Fabrication 26
2.3.2 Mechanical and Impedance Test Procedures 28
2.3.3 In Situ Impedance Spectroscopy Setup 28
2.3.4 Polarized Light Microscopy 30
2.3.5 Thermogravimetric Analysis (TGA) 31
2.4 Experimental Results and Discussion 32
2.5 Continuum Model 44
2.5.1 Mass Balance 44
2.5.2 Elasticity 46
2.5.3 Coupling Diffusion and Elasticity 47
2.5.4 Small Deformation Development 49
2.6 Conclusions 50
CHAPTER 3: THE INVESTIGATION OF MOLECULAR WEIGHT BLENDS IN PURE AND NANOCOMPOSITE POLYETHYLENE OXIDE ELECTROLYTES 51
3.1 Overview 51
3.2 Introduction 51
3.3 Methods 54
3.3.1 PEO 100k/600k Mw Electrolyte Fabrication 54
3.3.2 PEO/GO 100k/600k Mw Nanocomposite 54
3.3.3 Thermogravimetric Analysis (TGA) 54

3.3.4 Mechanical Testing *55*

3.3.5 Impedance Testing *55*

3.3.6 In Situ Impedance Spectroscopy Setup and Test Procedure ..

..... *56*

3.3.7 Differential Scanning Calorimetry *57*

3.3.8 Scanning Electron Microscopy *57*

3.4 Results and Discussion 58

3.4.1 Differential Molecular Weight PEO Blends *58*

3.4.2 Differential Molecular Weight Polymer Nanocomposite Blends

..... *62*

3.4.3 Strain-Dependent Ion Conductivity *66*

3.5 Conclusions 68

CHAPTER 4: STRETCHABLE LITHIUM ION BATTERY DISPLAYING ENHANCED PERFORMANCE WITH STRAIN 70

4.1 Overview 70

4.2 Introduction 70

4.3 Methods 73

4.3.1 Stretchable Battery Fabrication *73*

4.3.2 Battery Testing *74*

4.3.3 Mechanical Testing *75*

4.4 Results and Discussion 75

4.4.1 VHB Encapsulation Material *75*

4.4.2 Stretchable Battery Mechanical Analysis *78*

4.4.3 Electrochemical Analysis 80

4.5 Conclusions 84

CHAPTER 5: CONCLUSIONS AND FUTURE WORK 86

5.1 Conclusions 86

5.2 Future Work 89

5.2.1 Battery Development 89

5.2.2 Fundamental Studies 90

REFERENCES 92

List of Figures

Figure 1.1 Ragone plot....1

Figure 1.2 Battery charge and discharge behavior 3

Figure 1.3 Capacity and voltage window comparison of various cathode and anode chemistries. 6

Figure 1.4 SEM images of pristine silicon (a) nanowires and (b) nanotubes prior to cycling. SEM images of SEI formation over the silicon (c) nanowires and (d) nanotubes after 200 cycles. 7

Figure 1.5 Example of volumetric expansion in a lithium ion battery silicon anode....8

Figure 1.6 Examples of nanostructured electrode architectures including (a) microbeads, (b) nanotubes, (c) porous structures, and (d) nanowires. 9

Figure 1.7 Arrhenius plot of ion conductivity of various liquid, hard solid, and solid polymer electrolytes. 11

Figure 1.8 Depiction of bulk resistance measurement for solid and gel polymer electrolytes using the obtained Nyquist plot from electrochemical impedance spectroscopy. 13

Figure 1.9 Images of (a) graphene paper and (b) graphene paper with vertically aligned carbon nanotubes and (c) a schematic of a flexible battery with 3D interconnected graphene foam electrodes. 17

Figure 1.10 Left: schematic of PEO/GO/Li salt membrane. Right: (a) images of flexible PEO/GO electrolyte based lithium ion battery powering an LED, (b) schematic of flexible battery materials and configuration. 18

Figure 1.11 SEM image and element mapping of (a,b) conductive silver fabric, (c,d) fabric embedded with MnO_2, (e,f) fabric embedded with Zn particles. (g,h) SEM images of spring-like carbon nanotube fibers.... 20

Figure 1.12 Photographs of stretchable batteries developed by (a) Xu et al., [87] (b) Kettlgruber et al., [92] and (c,d) Song et al. [93] 21

Figure 2.1 Plot of 600,000 Mw PEO Poisson's ratio 27

Figure 2.2 *In situ* impedance spectroscopy setup during tensile stress-strain testing. (a) Electrode is in open position, (b) closed electrodes, (c) schematics of the experimental components [86] 28

Figure 2.3 Comparison of the effects of micro voids and stretching on ion conductivity [86] 29

Figure 2.4 Effect of (a) moisture and (b) electrode to electrolyte area on bulk PEO resistivity [86] 30

Figure 2.5 Thermogravimetric analysis (TGA) of PEO electrolyte at different drying times [86] 31

Figure 2.6 TGA at room temperature showing moisture absorption over time for (a,b) 600,000 Mw PEO and (c,d) 400,000 Mw PEO [86] 32

Figure 2.7 Tensile stress-strain behavior of PEO (a) at various strain rates (b) magnified curve below 20% strain, (c) stress-strain hysteresis effect, and (c) photos of PEO under tensile deformation [86] 32

Figure 2.8 (a) Fitted Nyquist plots for PEO stretched from 0 to 0.4 cm; equivalent circuit fit (inset), Nyquist plots with equivalent circuit fit curves at (b) 0 cm, (c) 0.2 cm, and (d) 0.4 cm deformation [86] 35

Figure 2.9 (a,c) Ion conductivity vs. deformation in through and in-plane directions, respectively. (b,d) Conductivity enhancement vs. strain in through and in-plane directions, respectively. [86] 36

Figure 2.10 Percent ion conductivity enhancement vs. axial strain in wet and dry environments for (a) 600k Mw PEO and (b) 400k Mw PEO [86].....39

Figure 2.11 Depiction of semi-crystalline polymer microstructure at various stages of tensile deformation [86] 40

Figure 2.12 Polarization Light Microscopy (PLM) images of unstretched (top) and stretched (bottom) PEO. (a-b) 50x magnification, (c-d) 100x, (e-f) 200x, and (g-h) 500x magnifications. [86] 40

Figure 3.1 TGA of various molecular weight blend polymers comparing decomposition temperatures 55

Figure 3.2 In situ ion conductivity set up 56

Figure 3.3 (a) Elastic modulus, (b) yield strength and ultimate tensile strength, (c) % elongation, and (d) photo images of a PEO sample subject to tensile deformation. 58

Figure 3.4 (a) Log scale ion conductivity and (b) glass transition temperature of PEO molecular weight blends.....59

Figure 3.5 SEM images of PEO molecular weight mixtures 60

Figure 3.6 Close-up SEM images of the 0%, 25%, 50% and 100% PEO molecular weight blends. 62

Figure 3.7 Schematic of unfilled (left) and filled PEO (right) depicting how nanofillers affect the polymer chain conformation.....62

Figure 3.8 Comparison of (a) Elastic modulus, (b) yield strength, (c) % elongation, and (d) ultimate tensile strength of PEO molecular weight blends and PEO blends + 1% GO 63

Figure 3.9 Comparison of (a) Log scale ion conductivity, (b) glass transition temperature 65

Figure 3.10 SEM images of (a) 100kMw PEO and (b) 100kMw PEO + 1% GO 65

Figure 3.11 (a) logarithmic ion conductivity deformed 25% samples vs. tensile strain and (b) enhancement in ion conductivity vs. tensile strain ...67

Figure 4.1 (a) Diagram of stretchable battery with (b, c, d) SEM images of the stretchable battery cross-section. 73

Figure 4.2 Pictures of (a) the stretchable battery experimental setup, (b) a battery under tensile strain, and (c) a pinned battery. 74

Figure 4.3 (a) Table of VHB mechanical properties, (b) VHB stress-strain curve, (c) photo images of VHB under tensile load, (d) adhesive strength-strain curve, and (e) photo images of the peeling test.....76

Figure 4.4 Plots of the (a) specific capacity and (b) coulombic efficiency vs. cycle of an unstrained battery tested outside of the glove box. (c) Corresponding images of battery degradation with cycle. 77

Figure 4.5 Plots comparing the (a) specific capacity vs. cycle and (b) coulombic efficiency vs. cycle of two batteries tested inside and outside of the glove box. 78

Figure 4.6 Comparison of electrolyte and battery stress-strain curves, table of mechanical properties for the 25% 100k Mw PEO electrolyte, VHB, and battery, photo images of the battery under tensile loading 79

Figure 4.7 Area capacity vs. cycle and coulombic efficiency vs. cycle for each strain increment of the battery 80

Figure 4.8 SEM images of pristine (a) graphite and (c) $LiFePO_4$ electrodes. SEM images of used (b) graphite and (d) $LiFePO_4$ electrodes. 82

Figure 4.9 (a) Nyquist plots at 0%, 2%, 5%, and 10% strains with equivalent circuit inset and (b) voltagramm of the stretchable battery at the corresponding strain increments. 83

List of Tables

Table 2.1 Mechanical properties of thin-film 600,000 Mw PEO/$LiClO_4$ [86]..... 33

Table 2.2 Out-of-Plane and In-Plane ionic conductivity of unstretched 600,000 Mw PEO/$LiClO_4$ [86] 37

Table 2.3 Comparison of through-plane and in-plane CSDICE values [86] 42

Table 3.1 Comparison of mechanical properties of filled and unfilled PEO molecular weight blends. 64

Table 3.2 Average ion conductivity, glass transition temperature, % crystallinity, and melting temperature for all PEO molecular weight blends and PEO blends + 1% GO.....66

Chapter 1: Introduction

1.1 Energy Crisis

Global energy demands are rapidly growing. The United States is currently the 2nd largest energy consumer in the world. Majority of energy consumed in the US is produced from fossil fuels, a non-renewable sources of energy, taking millions of years to reproduce. Furthermore, burning fossil fuels generates greenhouse gases, which are widely considered to be a cause of global warming [1-7].

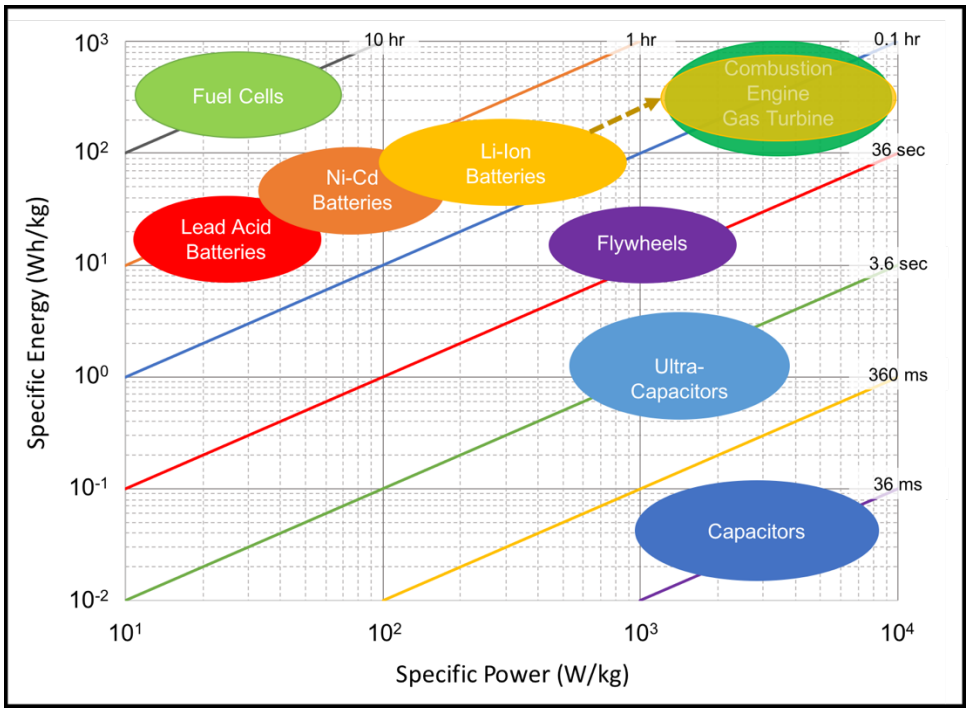

Figure 1.1 Ragone plot

There is a global effort to utilize alternative energy sources in order to lessen our dependence on fossil fuels. Renewable energy, including solar and wind, is a popular "green" alternative energy source. However, energy sources such as these are intermittent and for continuous use it is necessary to store the excess energy

produced. Batteries are one storage option, storing energy in the form of chemical potential difference.

Lithium ion batteries are of particular interest in the energy storage industry because they have a high energy density and power density compared to other battery chemistries [1-5], as seen in the Ragone plot in **Figure 1.1**. An ideal lithium ion battery would have an energy and power density similar to a combustion engine.

1.2 Lithium Ion Batteries

Lithium batteries were first introduced in the 1970s. Lithium is the lightest of all metals, the strongest reducing agent with the greatest electrochemical potential, and has an extremely large theoretical specific capacity, making it an attractive material for batteries. Unfortunately, attempts to develop rechargeable lithium batteries failed due to the inherent instability of lithium metal. Because of this, researchers developed non-metallic lithium batteries using lithium ions. Although lithium-ion batteries have a slightly lower energy density than lithium metal batteries, they remedy the major safety concerns attributed to the use of lithium metal.

Batteries are electrochemical energy storage devices that separate positive and negative charges to do work. All batteries work in a similar fashion and require a positive electrode (cathode), negative electrode (anode), and an electrolyte. Battery electrodes are electrically conducting materials chosen based on their reduction potential and chemical compatibility. The electrolyte is an electrically insulating and ionically conducting medium that separates the cathode and anode.

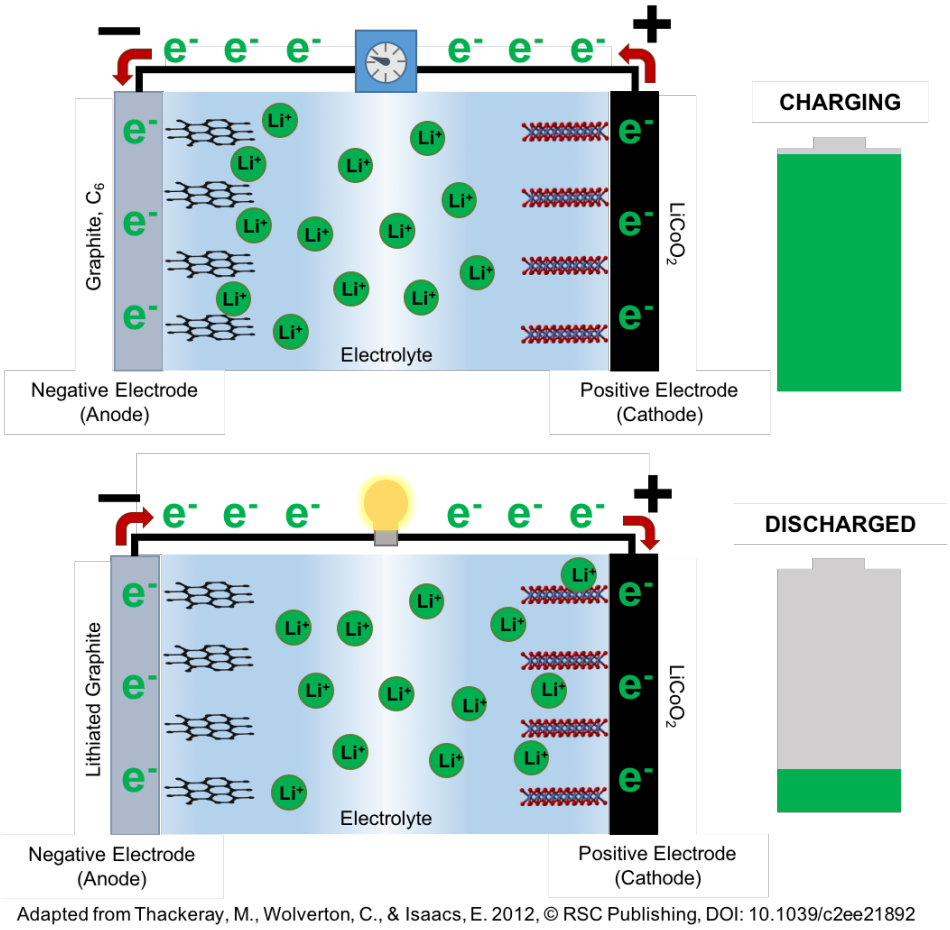

Figure 1.2 Battery charge and discharge behavior

Lithium ion batteries are rechargeable, meaning that the electrochemical reaction that occurs during discharging can be reversed by applying power to the cell, allowing the battery to recharge. Conventional lithium ion cells contain a lithium cobalt oxide ($LiCoO_2$) cathode and a graphite anode. Conventional cells often use an organic liquid electrolyte and require a thin, polymeric separator that prevents the electrodes from touching and causing a battery short. When charging, lithium ions move from cathode to anode and upon discharge ions move from anode to cathode. Being unable to travel across the electrically insulating electrolyte,

electrons are forced to flow through the external circuit during their respective charge and discharge cycles, diagramed in **Figure 1.2**.

1.2.1 Material Selection

The chemical driving force on the lithium ions within the electrolyte is the Gibbs free energy, defined in **Equation 1.1**

$$\Delta G = \sum \Delta G_{f(products)} - \sum \Delta G_{f(reactants)} \quad (1.1)$$

$$= \mu^e_{Li} - \mu^e_{Li^+}$$

$$= -z\phi_{Li}F \ ,$$

where ΔG is Gibbs free energy, μ^e is electrochemical potential, ϕ is electrostatic potential, z is the number of electrons per mole of product, and F is Faraday's constant (96485 Coulombs/mol).

The Gibbs free energy, working in one direction, is balanced by an electrostatic driving force in the opposite direction, which is the electrochemical potential. Using the Gibbs free energy, we can calculate the voltage between the battery electrodes.

The Nernst equation is derived from the Gibbs free energy and is used to determine the cell potential under non-equilibrium conditions or at any point during the electrochemical reaction. The Nernst equation is defined as

$$\mathrm{E} = E_0 - \frac{RT}{zF}\ln(Q) \ , \quad (1.2)$$

where E is electric potential, E_0 is the reduction half-cell potential, R is the universal gas constant, T is temperature, and Q is the reaction quotient. These equations are useful in choosing new materials used for lithium ion batteries as well as better understanding the electrochemical reaction occurring within the cell.

The goals of current research in lithium ion batteries includes finding materials with a high capacity and rate capability, increasing the battery life and cyclability, and addressing safety concerns. Making adjustments to any of the three major components of the battery can affect the overall performance.

When choosing battery component materials, it is important to use chemically stable and chemically compatible materials for safety and for longevity. Maximizing the amount of energy stored in the battery is dependent on the materials chosen for the electrode materials. The maximum theoretical specific energy (MTSE) can be determined using **Equation 1.3**

$$MTSE\left[\frac{Wh}{kg}\right] = \frac{|\Delta G_r|}{3.6\, W_{reactants}}, \tag{1.3}$$

where $W_{reactants}$ is the weight of the reactants. This value is especially important as the world continues to manufacture devices at smaller and smaller scales and materials with a larger MTSE value are preferred.

To maximize energy potential stored in the battery, there should be a large potential difference between the chosen cathode and anode active materials. **Figure 1.3** depicts the potential differences of various cathode and anode materials commonly used in lithium ion battery research. **Figure 1.3** also compares cathode

and anode capacities. The battery capacity is a material dependent property that quantifies the amount of charge stored in the battery. Capacity fading, or loss of capacity over time, of the battery is common. Loss of capacity implies that lithium ions are being trapped, thus preventing the full lithiation or delithiation of battery electrodes. Solid electrolyte interphase (SEI) formation is one cause for capacity fading. SEI is a thin, passive layer consisting of organic and inorganic electrolyte decomposition products that forms over the anode surface, as seen in **Figure 1.4**.

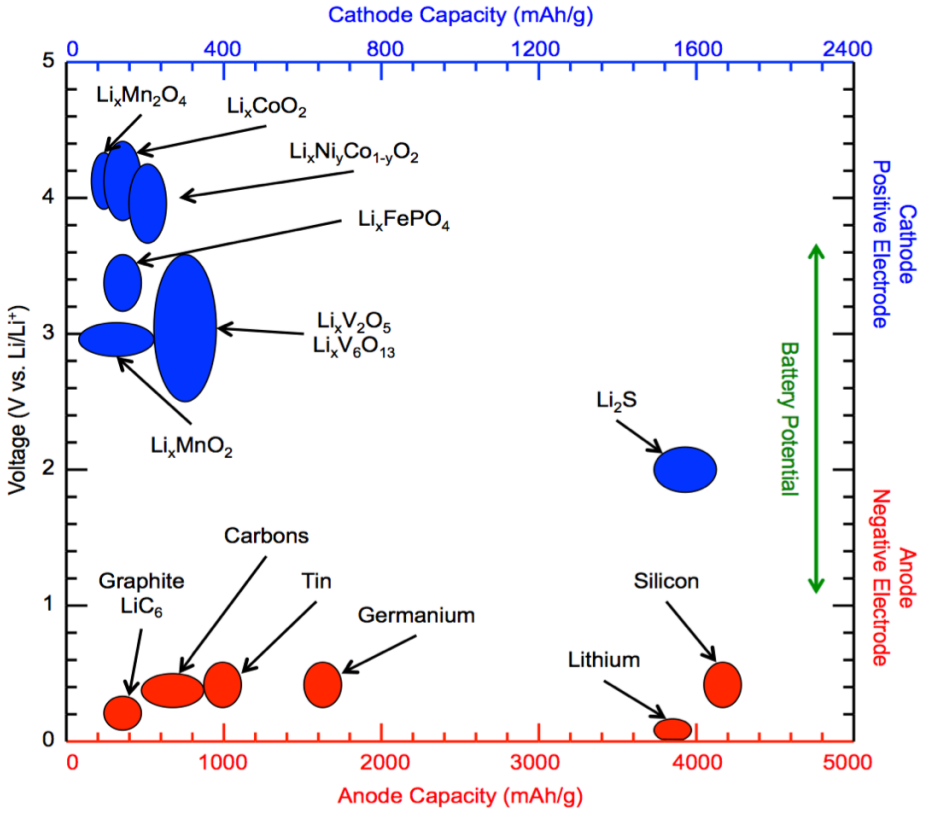

Adapted from Landi et al. 2009, ©RSC Publishing, DOI: 10.1039/b904116h

Figure 1.3 Capacity and voltage window comparison of various cathode and anode chemistries.

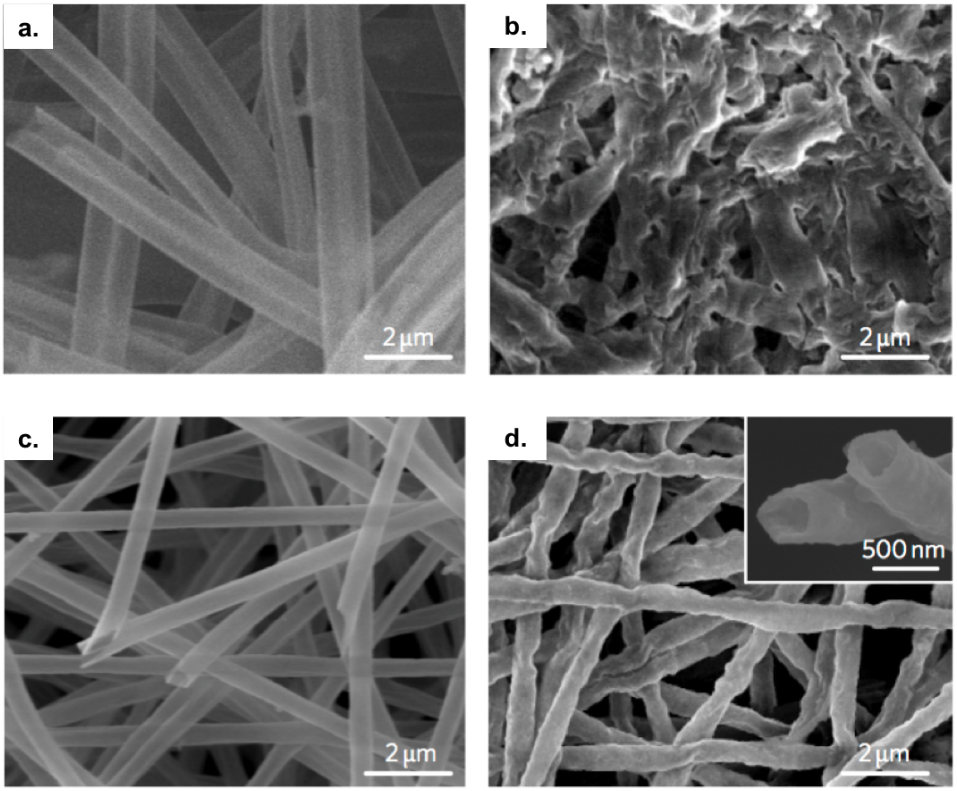

Cui et al., 2012, © Nature Publishing Group, DOI: 10.1038/NNANO.2012.35

Figure 1.4 SEM images of pristine silicon (a) nanowires and (b) nanotubes prior to cycling. SEM images of SEI formation over the silicon (c) nanowires and (d) nanotubes after 200 cycles.

Improving battery capacity through material selection and design of electrode architectures is a popular area of research within the lithium ion battery field [6,8-17]. For decades there has been a great deal of attention in developing and utilizing high capacity anode materials. Silicon is one such example. Silicon is an attractive anode material because of its theoretical specific capacity of 4200 mAh cm^{-2}; the highest specific capacity of known lithium ion battery anode materials [14]. One of the challenges with implementing silicon-based anodes has to do with silicon's large volumetric expansion of up to a 400% [6,14,16,18-22]. Volumetric expansion of the electrode material can be directly related to capacity loss or battery

failure [18]. During cycling, ions are inserted to and extracted from either the anode or cathode causing mass transfer and subsequent volume changes, as depicted in **Figure 1.5**. These volume changes can be severe enough to break the active material free from the electrode, resulting in capacity fade or create an electrically conducting bridge between electrodes, also known as shorting.

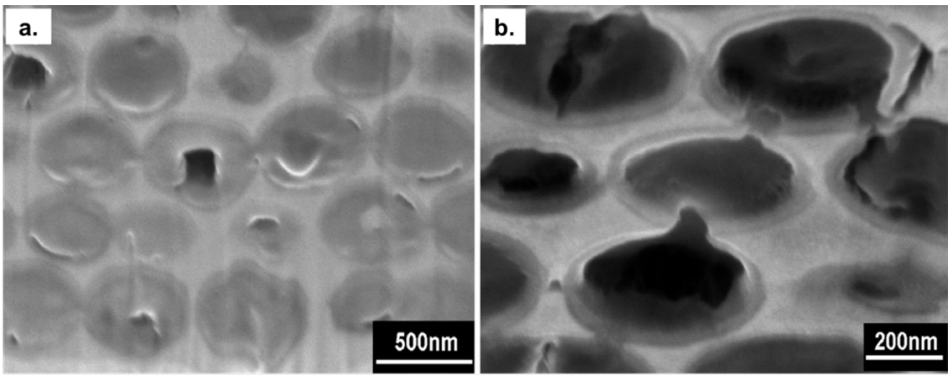

Figure 1.5 Example of volumetric expansion in a lithium ion battery silicon anode

One method used to minimize expansion effects of silicon, and other high capacity materials, is through nanostructuring. Nanostructuring the electrode surface provides a larger anode surface area and increases the number of reaction sites for lithium insertion, thus increasing the overall capacity of the anode, while providing space for material expansion. Additional benefits of the electrode architecture include enhanced ion conductivity and ultra-fast charge and discharge capability. Some examples of nanostructured architectures include microbeads, nanotubes, porous structures, and nanowires, seen in **Figure 1.6** [17,23-25].

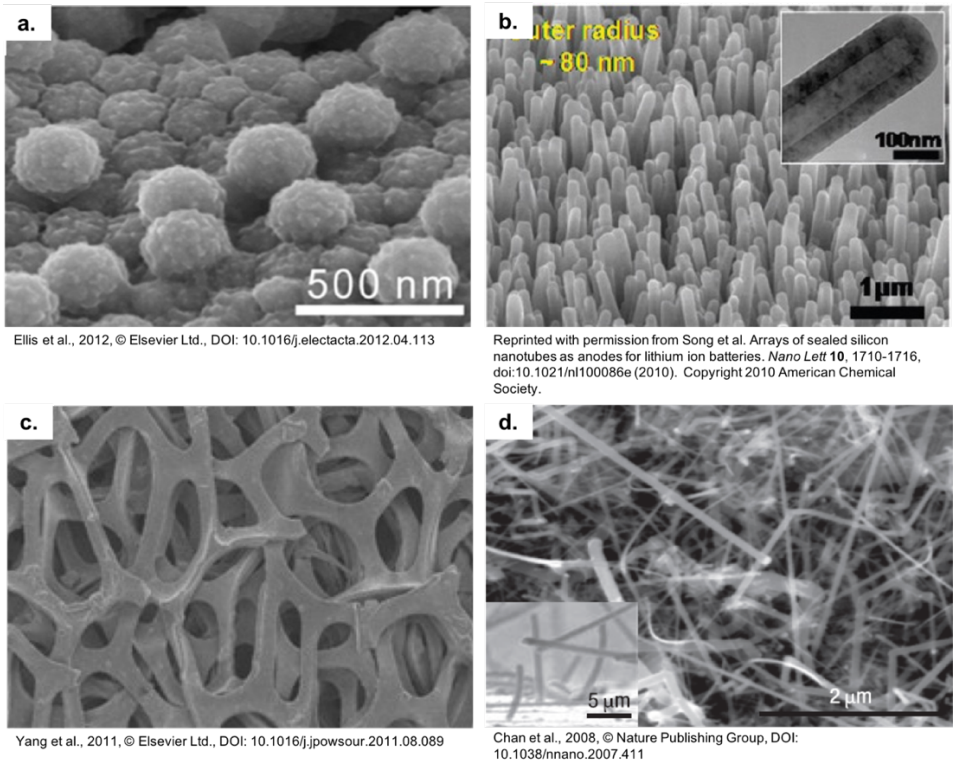

Ellis et al., 2012, © Elsevier Ltd., DOI: 10.1016/j.electacta.2012.04.113

Reprinted with permission from Song et al. Arrays of sealed silicon nanotubes as anodes for lithium ion batteries. *Nano Lett* **10**, 1710-1716, doi:10.1021/nl100086e (2010). Copyright 2010 American Chemical Society.

Yang et al., 2011, © Elsevier Ltd., DOI: 10.1016/j.jpowsour.2011.08.089

Chan et al., 2008, © Nature Publishing Group, DOI: 10.1038/nnano.2007.411

Figure 1.6 Examples of nanostructured electrode architectures including (a) microbeads, (b) nanotubes, (c) porous structures, and (d) nanowires.

1.2.2 Safety

Although researchers have taken great strides in improving battery performance and capability, it is important to remember that safety is the number one concern with using conventional lithium ion batteries. News of a Boeing 787 Dreamliner fire was released in 2012 and 2013. After an investigation was launched, thermal runaway of the lithium ion battery was reported to be the cause of the fire [26]. Thermal runaway most commonly occurs in lithium ion batteries utilizing an organic liquid electrolyte. In a thermal runaway event, overheating, abuse, or an internal short circuit heats the flammable electrolyte material, causing it to vaporize and build pressure within the battery. Rapid self-heating occurs when the battery

reaches a critical temperature, causing decomposition of the toxic battery cathode [27-35]. The heat and pressure build up cause a catastrophic event. Furthermore, the energy released by a battery cell in thermal runaway can be enough to heat neighboring cells and cause thermal runaway propagation.

Although there has been substantial work in trying to improve lithium ion battery safety through liquid electrolyte additives and electrode coating, news of battery fires continues to be released. Tesla battery fires have occurred in 2013 and 2016, there was widespread news of hover board battery fires in 2015 and 2016 [36], and, most recently, there has been extensive media coverage of the Samsung Note 7 battery fires. An alternative method for enhancing battery safety and minimizing the potential for thermal runaway is to replace the conventionally used liquid electrolyte with a solid and less flammable electrolyte, particularly solid ceramic or solid polymer.

1.3 Battery Electrolytes

A battery electrolyte is an electrically insulating medium responsible for facilitating ion transport between the battery anode and cathode. Lithium ion battery electrolytes can be separated into three main categories: liquid, hard solid, and polymer.

1.3.1 Characterization

Electrolytes are often characterized by their thermal and electrochemical stability, transference number, and ion conductivity [37]. The electrolyte material

must be thermally and electrochemically stable to safely and reliably operate in a wide range of temperatures and within a 0 - 4.5V window to be compatible with lithium ion cathode materials. The electrolyte transference number describes the fraction of lithium ion charges that are transferred from one electrode to the other. A transference number of one is ideal, suggesting that all lithium ions are successfully moving across the electrolyte.

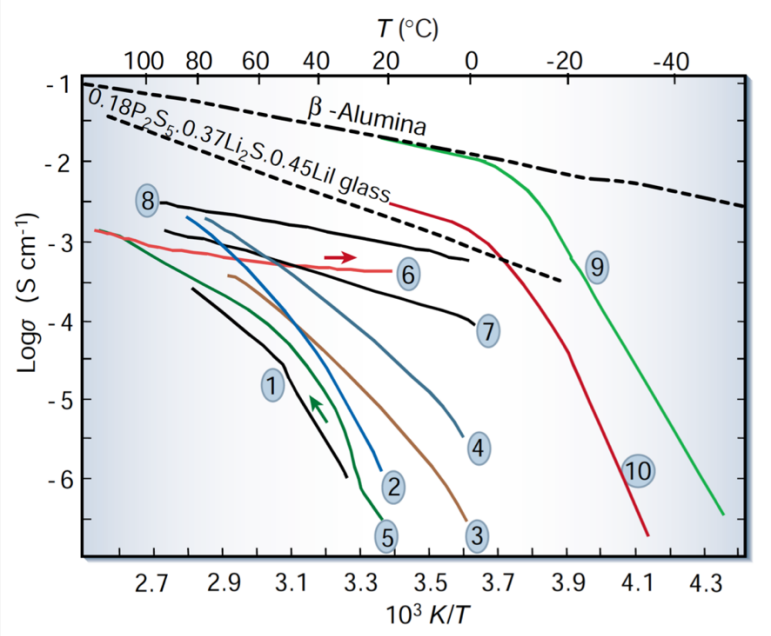

1. First generation PEO-$LiCF_3SO_3$; 2, new solutes with high-dissociation PEO-$Li[(CF_3SO_2)_2N]$; 3, low-T_g combination polymer; 4, plasticized polymer electrolyte PEO-$Li[(CF_3SO_2)_2N]$+25% w/w PEG-dimethylether (molecular weight, 250); liquid crystalline polymer electrolytes; 5, heating curves; 6, cooling curve; gel-type polymer (X-linked PEO dimethacrylate-$Li[(CF_3SO_2)_2N]$-PC 70%); 8, liquid electrolyte PC/DME $LiCF_3SO_3$; 9, liquid electrolyte EC/DMC-$LiPF_6$ at low temperature; 10, gel electrolyte P(VDF-HFP)/EC/DMC-$LiPF_6$

Figure 1.7 Arrhenius plot of ion conductivity of various liquid, hard solid, and solid polymer electrolytes.

The ion conductivity of the electrolyte is arguably its most important characteristic as it broadly describes the electrolyte's ability to transport ions between electrodes. Liquid, hard solid, and polymer electrolytes have different ion

conductivities owing to their different molecular structures. **Figure 1.7** compares the ion conductivity of liquid, gel, and polymer electrolytes at varying temperatures.

Ion conductivity is dependent on the electrolyte's dimensions and bulk resistance, as seen in **Equation 1.4**

$$\sigma = \frac{d}{R_b A}, \tag{1.4}$$

where σ is ion conductivity, d is the electrolyte thickness, R_b is measured bulk resistance of the material, and A is the electrolyte surface area. Electrochemical impedance spectroscopy is often employed to measure the electrolyte resistance. The resistance of solid or gel polymer electrolytes can be approximated by finding the real impedance at the intersection of the charge and mass transfer regions on the obtained Nyquist plot, depicted in **Figure 1.8**. A more accurate method for determining bulk resistance is to fit an equivalent circuit to the Nyquist plot and obtaining the value for $R_{electrolyte}$. The equivalent circuit used for modeling the impedance behavior of electrolytes is also seen in **Figure 1.8**.

The Nyquist plot can also be used to determine the contact resistance at the electrode-electrolyte interface, double layer capacitance, and the Warburg element. The double layer capacitance describes the charge polarization that occurs at the electrode-electrolyte interface and the Warburg element models ion diffusion across the electrolyte membrane. As a side note, the contact resistance value is often taken as the bulk electrolyte resistance in liquid electrolyte systems.

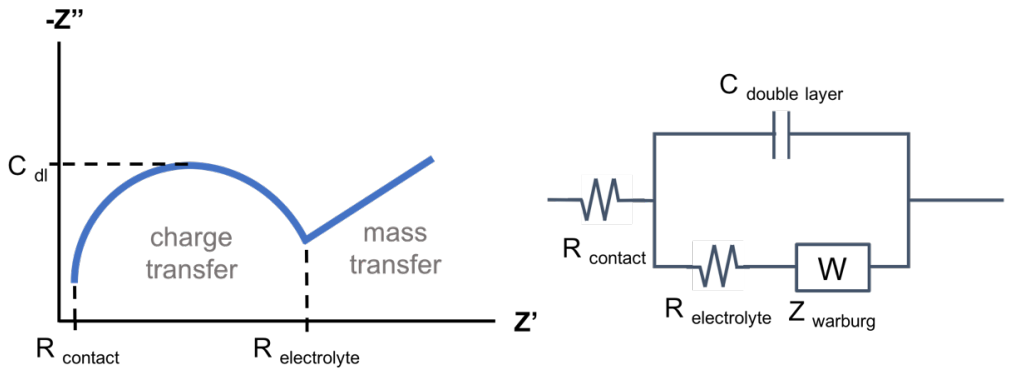

Figure 1.8 Depiction of bulk resistance measurement for solid and gel polymer electrolytes using the obtained Nyquist plot from electrochemical impedance spectroscopy.

1.3.2 Liquid

As previously mentioned, conventional lithium ion batteries contain an organic liquid electrolyte. Ideally, a liquid electrolyte should be able to dissolve a sufficient concentration of lithium salt, have a low viscosity to facilitate fast and efficient ion transport, be chemically stable, have a low melting temperature and a high boiling temperature [33]. Liquid electrolytes are able to achieve the highest ion conductivities and transference numbers due to the free and uninhibited movement of ions in the liquid medium. However, thermal and electrochemical instability have led to major safety concerns, as previously discussed.

In addition to organic liquids, ionic liquids also fall into the liquid electrolyte category. Ionic liquids contain molten salt, are able to achieve high ion conductivities, and are much safer than organic liquid electrolytes. However, the concern for leakage is present when using any liquid electrolyte. For these reasons, liquid electrolytes are not compatible with flexible and stretchable batteries as well as batteries designed for wearable and implantable electronics.

There has been a growing interest to move from liquid to solid electrolyte due to the general safety and stability concerns faced with the liquid electrolyte used in conventional lithium ion batteries [38-40], as previously discussed. However, using hard solid and solid polymer electrolytes have their own disadvantages such as poor interfacial contact with the electrodes [2-4,41-43].

1.3.3 Hard Solid

Hard solid electrolytes have shown great promise with reported room temperature ion conductivities on the order of 10^{-3} S cm^{-1}, compared to the 10^{-2} to 10^{-1} S cm^{-1} ion conductivity of liquid electrolyte [11,44,45]. Ion conductivity in hard solid electrolytes arises from Li^{+} ion hopping through the vacancy sites of the crystalline structure as it travels from one electrode to the other [29,31,46,47]. Hard solid electrolytes can operate safely within a large voltage window and are an excellent electrolyte option for high temperature applications because of their high electrochemical, thermal, and mechanical stability [11,29,47]. Unfortunately, its applications aer limited due to its incompatibility with flexible and stretchable electronic devices; the future in technology.

1.3.4 Polymer

Solid polymers are an excellent electrolyte alternative for flexible and stretchable lithium ion batteries. They are deformable without the potential hazards and safety concerns associated with conventional lithium ion batteries. Additional advantages to using solid polymer electrolytes over liquid electrolytes

includes non-volatility, no leaks, compatibility with lithium metal, improved shock resistance, better overheat and overcharge allowance, and a lower cost [33]. However, solid polymer electrolytes have a lowest ion conductivities of the three electrolyte classes, usually on the order of 10^{-7} S cm^{-1} to 10^{-8} S cm^{-1}, as well as poor interfacial contact with the electrodes [48-52].

Methods for enhancing the ion conductivity include polymer blends, use of nanofillers, and plasticization [49-69]. Some of the highest reported conductivity values for solid polymer electrolyte (SPE) are on the order of 10^{-4} S cm^{-1}, but these electrolytes are often plasticized and compromise the safety and mechanical integrity of the electrolyte [66-68].

It is widely agreed upon that ion transport in solid polymer electrolytes is dependent on the chain segmental motion of the polymer host, suggesting that a higher degree of amorphicity correlates to enhanced ion conductivity [66-68,70-79]. However, little is known about how lithium ions move through the SPE. One accepted model is based on the free volume theory and assumes that lithium ions are transported by occupying the free volume of amorphous polymer chains. The ions hop from free volume to free volume and from polymer chain to polymer chain as they travel across the electrolyte membrane. Ion conductivity, based on the free volume theory, is related to the diffusivity of ions through the polymer [78].

Although polymer electrolytes exhibit low ion conductivities, the appeal of solid polymer electrolytes lies in their compatibility with next generation flexible and stretchable electronic devices [80-87]. The inherent safety and deformability of

polymer electrolytes make them ideal electrolyte candidates for use in wearable and implantable device applications

1.4 Next Generation Batteries

There is a growing need to develop flexible and stretchable batteries that are compatible with wearable, implantable, and conformable technologies. The challenges in creating such a battery lies in designing a mechanically sound, yet deformable battery without compromising the battery's electrochemical performance, including energy density and capacity. Understanding the effect of mechanical deformation on the electrochemical performance, stability, and safety of the battery, and its components, is necessary to successfully develop flexible and stretchable lithium ion batteries.

1.4.1 Flexible Batteries

The design and development of flexible lithium ion batteries is a popular area of research and most of the published work focuses on creating flexible battery electrodes. One method for creating flexible electrodes is to develop an intrinsically flexible active material [9]. Common free-standing and flexible electrodes are carbon-based due to carbon's electrochemical ability and mechanical flexibility. In 2011, Li et al., developed a flexible electrode by growing vertically aligned carbon nanotubes onto a free-standing graphene paper substrate, seen in **Figure 1.9 a** and **b**. They successfully built a flexible battery capabable of achieving a high discharge capacity of 310 mAh g^{-1}, compared to the 330 mAh g^{-1} theoretical capacity of graphite [88].

Alternatively, flexible electrodes can also be created by adhering the active materials onto flexible and self-standing supports [9]. In 2012, Li et al., developed flexible lithium ion battery electrodes using graphene foam substrate, depicted in **Figure 1.9c**. The porous structure allows the electrodes to be light, flexible, and capable of ultrafast charge and discharge rates. Additionally, the graphene provides excellent electronic conductivity. Lithium iron phosphate ($LiFePO_4$), as the cathode active material, and lithium titanate ($Li_4Ti_5O_{12}$), as the anode active material, were then deposited onto the graphene foam substrate. These batteries could sustain repeated bending to a radius of curvature less than 5mm without suffering structural failure and performance losses. Furthermore, Li et al., were able to discharge their battery at rates up to 200C [77].

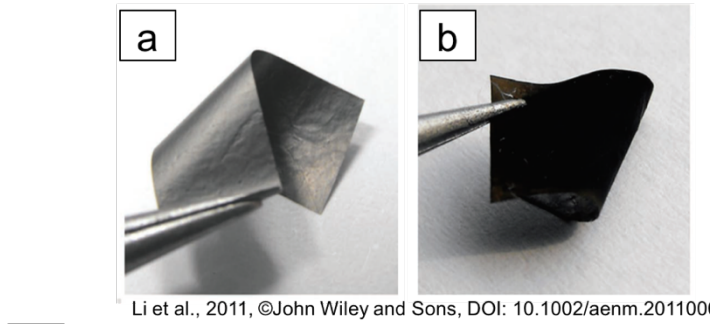

Li et al., 2011, ©John Wiley and Sons, DOI: 10.1002/aenm.201100001

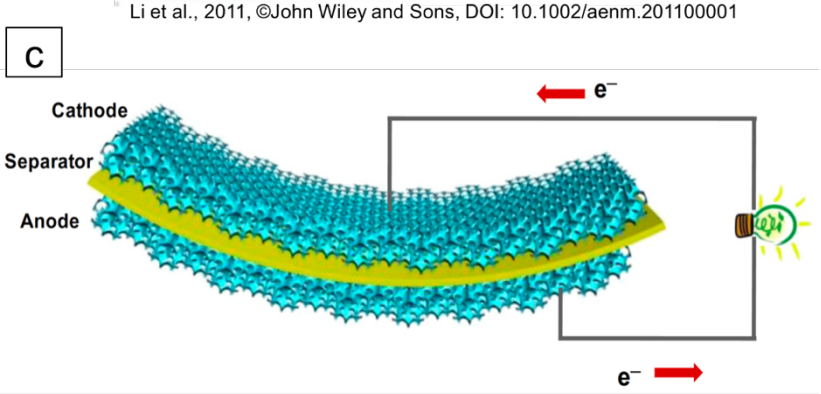

Li et al., 2012, ©National Academy of Sciences

Figure 1.9 Images of (a) graphene paper and (b) graphene paper with vertically aligned carbon nanotubes and (c) a schematic of a flexible battery with 3D interconnected graphene foam electrodes.

Designing mechanically and electrochemically stable electrodes for flexible battery applications is important, but developing a mechanically and electrochemically compatible battery electrolyte is equally important. This is especially true in scenarios where devices will be worn near or in the body. Solid polymer electrolytes are an excellent electrolyte alternative, as discussed in the previous section. Furthermore, substituting the liquid electrolyte for a solid electrolyte would eliminate any concerns of leakage and allow more freedom in the design of the flexible battery [89]. However, the difficulty in implementing SPEs lies in their inherent low ion conductivity, due to the fact that ion diffusion through solids does not occur as freely as in liquids, and the large interface resistance between the electrode and electrolyte layers.

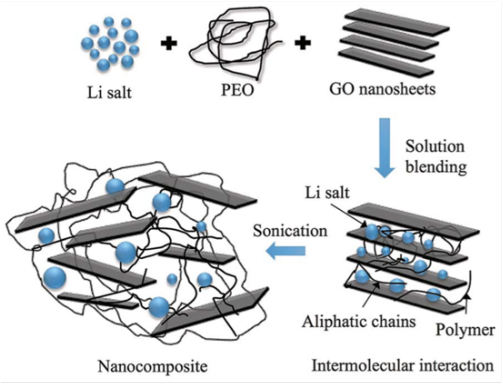

Yuan et al. 2014 © RSC Publishing, DOI:10.1039/c4ra07919a – Reproduced by permission of The Royal Society of Chemistry

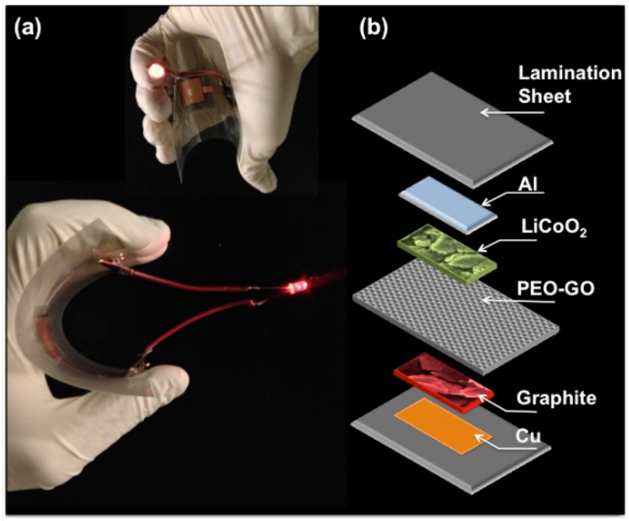

Kammoun et al. 2015 © RSC Publishing, DOI:10.1039/x0xx00000x – Reproduced by permission of The Royal Society of Chemistry

Figure 1.10 Left: schematic of PEO/GO/Li salt membrane. Right: (a) images of flexible PEO/GO electrolyte based lithium ion battery powering an LED, (b) schematic of flexible battery materials and configuration.

As previously mentioned, introducing nanofillers into the SPE is one method for enhancing ion conductivity by opening up polymer chains, increasing free

volume, and reducing the degree of tortuosity in the ion path [62]. In 2014, Yuan et al., developed a poly(ethylene oxide) (PEO) based electrolyte that included a 1%wt. content of graphene oxide (GO), diagramed in **Figure 1.10**. They demonstrated that the addition of GO enhanced ion conductivity by two orders of magnitude, from 10^{-7} S cm^{-1} to 10^{-5} S cm^{-1} [34].

In 2015, Kammoun et al., used this same PEO-based nanocomposite electrolyte in a flexible lithium ion battery with conventional lithium cobalt oxide ($LiCoO_2$) and graphite electrodes, seen in **Figure 1.10**. To further enhance battery performance by reducing the electrode-electrolyte interface resistance, Kammoun et al., added a small amount of liquid electrolyte (<5%wt.) to the active material surfaces of the battery electrodes and fed the assembled battery through a laminating machine, during which the heat and pressure applied enhanced the interface contact. This battery was reported to achieve an area capacity of approximately 0.1 mAh cm^{-2}, which is fairly high relative to other polymer-based solid state batteries with less than a 5%wt. liquid electrolyte content. These batteries were bent to a radius of curvature or 18.9 mm and maintained 93% of its capacity after 6000 bending cycles. Furthermore, the bent batteries showed improved capacity compared to their flat counterparts, likely due to the increase in contact pressure between the electrode and electrolyte layers [81].

1.4.2 Stretchable Batteries

Building stretchable batteries is even more challenging than building flexible batteries due to the inherent inelasticity conventional battery components. One

method for developing stretchable batteries is to deposit the battery active material onto a stretchable substrate. In 2012, Gaikwad et al., built stretchable alkaline batteries using silver fabric electrodes. The fabric base allowed the electrodes to reach strains upwards of 100% while the silver acted as the electrically conductive current collector. The fabric electrodes were soaked in an active material slurry with manganese dioxide (MnO_2) acting as the cathode and zinc oxide (ZnO) acting as the anode. SEM images and element mapping of these fabric electrodes are displayed in **Figure 1.11**. Using an appropriate electrolyte solution, these batteries were able to achieve a 3.875 mAh cm^{-2} areal capacity at a 100% strain. The process used by Gaikwad et al., is not exclusive to alkaline batteries and can be used with different battery chemistries [90].

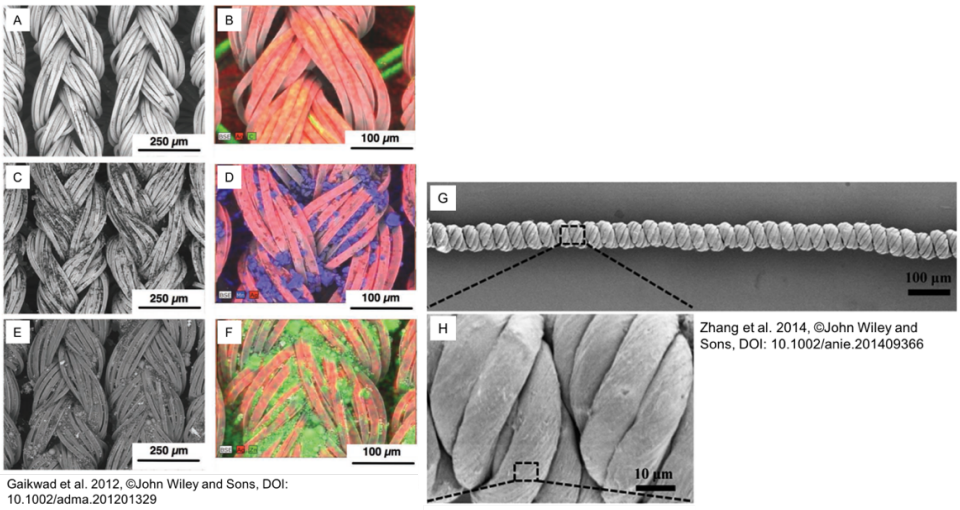

Figure 1.11 SEM image and element mapping of (a,b) conductive silver fabric, (c,d) fabric embedded with MnO_2, (e,f) fabric embedded with Zn particles. (g,h) SEM images of spring-like carbon nanotube fibers

Similarly, in 2014 Zhang et al., developed elastically stretchable electrodes using carbon nanotube fiber springs, seen in **Figure 1.11 g** and **h**. The fibers were

immersed in a slurry of $LiMn_2O_4$ (cathode) or $Li_4Ti_5O_{12}$ (anode) to absorb the battery active material. The battery showed promising cyclability, maintaining 92.1% of its original discharge capacity over 100 cycles. Additionally, the battery performance remained stable after 300 stretching cycles. However, capacity did decrease with strain, dropping to 85% of its original capacity at a 100% strain [91].

Another option for developing stretchable batteries is through the battery design. In 2013, Xu et al., developed a lithium ion battery capable of reaching upwards of a 300% strain, seen in **Figure 1.12a**. The battery consists of multiple cells that are electrically connected using small springs. This allows for large deformations without mechanically compromising the battery components. The charging and discharging profiles at a 0% and 300% strain are nearly identical, implying that the effect of strain on electrochemical performance is negligible [87].

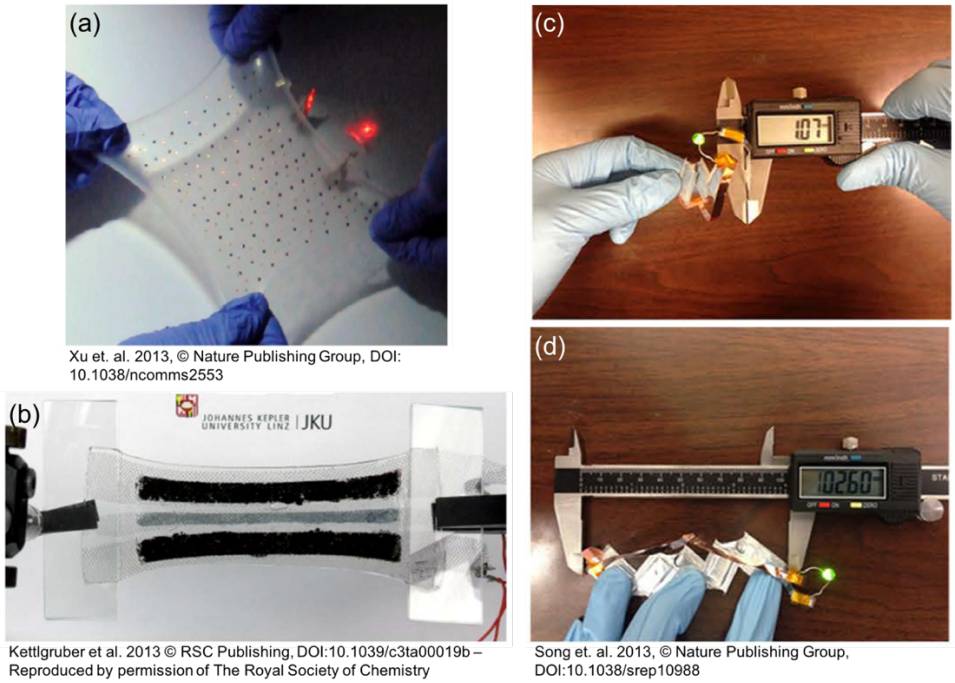

Xu et. al. 2013, © Nature Publishing Group, DOI: 10.1038/ncomms2553

Kettlgruber et al. 2013 © RSC Publishing, DOI:10.1039/c3ta00019b – Reproduced by permission of The Royal Society of Chemistry

Song et. al. 2013, © Nature Publishing Group, DOI:10.1038/srep10988

Figure 1.12 Photographs of stretchable batteries developed by (a) Xu et al., [87] (b) Kettlgruber et al., [92] and (c,d) Song et al. [93]

Similarly, Kettlgruber et al., developed a stretchable alkaline battery in 2013, depicted in **Figure 1.12b**. Manganese dioxide and zinc were made into electrode pastes. The pastes were spread over an elastomer substrate is different sections to prevent shorting. Finally, an electrolyte gel was spread over the electrode rows to facilitate ion transport. The normalized capacity vs. cycle profiles of the battery vary minimally at different strains [92]. However, the battery developed by Xu et al., and the battery developed by Kettlgruber et al., both experience rapid capacity fade, likely caused by the inability to ensure an air-tight seal by the encapsulating materials.

Song et al., took a slightly different approach in building their stretchable battery. Their battery design is inspired by the Japanese art of kirigami and combines cutting and folding the battery into patterns that are expandable. **Figure 1.12c** and **d** demonstrate how these batteries "stretch". This battery was repeatedly cycled at its most compact and most stretched states. Results show that the capacity and coulombic efficiency are negligibly affected by stretching [93].

1.5 Overview of this Dissertation

The main goal of this doctoral research is to investigate the fundamental relationship between mechanical tensile strain and ion conductivity in solid polymer electrolyte used in lithium ion battery. The specific polymer studied is a commonly used solid electrolyte, namely, polyethylene oxide (PEO). Furthermore, the effects of tensile strain on the electrochemical performance of a sliding stretchable battery based on the stretchable solid PEO electrolyte were experimentally evaluated.

In addition to providing scientific insights into strain- ion conductivity coupling in polymer electrolytes, the results of this study can lead to a more effective design and development of a fully stretchable Li-ion battery in near future.

This thesis is divided into five chapters with three primary research chapters. Chapter 1 provides a brief introduction to lithium ion batteries and their electrolytes, challenges faced, published research progress, and an overview of the work presented in this dissertation. Chapter 2 is a fundamental study investigating the effect of tensile strain on the mechanical and electrochemical properties of solid PEO electrolyte using an innovative, *in situ* impedance spectroscopy technique in order to determine the feasibility of incorporating solid PEO into a stretchable lithium ion battery. Chapter 3 is an optimization study aimed to develop a solid PEO electrolyte with optimal mechanical and electrochemical properties through blending high and low molecular weight PEO. Furthermore, nanofillers are introduced into the molecular weight blended electrolytes and the mechano-electrochemical properties of the unfilled and nanocomposite polymers are compared. Chapter 4 tests the optimized molecular weight blended PEO electrolyte, determined in Chapter 3, in a stretchable lithium ion battery with a sliding electrode design and the effect of electrolyte strain on battery performance is investigated. Chapter 5 summarizes the conclusions drawn from the presented work and provides suggestions for future and continued work in the successful design and development of a fully stretchable lithium ion battery.

Chapter 2: *In Situ* Study of Strain-Dependent Ion Conductivity of Stretchable Polyethylene Oxide Electrolyte

2.1 Overview

There is a growing interest in developing stretchable lithium ion batteries for various deformable applications including medical implants and wearable electronic devices. Solid polymers are ideal electrolyte candidates for such applications for their mechanical and chemical stability. The feasibility of implementing solid polymer electrolytes into fully stretchable batteries is explored as this work elucidates the relationship between tensile deformation and ion conductivity of solid polyethylene oxide (PEO) electrolyte through an *in situ* study. Mechanical and electrochemical testing supported by polarization light microscopy (PLM) reveal critical insights into the microstructural changes of strained PEO and its potential effects on ion conductivity.

2.2 Introduction

Advancements in mobile technologies have driven the demand for small, thin, and flexible energy storage devices [9,49,89]. The constant evolution of electronic devices has sparked a growing interest in developing stretchable lithium ion batteries to be compatible with irregularly shaped and stretchable applications, including medical implants, textiles, and stretchable electronics [87,90-92]. To date, majority of the published research aimed to developing stretchable batteries is

focused on creating stretchable electrodes [90-92]. This study focusses on the potential use of solid polymer electrolytes (SPEs) in a fully stretchable battery.

Conventional lithium ion batteries use organic liquid electrolytes for their superior ion conductivity at room temperature. However, the poor chemical and mechanical stabilities of these electrolytes make them unfit for use in deformable device applications [79]. In contrast, SPEs display superior mechanical and chemical stability, but cannot achieve comparable ion conductivities at room temperature [34,62,81,83,86]. Methods for enhancing the ion conductivity of SPEs, including plasticization or using low molecular weight polymers, are often at the sacrifice of mechanical strength. Alternatively, using nanofillers [34,58,62,64,81,94] or polymer blending [40,51,57,60,66,95-97] has shown to enhance ion conductivity while maintaining mechanical stability.

It is widely agreed upon that the ion conductivity of polymer electrolytes arises mainly from the amorphous phase of the polymer host. Lithium ions are transported across the electrolyte membrane via the thermally driven motion of the polymer chain segments [98]. The ion conductivity of polyethylene oxide (PEO) based electrolytes, one of the most extensively studied class of polymer electrolytes, is generally governed by the complex interplay of ion migration along the helical chains of the PEO and its chain segmental motions [60].

Golodnitsky et al. [50,73-75,99-103], previously studied the effect of tensile strain on ion conductivity of hot-pressed PEO and reported that stretching caused a 3-40 fold ion conductivity enhancement in the stretching axis (in-plane) [101-103], but a

decline in conductivity in the perpendicular axis (through-plane). They attributed this behavior to polymer chain stiffening, PEO helices alignment, and suppression of ion hopping along chains [102].

The present work investigates the effect of tensile deformation on the ion conductivity of thin-film 600k molecular weight (Mw) PEO/$LiClO_4$ electrolyte samples via *in situ* impedance spectroscopy (**Figure 2.2**). Contrary to previous studies, the current work demonstrates ion conductivity enhancement with axial stretching in both in-plane and through-plane directions. This enhancement behavior is believed to stem from the mechanically forced disentanglement of polymer chains in the amorphous region of the semi-crystalline polymer, resulting in less encumbered ion transport across the electrolyte membrane.

2.3 Methods

2.3.1 Polymer Electrolyte Fabrication

Thin-film solid polyethylene oxide (PEO) electrolyte is prepared in our laboratory using a solution-casting method. The amounts of PEO (Aldrich), the polymer, and lithium perchlorate ($LiClO_4$) (99.99%, Aldrich), the salt, used in the electrolyte are determined based on a 16:1 ratio of oxygen to lithium. Typically, 2g of PEO and 0.3g of $LiClO_4$ are dispersed in anhydrous acetonitrile (99.9%, Sigma-Aldrich) and stirred at room temperature for 24 hours. The mixture of electrolyte solution is then dried at 50 ^{o}C under a slight vacuum for a 24 hours, creating a polymer film approximately 200 - 300 μm thick. Finally, the electrolyte films are

transferred to the argon-filled VAC glove box where they continue to dry at room temperature for a minimum of 48 hours prior to use to ensure the removal of any residual acetonitrile solvent. When not in use, all electrolyte films are stored in the glove box.

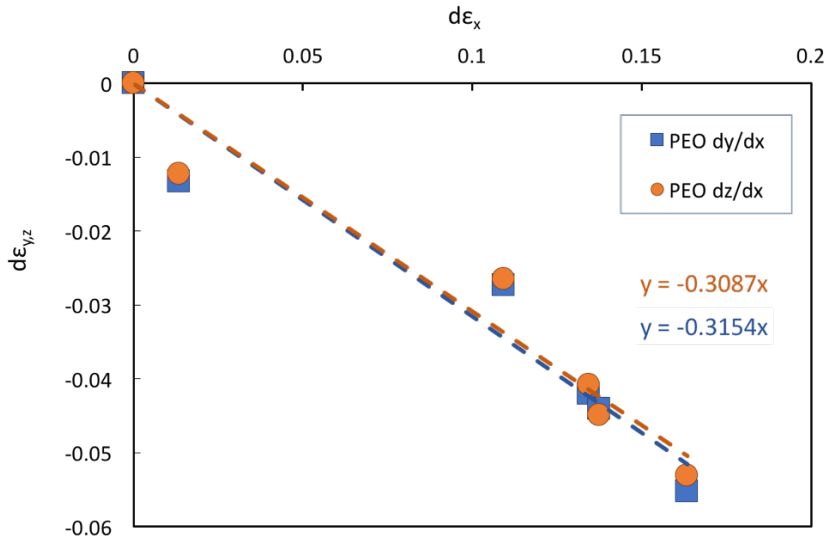

Figure 2.1 Plot of 600,000 Mw PEO Poisson's ratio

Mechanical testing of the polymer electrolyte films was conducted outside of the glove box at ambient room conditions. The thin-film polymer electrolyte samples were loaded into a MARK-10 ESM301L motorized test stand and strained at 0.5, 3.5, and 35 mm/min to investigate the effect of strain rate on tensile stress-strain curve of the viscoelastic material. Stress-strain cyclic tests were conducted on the PEO electrolyte film for 6 load/unload cycles to observe hysteresis effects. Furthermore, Poisson's ratio ($\nu = 0.3$) of the PEO membrane was experimentally determined and plotted in **Figure 2.1**.

2.3.2 Mechanical and Impedance Test Procedures

For the in situ impedance measurements, the electrolyte membrane was stretched at a strain rate of 3.5mm/min. Through-plane and in-plane *in situ* complex impedance spectra [104,105] of the solid polymer were obtained in the frequency range of 10MHz-1Hz using an Autolab multichannel potentiostat fitted with an FRA module for conducting electrochemical impedance spectroscopy (EIS) measurements.

2.3.3 In Situ Impedance Spectroscopy Setup

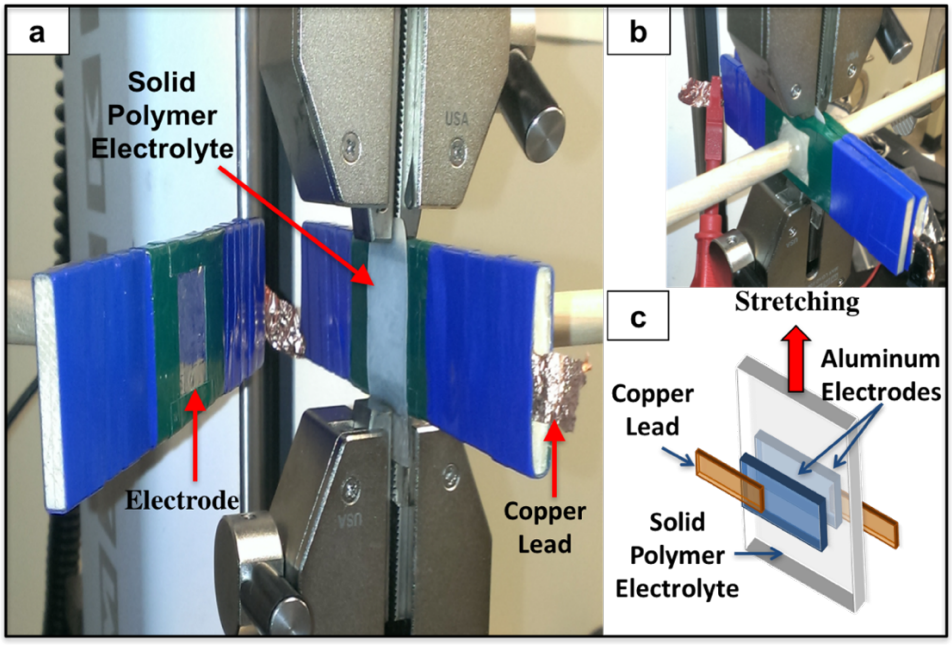

Figure 2.2 *In situ* impedance spectroscopy setup during tensile stress-strain testing. (a) Electrode is in open position, (b) closed electrodes, (c) schematics of the experimental components [86]

A layer of aluminum foil was attached to two wooden columns using a double-sided adhesive. Electrical insulating tape was used to mark off two identically sized squares and the exposed aluminum foil area acted as the electrodes.

The two wooden columns, held in place using ring stands, were placed on either side of the sample such that the exposed aluminum surfaces were in contact with the polymer electrolyte, as seen in **Figure 2.2**.

Plastic pins were then placed across the wooden columns and used to minimize the contact resistance between the polymer and the electrodes. Finally, the copper leads were connected to the Autolab potentiostat for impedance spectroscopy. The Nyquist plots from impedance spectroscopy of the polymer electrolyte film were obtained as the polymer was stretched in approximately 0.5mm increments.

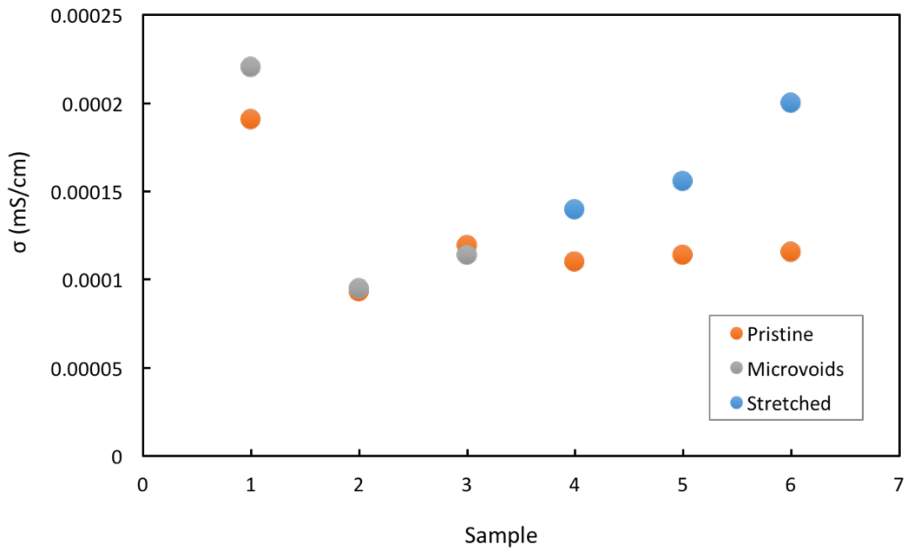

Figure 2.3 Comparison of the effects of micro voids and stretching on ion conductivity [86]

In situ impedance spectroscopy tests were conducted both at ambient and dry conditions. Furthermore, the effect of variation in the ratio of the electrode to electrolyte areas during the tensile deformation of the polymer electrolyte was investigated. The established baseline measurements for micro-void formation

(**Figure 2.3**) and room condition and area variation (**Figure 2.4**) were considered during the calculation of the ion conductivity of stretched polymer in order to precisely isolate the effect of tensile deformation on the ion conductivity of PEO/$LiClO_4$ film.

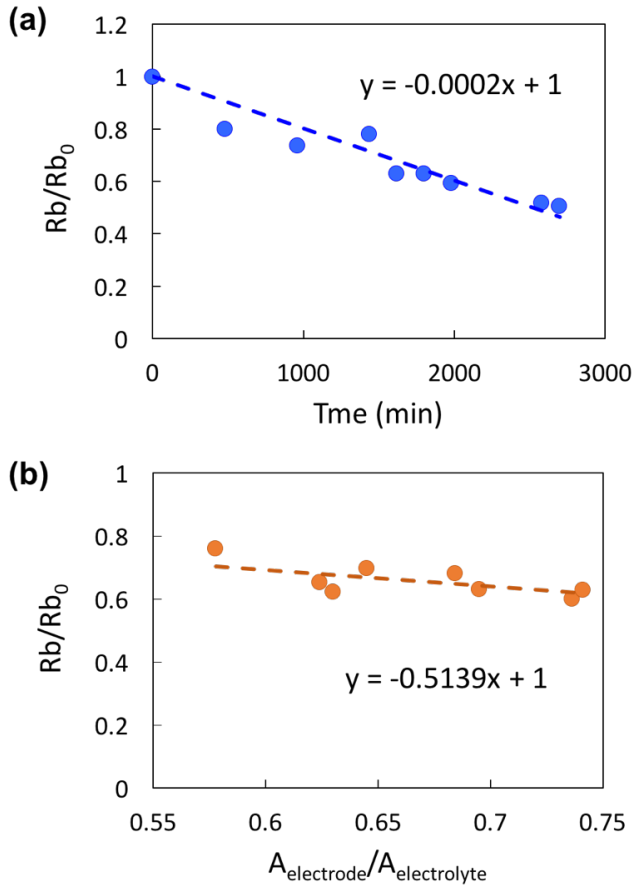

Figure 2.4 Effect of (a) moisture and (b) electrode to electrolyte area on bulk PEO resistivity [86]

2.3.4 Polarized Light Microscopy

Polarized light microscopy (PLM) was used to qualitatively observe the effect of tensile strain on the polymer electrolyte at the molecular level. PLM uses polarized light to illuminate the sample and provides greater contrast in microscope

images. For this study, PLM was used to observe and compare the degree of amorphicity in stretched and unstretched PEO samples.

2.3.5 Thermogravimetric Analysis (TGA)

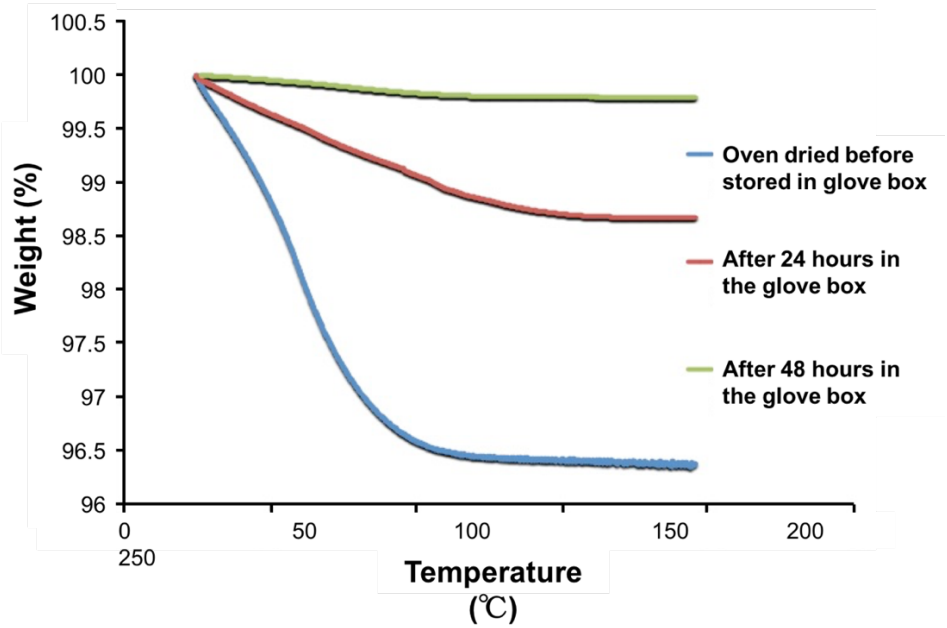

Figure 2.5 Thermogravimetric analysis (TGA) of PEO electrolyte at different drying times [86]

Thermogravimetric analysis (TGA) desorption test was performed using TA Instruments TGA from 25 °C to 200 °C to verify the drying process of the PEO electrolyte films. The TGA of PEO electrolyte at various drying times is depicted in **Figure 2.5.** TGA absorption test at room temperature (**Figure 2.6)** was performed to quantify the moisture content in PEO absorbed over time when exposed to the ambient environment.

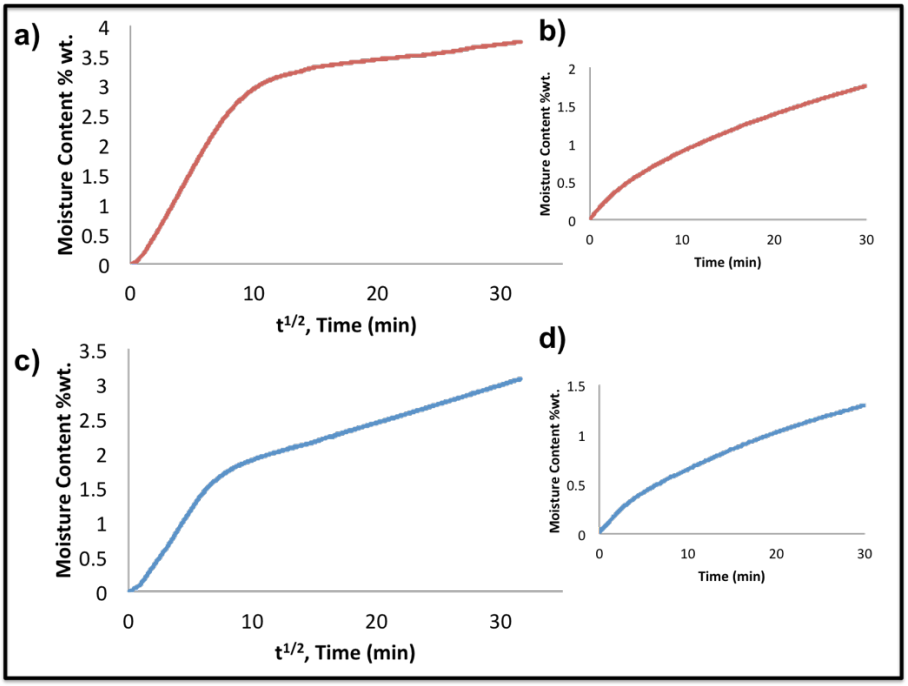

Figure 2.6 TGA at room temperature showing moisture absorption over time for (a,b) 600,000 Mw PEO and (c,d) 400,000 Mw PEO [86]

2.4 Experimental Results and Discussion

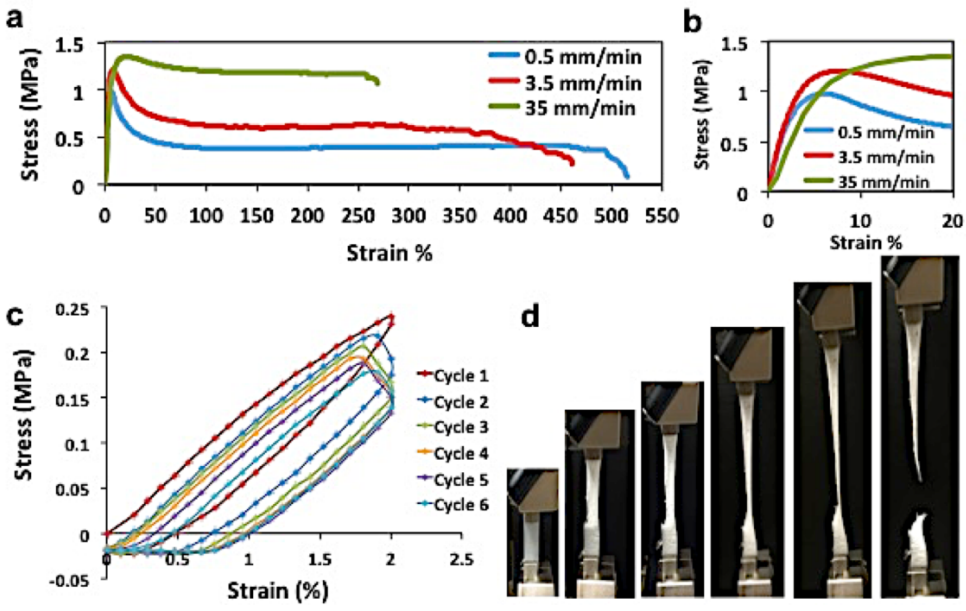

Figure 2.7 Tensile stress-strain behavior of PEO (a) at various strain rates (b) magnified curve below 20% strain, (c) stress-strain hysteresis effect, and (c) photos of PEO under tensile deformation [86]

Figure 2.2 shows the experimental setup used for the tensile displacement of stretchable polymer electrolyte subjected to simultaneous, through-plane impedance spectroscopy. **Figures 2.7a** and **2.7b** depict the representative stress-strain plots for solid PEO film at different strain rates (0.5, 3.5, and 35 mm/min) at 25°C. The average yield strength, ultimate tensile strength, and poison's ratio are also reported in **Table 2.1**.

Table 2.1 Mechanical properties of thin-film 600,000 Mw PEO/$LiClO_4$ [86]

PEO		Elastic Modulus (MPa)	Yield Strength (MPa)	UTS (MPa)	Poisson's Ratio
Temperature (℃)	Strain Rate (mm/min)				
18	3.5	17.99	0.81	1.26	0.23
25	0.5	39.5	0.74	1.10	0.24
	3.5	39.7	0.83	1.20	0.24
	35	20.9	0.91	1.35	0.24

If the behavior of a specimen is predominantly elastic in nature, the stresses are generally governed by forces carried within the amorphous and crystalline phase structures as well as viscous forces [106]. Semi-crystalline PEO exhibits a small elastic range, less than a 5% strain, at room temperature. This is expected as PEO is known to have a high degree of crystallinity (i.e. 60%) at room temperature, thus causing a relatively low ion conductivity at room conditions. For a specimen that exhibits tensile necking, a maximum stress occurs indicating the onset of yielding, which is accompanied by a drop in stress in the engineering stress-strain curve. Void nucleation and growth occurs at yielding, which can be confirmed visually by the observed stress whitening. The degree of void nucleation and growth is dependent

on whether or not particles are in contact with the void surfaces, which constrains the void [107].

Observed in the tensile behavior of the PEO specimen, shown in **Figure 2.7c**, is that the unload path differs from the load path, forming a hysteresis loop that could thermodynamically result in heat generation especially at high cycles [108-110]. Upon tensile reloading of the specimen in subsequent cycles, a noticeable drop in stress is observed at fixed strain. This is a feature of the viscoelasticity of the semi crystalline polymer and indicative of a type of mechanical damage [111]. Further cyclic loading shows a monotonic change in stress with cyclic loading which appears to approach an asymptotic value [112].

Figures 2.8a and **2.8b** show the through-plane Nyquist plots for one sample of PEO stretched from 0 cm to 0.4 cm in 3D and 2D representations, respectively. The through-plane (z-axis) ion conductivity, σ_z of the electrolyte samples can be calculated using **Equation 2.1**

$$\sigma_z = \frac{d}{R_b A}, \tag{2.1}$$

where d is the thickness of the electrolyte sample, R_b is the bulk resistance and A is the surface area of the electrolyte in contact with the electrode. The bulk resistance of the electrolyte can be estimated as the real impedance where the high frequency semi-circle and low frequency line intersect on the Nyquist plot. More accurately, electrolyte bulk resistance is determined from fitting of the equivalent electrochemical circuit to the Nyquist data (**Figure 2.8a**, inset).

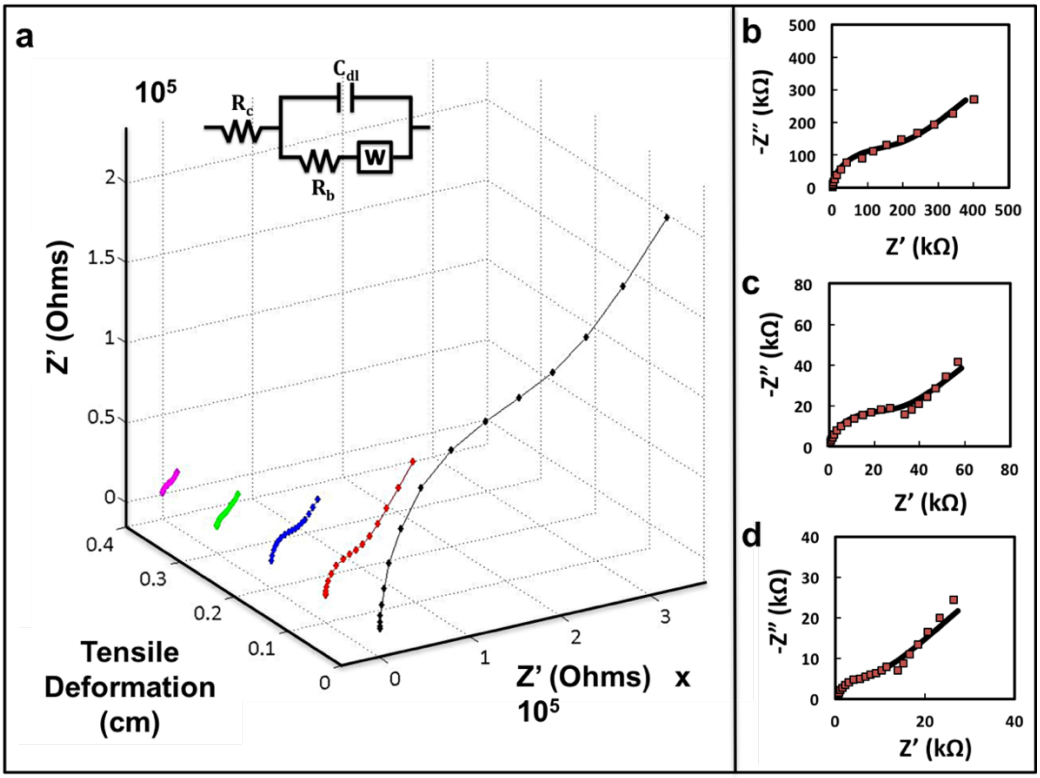

Figure 2.8 (a) Fitted Nyquist plots for PEO stretched from 0 to 0.4 cm; equivalent circuit fit (inset), Nyquist plots with equivalent circuit fit curves at (b) 0 cm, (c) 0.2 cm, and (d) 0.4 cm deformation [86]

The through-plane ion conductivity is the typical conductivity used when characterizing an electrolyte for battery use because of the configuration of the cell where the electrolyte is sandwiched between the two electrodes. In this study, however, the in-plane (y-axis) conductivity was also determined in order to better understand the effect of axial strain on ion conduction through PEO. The in-plane ion conductivity, σ_{xy} can be calculated using **Equation 2.2**

$$\sigma_{xy} = \frac{L}{R_b W t}, \tag{2.2}$$

where L is the distance between the electrodes, W is the width of the sample and t is the sample thickness.

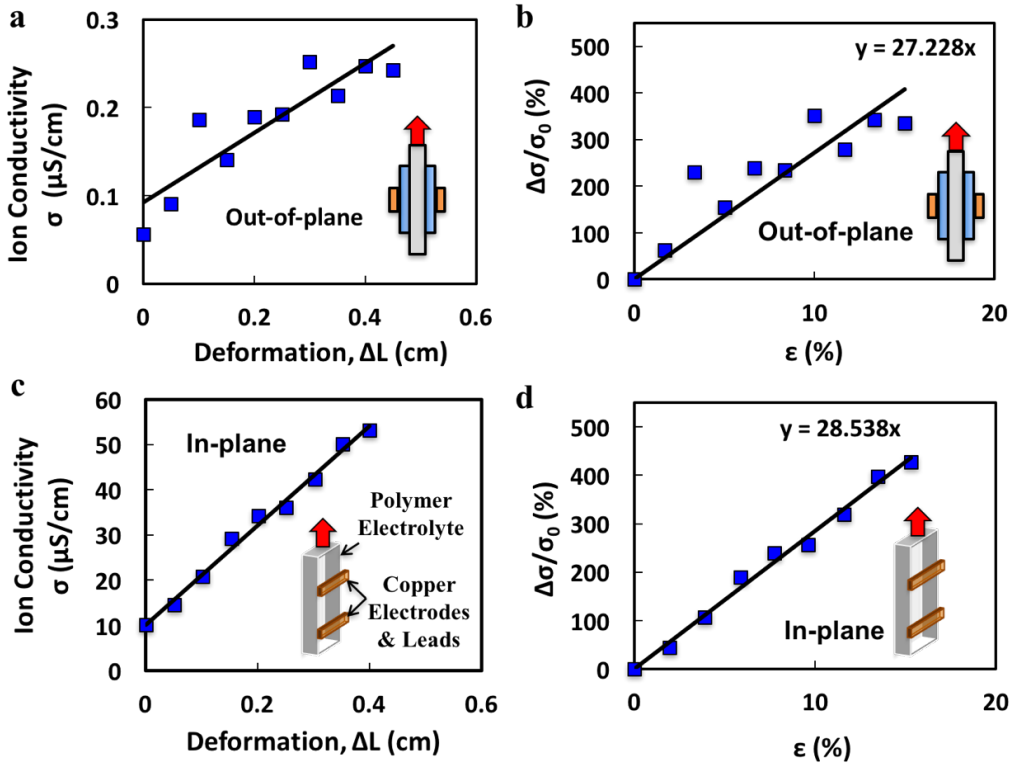

Figure 2.9 (a,c) Ion conductivity vs. deformation in through and in-plane directions, respectively. (b,d) Conductivity enhancement vs. strain in through and in-plane directions, respectively. [86]

Analysis of the data shows a clear effect of tensile deformation due to axial loading on ion conductivity in the PEO/Li salt polymer electrolyte, as seen in **Figure 2.9**. The observed through-plane ion conductivity of unstretched PEO/ $LiClO_4$ sample, depicted in **Figure 2.9a** and **Table 2.2**, is $5.6x10^{-8}$ $S.cm^{-1}$ measured at about 18°C. This value corresponds well to other published values for 600,000 M_w PEO [102,113,114]. The unstretched in-plane ion conductivity at the same temperature, in **Figure 2.9c**, was observed to be 10^{-6}, two orders of magnitude greater than that of the through-plane configuration. This phenomenon has been observed previously in several polymers and can be attributed to the order and orientation of polymer grains in the thin-film electrolyte [61,102,115]. At a slightly higher temperature of 25 °C,

both in-plane and through-plane ion conductivities increase as expected due to the thermally induced increase in both ion mobility and polymer segmental motion which can facilitate ion hopping between the coordinate sites on the polymer chains.

Table 2.2 Out-of-Plane and In-Plane ionic conductivity of unstretched 600,000 Mw PEO/$LiClO_4$ [86]

Temperature (℃)	Ion Conductivity (S/cm)	
	Through-plane	In-plane
18	5.6×10^{-8}	1.0×10^{-6}
25	1.5×10^{-7}	4.6×10^{-5}

Figure 2.9a expresses the average ion conductivity versus tensile deformation distance and **Figure 2.9b** depicts the average normalized ion conductivity of PEO with respect to strain for the through-plane configuration. **Figures 2.9c-d** show the same information for the in-plane configuration. Both conductivity directions show a similar and steady ion conductivity growth during axial deformation, achieving an approximate 4-fold increase in ion conductivity at a 15% strain.

Since the mechanical deformation and impedance spectroscopy of the polymer films were mainly performed in the ambient environment, further experiments were conducted to evaluate the potential effects of ambient moisture on ion conductivity during tensile deformation. **Figure 2.3a** shows the bulk resistance of an unstretched PEO film exposed to the ambient environment and **Figure 2.6** depicts the percent weight of absorbed moisture over time. For short periods of time, comparable to the testing times in this study (i.e. about 15 minutes),

the results show that small amount of absorbed moisture has a negligible direct effect on the ion conductivity of unstretched PEO (**Figure 2.3a**).

Figure 2.10 compares the percent change in ion conductivity with respect to the axial strain for 600,000 Mw PEO samples both inside and outside of the dry glove box. The results demonstrate that the ion conductivity of the PEO increases with strain in both ambient and dry environments. However, the ion conductivity of the polymer electrolyte appears to increase at a slower rate in the dry environment. This indicates that plasticization coupled with mechanical deformation of PEO electrolyte can lead to higher enhancement of ion conductivity. Tests on both plasticized and unplasticized PEO samples can offer insight into the potential electrochemical performance of PEO in a flexible or stretchable battery. Because most SPEs have relatively lower ion conductivities at room temperature, it is common practice to plasticize the solid polymer electrolyte inside a battery in order to enhance its ion conductivity and interface contact with the electrodes.

The increasing trend in ion conductivity with axial tensile strain infers that the structural changes induced in the polymer electrolyte results in altered and improved ion conduction. We hypothesize that the stretching and aligning of the amorphous polymer chains decreases the degree of tortuosity in the polymer, allowing for faster, and less obstructed ion transport through the polymer electrolyte.

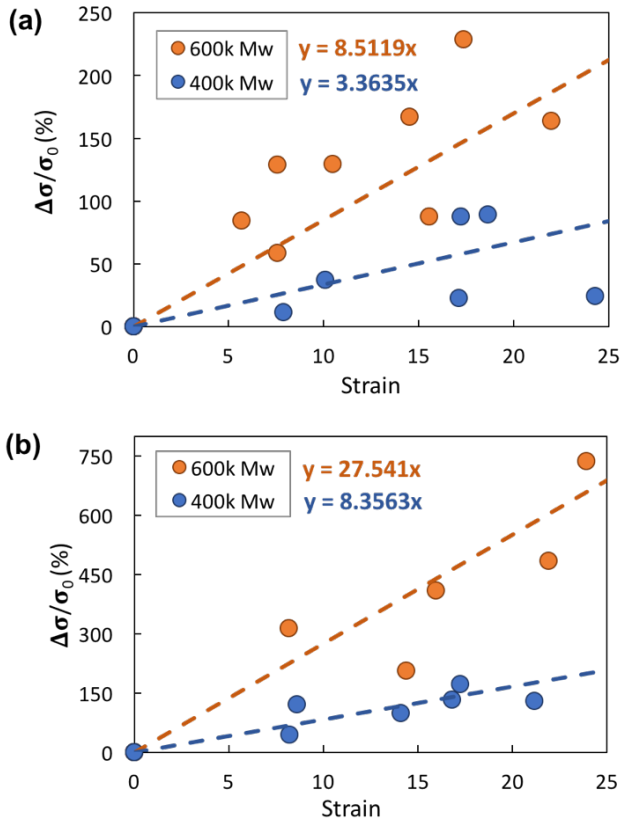

Figure 2.10 Percent ion conductivity enhancement vs. axial strain in wet and dry environments for (a) 600k Mw PEO and (b) 400k Mw PEO [86]

To better understand the mechanisms behind the ion conductivity enhancement in PEO, we shall delve deeper into the microstructural characteristics of the polymer. Semi-crystalline PEO consist of two phases, a crystalline phase and an amorphous phase as depicted in **Figure 2.11**. In the crystalline phase, the ordered polymer chains align themselves in regions called crystallites. The amorphous phase of semi-crystalline PEO is generally present on the edges of the crystallites where the polymer chains are arranged in disordered, twisted and entangled conformations. The polymer chains in the amorphous regions predominantly tie one crystallite to another.

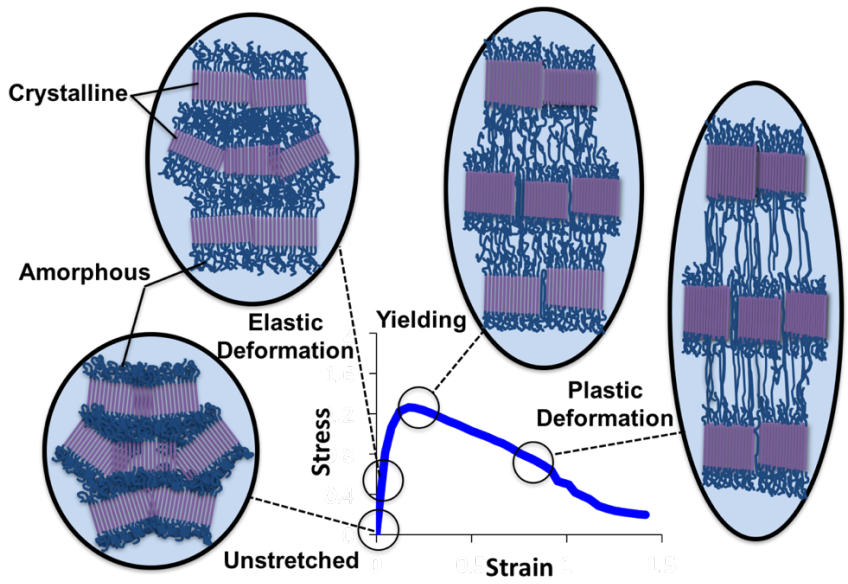

Figure 2.11 Depiction of semi-crystalline polymer microstructure at various stages of tensile deformation [86]

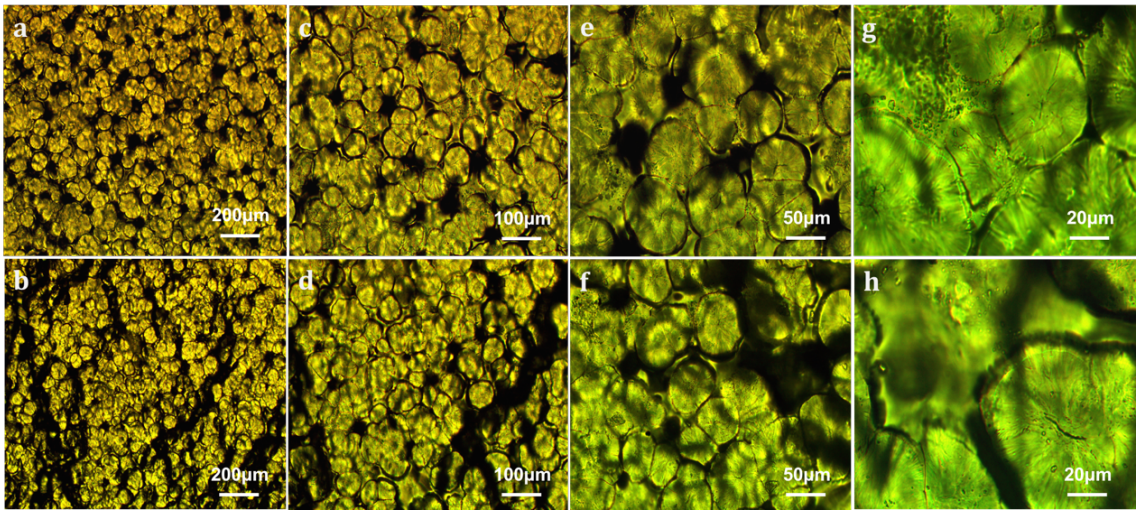

Figure 2.12 Polarization Light Microscopy (PLM) images of unstretched (top) and stretched (bottom) PEO. (a-b) 50x magnification, (c-d) 100x, (e-f) 200x, and (g-h) 500x magnifications. [86]

To provide further insight into the effect of stretching on the molecular structure of the polymer electrolyte, polarization light microscopy (PLM) was performed on the PEO electrolyte samples. The PLM images in **Figure 2.12** are of

the PEO/$LiClO_4$ film in unstretched and stretched states at various magnifications. The images show a contrast of color where dark regions suggest amorphous phases and light regions indicate crystalline phases. The dark rings around the crystallites, visible at 100x-500x magnifications, are the entangled polymer chains tying one crystallite to its neighbor. The growth of dark regions, as the polymer transitions from the unstretched to stretched state, confirms a growth or extension of the amorphous regions as the chains stretch and disentangle.

The evolution of the microstructure of semi crystalline PEO is illustrated in **Figure 2.11**. For small applied stress and strain, the polymer chains elongate elastically. The amorphous regions grow and transmit loading that is carried by the crystalline grains, and crystallite blocks slide and begin to orient into the direction of applied load [106]. The mechanical response of the crystalline region is elastic while the response of the amorphous region possesses both elastic and viscoelastic behavior. Beyond the critical stress and the onset of yielding, favorably oriented crystalline grains subject to excessive shear begin to experience an increase in dislocations accompanied by transformation into fibrils [106,116]. With the increase in dislocations, void nucleation, growth and necking occur. As the process progresses the force carried dominantly by the crystallites shift to the amorphous regions until the chains are fully disentangled. These effects are believed to drive the nature of the stress-strain curves shown in **Figure 2.7**.

The strength of the polymer mainly depends upon the degree of crystallinity, temperature, and density among others. In polyethylene oxide, the amorphous

regions of the polymer are the most mechanically compliant part of the microstructure during applied tensile loading. The nature of inelastic deformation, or plasticity, in semi-crystalline polymers can be preceded by cavitation in the amorphous regions; however, the driving mechanisms depend on the strength of the crystallite grains and their susceptibility to shear deformation, void nucleation and growth [111,117-123].

It is widely agreed upon that ion transport in SPEs is heavily dependent on the chain segmental motions of the polymer host. Increased motion creates more coordination sites that lithium ions can use to migrate from one electrode to the other. This is why it has long been believed that order and crystallinity adversely affects the ion conductivity of polymer electrolytes. Additionally, the conformation of amorphous polymer chains plays an important role in ion conductivity. The conformation and strength of polymer chains are dependent on several factors including the solvent used as well as the drying time [116,120,123-126]. Collapsed chain conformations are inefficient ion conductors because they trap and create a more tortuous migration path for lithium ions. Minimizing tortuosity by disentangling and opening up polymer chains via stretching can enhance ion conduction by increasing the chain's ability to move, thus creating more coordination sites [64,66].

Table 2.3 Comparison of through-plane and in-plane CSDICE values [86]

Conductivity Direction	CSDICE (χ)
Through-plane	27.2
In-plane	28.5

Table 2.3 compares the slopes of the linear trends of the normalized conductivity versus strain data, which have been labeled as the coefficient of strain-dependent ion conduction enhancement (CSDICE). The CSDICE values for the through-plane and in-plane conduction are very similar, exhibiting values of 27.2 and 28.5, respectively. This suggests that ion conductivity growth in thin-film PEO with respect to the tensile strain is mainly an isotropic property, as growth in the through-plane and in-plane directions are found to be nearly the same. This further supports the theory that the conformations and entanglement of polymer chains unravel, which occurs in both the axial and lateral directions of the semi-crystalline polymer under tension.

Equation 2.3 is an empirical model for ion conductivity in stretched polyethylene oxide

$$\frac{\Delta\sigma}{\sigma_0} = \chi\varepsilon, \tag{2.3}$$

where σ_0 is the ion conductivity of the sample at an unstretched state, χ refers to the CSDICE (presented in **Table 2.3**), and ε is the strain. Based on the results obtained in this study, χ is an isotropic property, and therefore, **Equation 2.3** can be valid for modeling both the through-plane and in-plane conductivities of PEO under axial strain.

Future studies should focus on the effect of material factors on strain-dependent ion conductivity, including chemically induced conformations of the polymer chains (i.e. polymer type, blends, etc.), filler types and dimensions, and salt

chemistry, and provide further insight to the underlying phenomena through specialized experiments or numerical simulations. The effects of mechanical stress-strain cycling on the ion conductivity of polymer electrolyte should also be investigated in future work.

2.5 Continuum Model

A continuum model of the strain-dependent ion conductivity enhancement behavior of the PEO electrolyte has been developed that can explain the experimental observations[127]. The model couples mass diffusion and displacement equations in an effort to better understand the impacts of strain on ion diffusion, and will be discussed in detail in this section.

2.5.1 Mass Balance

Consider a small solid control volume, Pt, within a body, Ω, with an initial concentration of lithium ions. The mass of the lithium ions within the control value can be expressed as

$$\int_{P_t} N\rho dV = \int_{P_t} CdV, \tag{2.4}$$

where N, ρ, and C are the species mass fraction, density of the solid, and species concentration, respectively with V being the region volume [127,128]. The concentration of the ionic species can be reinterpreted in terms of species flux [43,127]. The net rate of lithium ions transported into the control volume is given as

$$-\int_{\partial P_t} \boldsymbol{\phi} \cdot \mathbf{n} dA + \int_{P_t} h dV, \tag{2.5}$$

where φ is the species flux, n is an outward normal unit vector indicating flux direction, A is the area of the flux control surface, and h is the ion supply for the body. Mass balance can then be rewritten as

$$\int_{P_t} \rho \dot{N} dV = \int_{P_t} \dot{C} dV = -\int_{\partial P_t} \boldsymbol{\phi} \cdot \mathbf{n} dA + \int_{P_t} h dV. \tag{2.6}$$

By applying the divergence theorem,

$$\int_{P_t} \left(\dot{C} + div\boldsymbol{\phi} - h\right) dV = 0 \tag{2.7}$$

and

$$\dot{C} + div\boldsymbol{\phi} - h = 0, \tag{2.8}$$

Equation 2.8, can be used to model mass diffusion through the control volume. For convenience, it can be assumed that there is no ion generation and set h=0 [43,127].

It is appropriate to use Fick's laws when mass diffusion is the product of a concentration gradient. However, in the case of a stretched electrolyte, mass diffusion is also affected by stress gradients [20,22,43,127-129]. Thus, the total ion flux must also account for ion diffusion through both concentration and stress gradients,

$$\phi_{Total} = -D_C \nabla \mathrm{C} - D_\sigma \nabla \sigma = Cv, \tag{2.9}$$

where D is the diffusion coefficient, σ is applied stress, and v is the velocity of the diffusing species. Total flux can be further expanded when the chemical potential gradient, which is the driving force behind ion diffusion, is considered, producing

$$\phi_{Total} = -M\mathrm{C}\nabla\mu$$

and (2.10)

$$D_C\nabla\mathrm{C}+D_\sigma\nabla\sigma = M\mathrm{C}\nabla\mu,$$

where μ is chemical potential and M is the mobility tensor of the lithium ion species [20,22,43,127,128,130].

2.5.2 Elasticity

Modeling elasticity can be derived using the first law of thermodynamics,

$$Q = W_0 - \frac{dE}{dt}, \quad (2.11)$$

where Q is the heat dissipation, W is external work or power, and E is the stored internal energy of the system. Assuming the body acts elastically, such that Q=0, equation 2.1l can be simplified to

$$W_0 = \frac{dE}{dt}. \quad (2.12)$$

Assuming all work on the body is purely mechanical, the external power supply can only be due to surface or body forces. The work equation can then be rewritten as

$$W = \int_{\partial P_t} \boldsymbol{t^e} \cdot \mathbf{v} dA - \int_{P_t} \mathbf{b_0} \cdot \mathbf{v} dV, \quad (2.13)$$

where $\mathbf{t^e}$ is the external traction applied to the control surface, $\mathbf{b_0}$ is the external body force applied to the body, and **v** denotes the velocity vector [127]. By using the definition of infinitesimal strain [18,20,21,106,127,128,131]

$$\varepsilon = \frac{1}{2}(\nabla \mathbf{u} + \nabla \mathbf{u}^T), \tag{2.14}$$

where ε is strain and $\mathbf{u}$ denotes the displacement vector, the stored internal energy of the system can be expressed as

$$E = \int_{P_t} U(\nabla \mathbf{u}) dV\ , \tag{2.15}$$

where U is the volumetric internal energy of the body [127]. Work, as defined in Equation 2.11, can be rewritten as

$$W = \int_{\partial P_t} \boldsymbol{t^e} \cdot \mathbf{v} dA - \int_{P_t} \mathbf{b_0} \cdot \mathbf{v} dV = \int_{P_t} \frac{\partial U}{\partial \varepsilon} \cdot \dot{\varepsilon} dV. \tag{2.16}$$

Applying the divergence theorem and rearranging terms yields

$$\int_{\partial P_t} \left[\mathbf{t^e} - \frac{\partial U}{\partial \varepsilon}\mathbf{n}\right] \cdot \mathbf{v} dA + \int_{P_t} \left[\mathrm{div}\left(\frac{\partial U}{\partial \varepsilon}\right) + \mathbf{b_0}\right] \cdot \mathbf{v} dV = 0. \tag{2.17}$$

Substituting stress for the change in internal energy with strain results in the governing equation for elasticity [20-22,106,127,128,130-133],

$$\begin{aligned} &\mathrm{div}\boldsymbol{\sigma} + \mathbf{b_0} = 0 \\ &\boldsymbol{\sigma}\mathbf{n} = \mathbf{t^e}\ . \end{aligned} \tag{2.18}$$

2.5.3 Coupling Diffusion and Elasticity

To couple diffusion and elasticity, the energy due to diffusion must be considered in the total energy term [43,127,128],

$$E = \int_{P_t} U(\nabla \mathbf{u}, \mathrm{C}) dV\ . \tag{2.19}$$

Work exerted onto the body can then be expressed as

$$W = \int_{\partial P_t} \boldsymbol{t^e} \cdot \mathbf{v} dA - \int_{\partial P_t} \mu \boldsymbol{\phi} \cdot \mathbf{n} dA + \int_{P_t} \mu h dV \ . \tag{2.20}$$

By expanding the flux term, which is the chemical contribution to energy, the work equation can be written as

$$W = \int_{\partial P_t} \boldsymbol{t^e} \cdot \mathbf{v} dA - \int_{P_t} \left(\boldsymbol{\phi} \cdot \nabla \mu - \mu \dot{C} \right) dV \ . \tag{2.21}$$

Total heat dissipation is then defined as [127]

$$\begin{aligned} Q = \int_{P_t} \left(\mu - \frac{\partial}{\partial C} \right) \dot{C} dV + \int_{P_t} \left[\mathrm{div} \left(\frac{\partial U}{\partial \varepsilon} \right) + \mathbf{b}_0 \right] \cdot \\ \mathbf{v} dV - \int_{P_t} (\boldsymbol{\phi} \cdot \nabla \mu) dV + \int_{\partial P_t} \left[\mathbf{t^e} - \frac{\partial U}{\partial \varepsilon} \mathbf{n} \right] \cdot \mathbf{v} dA \ . \end{aligned} \tag{2.22}$$

So as not to violate the second law of thermodynamics, Q must be greater than or equal to zero. To do so, flux is defined as

$$\boldsymbol{\phi} = -\gamma \nabla \mu \ , \tag{2.23}$$

where γ is diffusivity and is a value greater than or equal to zero, to ensure that

$$\boldsymbol{\phi} \cdot \nabla \mu \leq 0. \tag{2.24}$$

The governing equations required for coupling diffusion and elasticity are as follows [127]:

$$\varepsilon = \frac{1}{2} \left(\nabla \mathbf{u} + \nabla \mathbf{u}^T \right) , \tag{2.25}$$

$$\sigma = \left(\frac{\partial U}{\partial \varepsilon} \right)_C \ ,$$

$$\mu = \left(\frac{\partial U}{\partial \mathrm{C}} \right)_\varepsilon ,$$

$$div\boldsymbol{\sigma} = 0,$$

$$\boldsymbol{\sigma} \cdot \mathbf{n} = \mathbf{t^e},$$

$$\boldsymbol{\phi} = -\gamma \nabla \mu \, ,$$

$$\dot{C} + \mathrm{div}\boldsymbol{\phi} - \mathrm{h} = 0.$$

2.5.4 Small Deformation Development

Assuming elastic behavior within the solid polymer electrolyte, the internal energy of the electrolyte at low strains can be defined using strain and lithium ion concentration with respect to initial concentration. The volumetric internal energy,

$$U = \frac{1}{2}\nabla \mathrm{u} \cdot \mathbb{C} \nabla \mathrm{u} + \alpha(C - C_o)Tr(\nabla u) + RTC\left[ln\left(\frac{C}{C_o}\right) - 1\right], \tag{2.26}$$

is the sum of the energy contributions due to elastic strain, diffusional strain, and concentration change, where $\mathbb{C}$ is the fourth order stiffness tensor, and RT is simply the product of temperature and Universal Gas constant [20,127]. Taking the volumetric internal energy differential, the governing equations in Equation 2.23 are reduced to

$$dU = \left.\frac{\partial U}{\partial \nabla u}\right|_C d\nabla u + \left.\frac{\partial U}{\partial C}\right|_\varepsilon dC \, ,$$

$$\mu = \left.\frac{\partial U}{\partial C}\right|_F = \alpha \nabla \cdot u + RTln\left(\frac{C}{C_o}\right), \tag{2.27}$$

$$\sigma = \left.\frac{\partial U}{\partial \nabla u}\right|_C = \mathbb{C}\nabla u + \alpha(C - C_o)\mathbf{I}.$$

Using these equations, the ion flux in terms of displacement and concentration is expressed as [127]

$$D_C \nabla \mathrm{C} + D_\sigma \nabla[\mathbb{C}\nabla u + \alpha(C - C_o)\mathbf{I}] = MC\nabla\left[\alpha\nabla \cdot u + RTln\left(\frac{C}{C_o}\right)\right]. \quad (2.28)$$

2.6 Conclusions

In summary, *in situ* impedance spectroscopy during the tensile deformation of stretchable PEO/$LiClO_4$ electrolyte film shows increase in both the through-plane and in-plane ion conductivities of the polymer electrolyte. This phenomenon is mainly attributed to the disentanglement of polymer chains during tensile deformation that consequently, reduce the degree of tortuosity in the path of ion transport. The increase in ion conductivity of PEO follows a linear trend, and the slopes of the normalized conductivity vs. strain data termed as the CSDICE, for both the through-plane and in-plane experiments exhibit values of 27.2 and 28.5, respectively. The similarity of these values suggests that the CSDICE is an isotropic property of the polymer electrolyte, describing the physical interactions of polymer chains during stretching. Furthermore, a continuum model of the strain-dependent ion conductivity enhancement behavior was developed. This model adequately models the mechanical and electrochemical coupling behavior of the PEO-based electrolyte seen in the *in situ* experiment.

Chapter 3: The Investigation of Molecular Weight Blends in Pure and Nanocomposite Polyethylene Oxide Electrolytes

3.1 Overview

The effect of differential molecular weight (Mw) blending on the mechanical and electrochemical properties of thin-film, solid polyethylene oxide (PEO) is explored. The mixture of large and small molecular weight PEO affects polymer chain packing, thus affecting both mechanical strength and ion conductivity of the electrolyte films. As the low molecular weight PEO content increases, the electrolyte loses its mechanical integrity, but shows enhanced ion conductivity. Furthermore, graphene oxide (GO) nanofillers is introduced to the molecular weight blended electrolytes and the mechanical and electrochemical properties of the nanofilled composites are studied. A 1%wt. GO content noticeably enhances the mechanical properties of the molecular weight blends, but does not uniformly enhance ion conductivity. The effect of graphene oxide on electrochemical performance appears to dominate over the effect molecular weight blending.

3.2 Introduction

In recent years, there has been a growing interest in developing flexible and stretchable energy storage devices to accommodate a wide range of applications including medical implants, textiles, and stretchable electronics [80-87,89-92,134-141]. The

superior attributes of lithium ion batteries, including energy density and efficiency, make them an attractive energy storage option for integration with such technologies. However, lithium ion batteries have recently been under severe scrutiny due to the growing media coverage of battery fires. Battery fires are the result of thermal runaway events, often caused by manufacturing defects or improper handling of the battery. Conventional batteries using an organic liquid electrolyte are more likely to undergo thermal runaway due to the mechanical, electrochemical, and thermal instability of the electrolyte, making them an irresponsibly unsafe electrolyte material for flexible, stretchable, and deformable batteries [28,32,33,35]. Furthermore, batteries using liquid electrolytes are often associated with the inherent disadvantages of leakage, dendrite growth, and solid electrolyte interphase.

Solid polymer electrolytes (SPEs) are a safer and more attractive electrolyte alternative for flexible and stretchable lithium ion batteries, offering the necessary mechanical, thermal, and electrochemical stability required for such applications [38,60,81,86,142]. In addition, SPEs offer the benefits of dendrite growth suppression and thin film manufacturability. Unfortunately, SPEs are known to have very low ion conductivities compared to other lithium-ion battery electrolytes.

Many methods for enhancing the ion conductivity of SPEs have been proposed including the use of nanoparticles [34,58,62,64,81] or creating polymer blends [55,57,68]. Furthermore, the molecular weight of the polymer matrix also affects the electrolyte's conductivity. For example, the ion conductivities of 600k and 100k

molecular weight poly(ethylene oxide) (PEO) have been reported to be 10^{-8} S cm^{-1} and 10^{-7} S cm^{-1}, respectively [34,86]. This order of magnitude variance in ion conductivity stems from the difference in the degree of amorphicity of the different molecular weights, with 100k PEO having a higher degree of amorphicity. Additionally, amorphicity of the polymer chains affects the mechanical strength and electrochemical properties of the polymer electrolyte material, with higher degrees of amorphicity corresponding to decreased material strength and enhanced electrochemical performance.

Many of the polymer blend studies for battery electrolyte applications involve cross-linking two or more different polymer materials [55,57,63,65,68,79,98,143]. There are limited studies investigating the effect of differential molecular weight PEO blends on polymer properties, most of which are related to drug delivery systems [96,144,145]. The present study takes the novel approach of investigating the effect of differential low (100k) and high (600k) molecular weight blends on the mechanical and electrochemical performance of PEO to determine an optimal balance of electrolyte properties for flexible and stretchable lithium ion batteries.

Previously, it was found that the addition of GO fillers could effectively improve both ion conductivity and mechanical properties of 100k Mw solid PEO electrolyte [34,62,81]. Here, we investigate how the inclusion of graphene oxide (GO) nanosheets to the PEO molecular weight blends affects the polymers' mechanical and electrochemical properties, and we can determine the influence of varying molecular weight on the degree of effectiveness of GO fillers.

3.3 Methods

3.3.1 PEO 100k/600k Mw Electrolyte Fabrication

The thin-film poly(ethylene oxide) electrolyte samples were prepared using a solution-cast method. 2g of PEO (Aldrich), with varying contents of 100k and 600k molecular weights, and 0.3g of $LiClO_4$ (99.99%, Aldrich) were dispersed in anhydrous acetonitrile (99.9%, Sigma-Aldrich). The electrolyte solutions were stirred at room temperature for 24 hours, then dried at 50°C under a slight vacuum. The films were then transferred to the argon-filled glove box and allowed to dry for an additional 96 hours prior to use in an effort to ensure solvent removal from the films.

3.3.2 PEO/GO 100k/600k Mw Nanocomposite

It is a common practice to introduce to solid polymer electrolytes as a means for enhancing ion conductivity, as previously discussed in section *1.3.4*. The nanofiller material used in this research is a graphene oxide (GO) powder (Graphene Supermarket) with layer dimensions of approximately 0.5-5 microns in length and width and 1.1±0.2nm in thickness. Based on previous work, all nanocomposite electrolyte films used in this study contain a 1% wt. GO [34].

3.3.3 Thermogravimetric Analysis (TGA)

A thermogravimetric analysis (TGA) desorption test was performed using a TA Instruments TGA from 25 ^{o}C to 750 ^{o}C. The decomposition temperature of the samples containing 0%wt., 25%wt., and 100%wt. 100k PEO, and 100%wt. 100k PEO

+ 1% GO were compared. The thermogram seen in **Figure 4.1** shows that the 25% blend has the highest decomposition temperature while also showing that the decomposition temperatures of the GO filled and unfilled polymer samples are similar, suggesting that a 1% GO content does not significantly impact the thermal properties of the material.

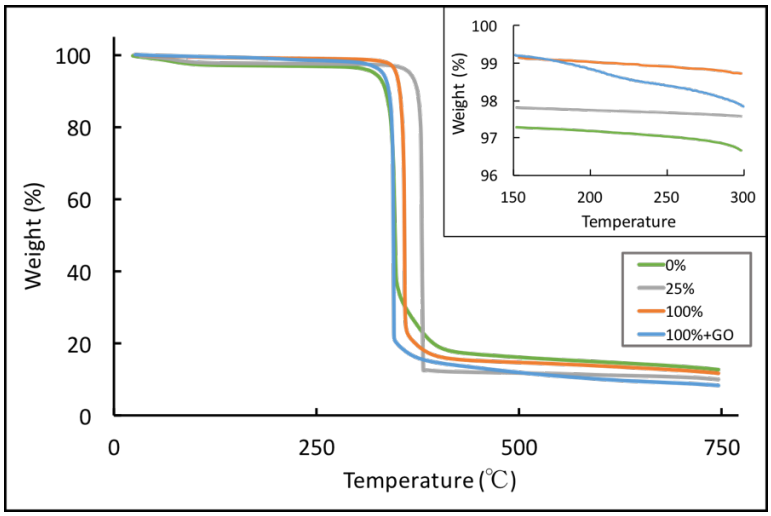

Figure 3.1 TGA of various molecular weight blend polymers comparing decomposition temperatures

3.3.4 Mechanical Testing

The molecular weight blend electrolyte samples were loaded into a MARK-10 ESM301L motorized test stand in ambient room conditions and strained at 10 mm/min. The yield strength, ultimate tensile strength, and Young's modulus were determined for each molecular weight blend.

3.3.5 Impedance Testing

The ion conductivities of the electrolyte films were calculated using the obtained bulk resistance values via electrochemical impedance spectroscopy. The

polymer samples were placed between two stainless steel electrodes connected to an Autolab multichannel potentiostat fitted with an FRA module. The bulk resistances of the samples were measured in the range of 1MHz-10Hz.

3.3.6 In Situ Impedance Spectroscopy Setup and Test Procedure

Figure 3.2 In situ ion conductivity set up

Figure 3.2 depicts the *in situ* impedance spectroscopy test setup. The polymer electrolyte sample was loaded into the MARK-10 ESM301L motorized test stand in ambient room conditions. Aluminum foil electrodes were placed on with either side of the electrolyte and clamped together using plastic pins in order to minimize the contact resistance between the electrode and the electrolyte. The aluminum foil electrodes were constructed in our lab by adhering a layer of

aluminum foil to wooden columns using a double-sided adhesive. Electrical tape was then used to mark off two identically sized aluminum foil rectangles. The exposed aluminum surfaces acted as the electrodes. Copper leads connected the aluminum foil electrodes to the Autolab potentiostat for impedance spectroscopy. The electrolyte samples were stretched in 0.5mm increments and impedance spectroscopy was performed at each increment in order to quantify the effect of strain on ion conductivity.

3.3.7 Differential Scanning Calorimetry

Generally, Differential Scanning Calorimetry (DSC) is used to detect phase transitions by measuring heat flow as a sample is heated and cooled. DSC is also commonly used to observe slighter physical changes including glass transition temperature (T_g), which is the temperature at which amorphous materials move from a brittle, glass-like state to a rubber-like state. For this research, DSC was also used to determine the %crystallinity and melting temperature of the polymer electrolyte materials.

3.3.8 Scanning Electron Microscopy

Scanning Electron Microscopy was employed to qualitatively observe the microstructural differences among the molecular weight PEO blend electrolyte samples. Additionally, SEM was used to observe how graphene oxide nanofillers affect the molecular weight blend polymers.

3.4 Results and Discussion

3.4.1 Differential Molecular Weight PEO Blends

As previously mentioned, solid polymer electrolytes offer enhanced safety and mechanical stability compared to their liquid counterparts. Thus, it is important to define their mechanical properties to assess their mechanical compatibility with flexible and stretchable batteries. The electrolyte films tested contain 0%, 12.5%, 25%, 37.5%, or 50%, by weight, 100k PEO with the remaining PEO content being 600k PEO. **Figure 3.3** plots the average elastic modulus, yield strength, ultimate tensile strength (UTS), and percent elongation of the PEO molecular weight blended electrolyte films.

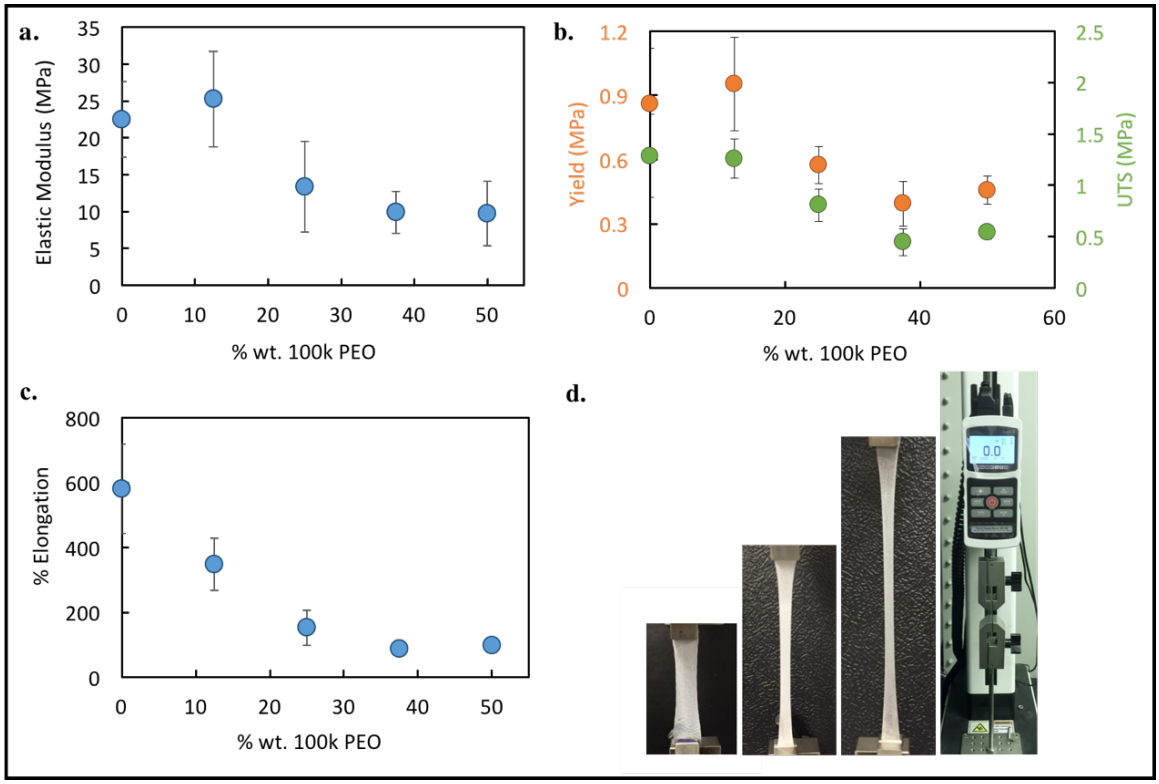

Figure 3.3 (a) Elastic modulus, (b) yield strength and ultimate tensile strength, (c) % elongation, and (d) photo images of a PEO sample subject to tensile deformation.

As expected, the strength of the molecular weight blends decreases with an increasing content of 100k PEO. This is because higher molecular weight polymers tend to be more mechanically stable because their longer molecular chains restrict chain mobility. Mechanical data was not obtained for polymer blends containing more than 50% 100k PEO because these polymers were too fragile and environmentally sensitive to be reliably and uniformly strained.

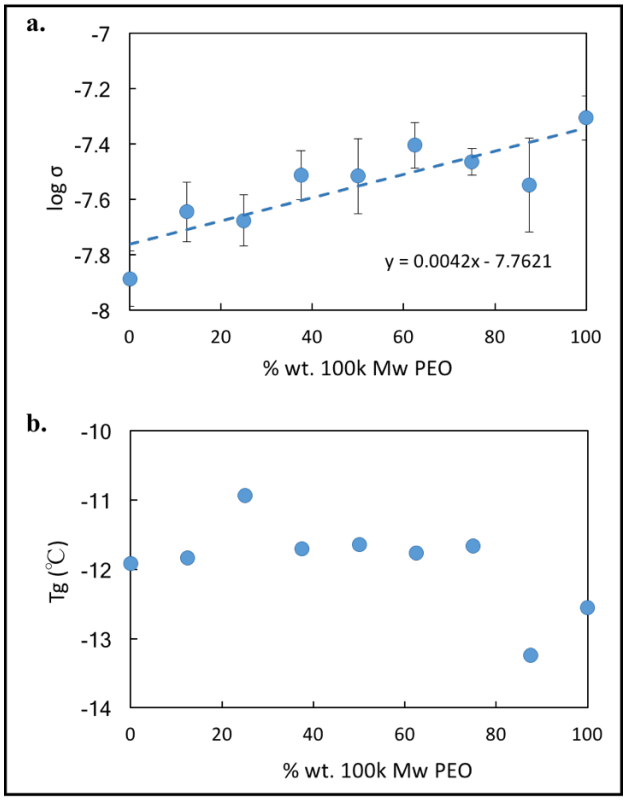

Figure 3.4 (a) Log scale ion conductivity and (b) glass transition temperature of PEO molecular weight blends

Mechanical strength and ion conductivity are inversely related in most electrolytes, including polymers. The material structure of the electrolyte dictates ease of ion transport, with liquids being the most effective medium. In polymer

electrolytes, lower molecular weight polymers exhibit higher conductivities due to shorter molecular chain lengths and increased chain motion [50,72,76,100-103,146,147], which is also the cause of their poor mechanical stability. The effect of molecular weight on ion conductivity is verified by the reported values of 10^{-8} S cm^{-1} and 10^{-7} S cm^{-1} for pure 600k Mw and 100k Mw PEO, respectively [34,86]. Thus, the ion conductivities for the molecular weight blended samples should increase with the % wt. of 100k PEO, as demonstrated in **Figure 3.4**.

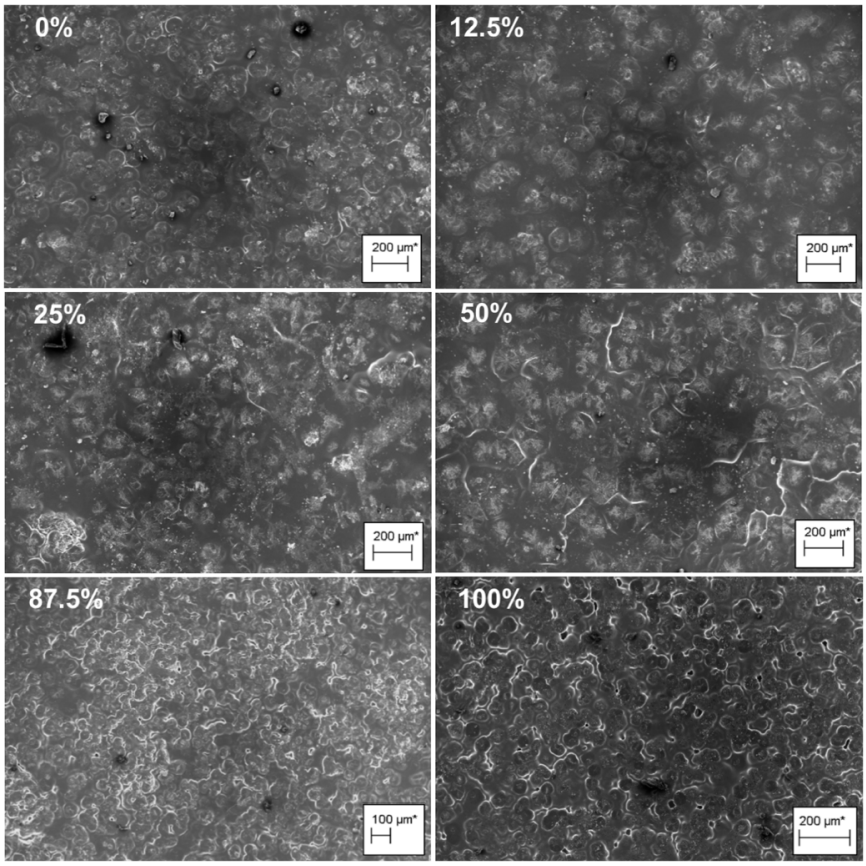

Figure 3.5 SEM images of PEO molecular weight mixtures

To further verify the ion conductivity data, a DSC analysis was performed to determine the glass transition temperatures (Tg) of the PEO blend samples. The

glass transition temperature corresponds to a material's degree of crystallinity with higher molecular weight polymers possessing higher glass transition temperatures due to the restricted motion of the long polymer chains. Similarly, lower molecular weight polymers often exhibit a lesser Tg due to the shorter molecular chains between the crosslinked points [147]. The DSC results, seen in **Figure 3.4b**, correlate well with the ion conductivity data and show an inverse trend with the 25% sample exhibiting the lowest glass transition temperature.

Scanning electron microscopy (SEM) was used to qualitatively evaluate the electrolyte structure. The images in **Figures 3.5** and **3.6** clearly demonstrates the effect of molecular weight on the electrolyte structure. **Figure 3.5** shows the changing ratio of large to small PEO crystals, which corresponds to the ratio of 600k Mw and 100k Mw PEO in the electrolyte films. The pure 600k Mw sample contains tightly packed polymer crystallites with clearly defined crystal edges, whereas the pure 100k Mw sample contains more loosely packed crystallites with no clearly defined edges. **Figure 3.6** provides close-up SEM images of the 0%, 25%, 50%, and 100% polymer films. These images more clearly show how molecular weight content affects polymer chain packing and ultimately, ion conductivity.

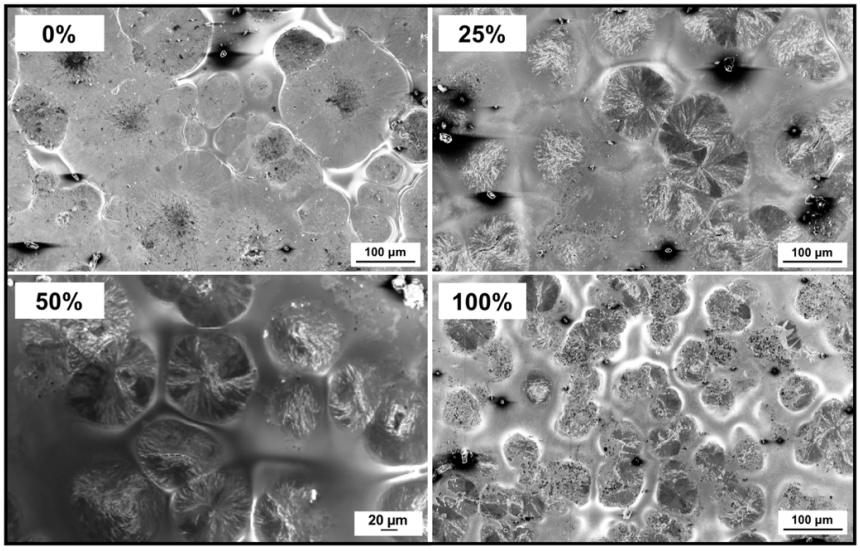

Figure 3.6 Close-up SEM images of the 0%, 25%, 50% and 100% PEO molecular weight blends.

3.4.2 Differential Molecular Weight Polymer Nanocomposite Blends

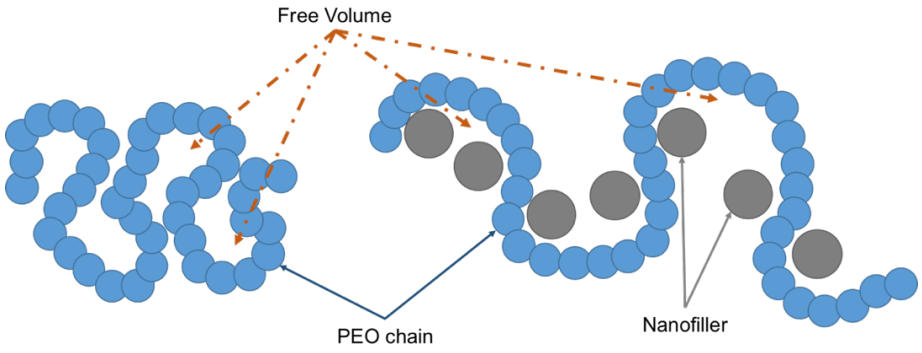

Figure 3.7 Schematic of unfilled (left) and filled PEO (right) depicting how nanofillers affect the polymer chain conformation

Introducing nanofillers to the polymer matrix has been shown to enhance ion conductivity of polymer electrolytes [34]. The positive role of nanofillers on electrochemical performance is believed to be a product of increased salt dissociation facilitated by high dielectric constant fillers, disentanglement of chain

conformations, and an increase in free volume of the polymer host, depicted in **Figure 3.7** [62].

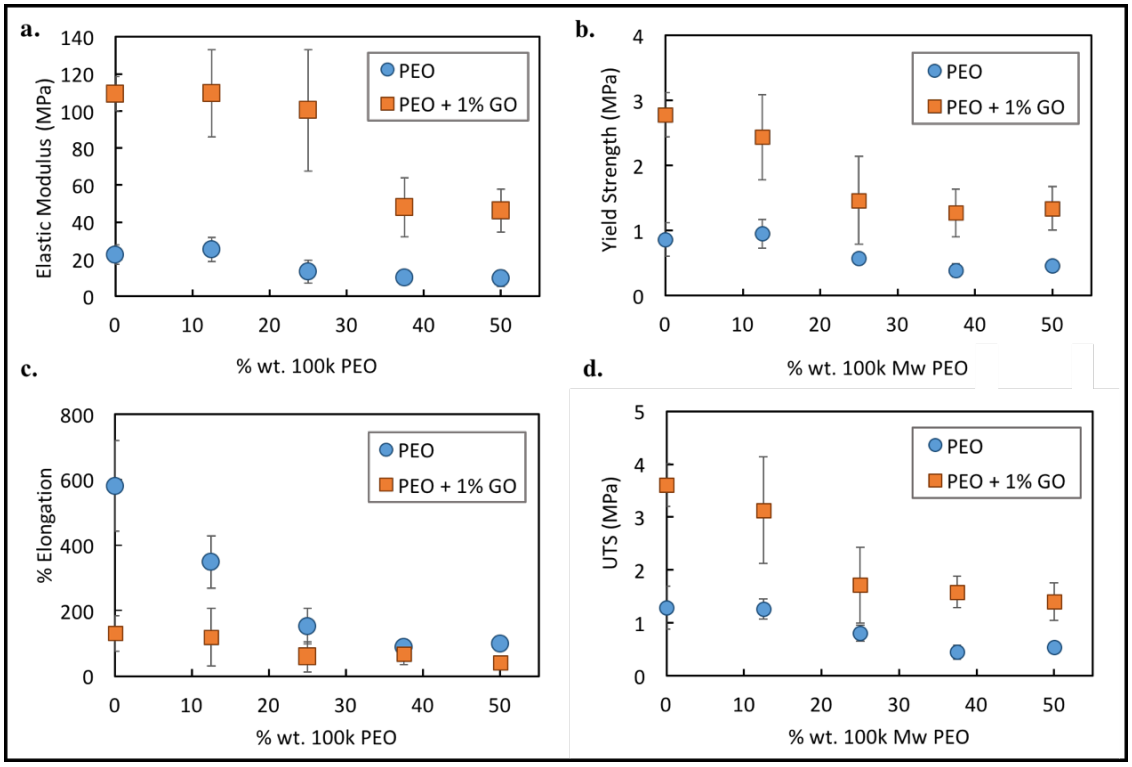

Figure 3.8 Comparison of (a) Elastic modulus, (b) yield strength, (c) % elongation, and (d) ultimate tensile strength of PEO molecular weight blends and PEO blends + 1% GO

The effect of graphene oxide (GO) nanoparticles on the mechanical and electrochemical properties of the molecular weight polymer blends was also investigated. The addition of nanoparticles to PEO changes the polymer matrix and consequently affects the electrolyte's properties, often causing an enhancement of both mechanical and electrochemical properties [34,64]. **Figure 3.8** compares the mechanical properties of the GO filled and unfilled PEO blends, showing a general enhancement of the elastic modulus, yield strength, and ultimate tensile strength in the nanocomposite blend samples. However, % elongation suffers suggesting that

the addition of graphene oxide causes the polymer blends to be more brittle. The mechanical properties of both the filled and unfilled PEO molecular weight polymer blends are summarized in **Table 3.1**.

Table 3.1 Comparison of mechanical properties of filled and unfilled PEO molecular weight blends.

% wt. 100k Mw PEO	Elastic Modulus (MPa)		Yield Strength (MPa)		UTS (MPa)		% Elongation	
	unfilled	+ 1% GO	unfilled	+ 1% GO	unfilled	+ 1% GO	unfilled	+ 1% GO
0	22.5	109	0.86	2.78	1.29	3.61	580	131
12.5	25.2	110	0.95	2.45	1.26	3.13	348	118
25	13.4	100	0.57	1.47	0.81	1.71	153	58.7
37.5	9.89	28.0	0.39	1.27	0.45	1.58	88.0	67.5
50	9.71	46.1	0.46	1.34	0.54	1.40	99.0	40.9

Figure 3.9a compares the ion conductivities of the GO filled and unfilled molecular weight blend samples. The effect of GO on ion conductivity increases with an increasing 100k Mw PEO content and is most pronounced in the pure 100k Mw PEO samples. While GO enhances the ion conductivity of all the molecular weight blends, GO appears to be most effective in opening up smaller entangled chain conformations, thus decreasing the degree of tortuosity in the path of ion transport. **Figures 3.9b** supports this ion conductivity trend by showing a decrease in glass transition temperature, with the GO filled PEO electrolytes showing a faster rate of change.

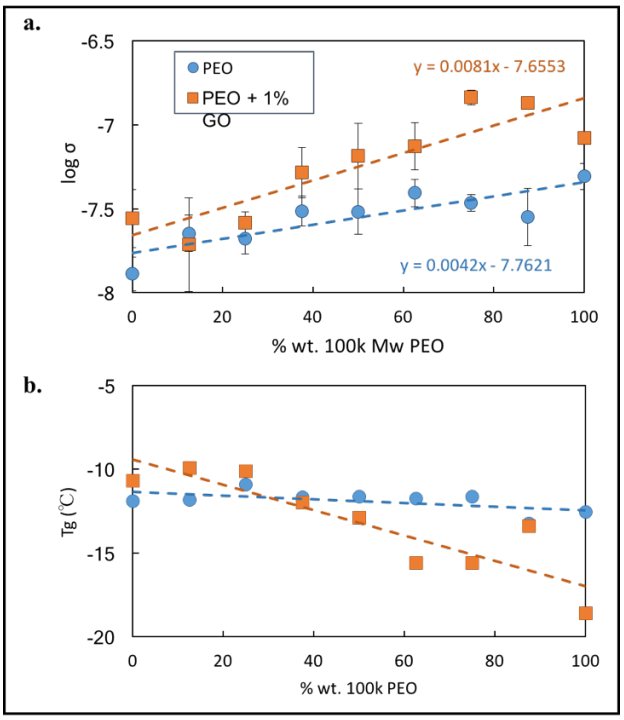

Figure 3.9 Comparison of (a) Log scale ion conductivity, (b) glass transition temperature

SEM images of GO filled and unfilled 100k Mw PEO electrolytes are compared in **Figure 3.10** to qualitatively observe the effect of on the electrolyte's molecular structure. **Table 3.2** summarizes the ion conductivity and DSC data for both the GO filled and unfilled PEO molecular weight blend electrolytes.

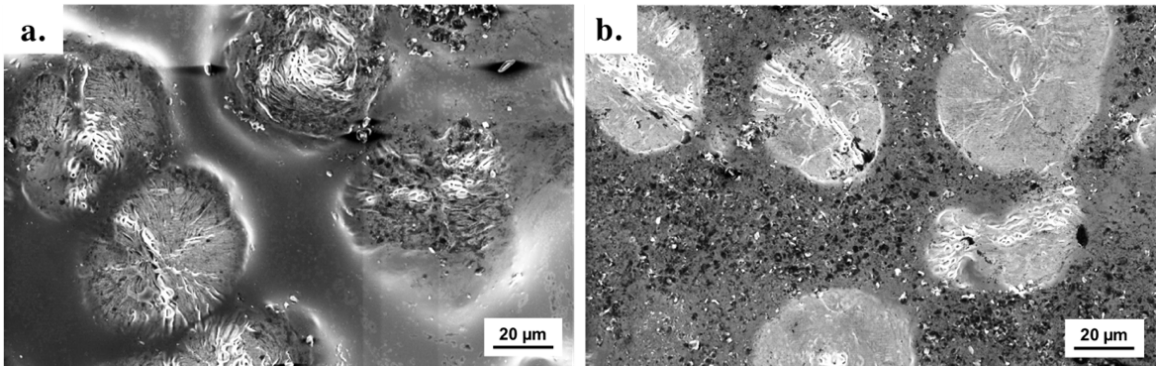

Figure 3.10 SEM images of (a) 100kMw PEO and (b) 100kMw PEO + 1% GO

Table 3.2 Average ion conductivity, glass transition temperature, % crystallinity, and melting temperature for all PEO molecular weight blends and PEO blends + 1% GO

% wt. 100k PEO	Log σ [S cm^{-1}]	T_g [℃]	X_c [%]	T_m [℃]
0	-8.2	-11.92	47.2	66.05
12.5	-7.5	-23.72	38.0	56.06
25	-7.3	-31.38	28.5	54.37
37.5	-7.4	-20.72	30.8	55.39
50	-7.5	-15.31	31.9	53.78
62.5	-7.7	-12.59	33.4	55.37
75	-7.7	-12.32	38.4	54.91
87.5	-7.5	-20.23	45.0	54
100	-7.2	-16.68	47.4	54.23
0 + 1% GO	-7.5	-10.7	17.8	57.29
12.5 + 1% GO	-7.6	-9.92	17.7	57.07
25 + 1% GO	-7.6	-10.13	12.2	55.93
37.5 + 1% GO	-7.1	-12	37.3	55.58
50 + 1% GO	-7.2	-12.91	34.4	55.65
62.5 + 1% GO	-7.0	-15.58	50.0	53.57
75 + 1% GO	-6.8	-15.59	55.4	54.8
87.5 + 1% GO	-6.9	-13.41	42.2	53.71
100 + 1% GO	-6.7	-18.6	51.4	54.82

The 25%wt. 100k Mw PEO blend was chosen for use in the stretchable lithium ion battery, described in Chapter 5, for its mechanical and electrochemical property balance. Although the GO filled samples exhibited enhanced mechanical strength and ion conductivity they also have small elastic strain regions. Comparing the filled and unfilled 25% blends, yielding occurred at a 1.5% strain in the GO filled samples versus a 4.3% strain in the unfilled samples.

3.4.3 Strain-Dependent Ion Conductivity

An in situ ion conductivity study was performed to investigate how strain affects ion conductivity in the 25% electrolyte. **Figure 3.11a** plots logarithmic ion

conductivity, showing an increase in conductivity as the samples are strained to 15%. **Figure 3.11b** depicts the normalized ion conductivity data with strain, where σ_0 is the unstrained conductivity. The slope of the linear trend, describing the rate of ion conductivity change with strain, is the coefficient of strain dependent ion conductivity enhancement (CSDICE). For the 25% blend, the CSDICE value is 28.453, similar to a previously reported value of 27.228 for pure 600k PEO [86]. The similarity in these CSDICE values is expected as the polymer host in the 25% blend consists mostly of 600k PEO.

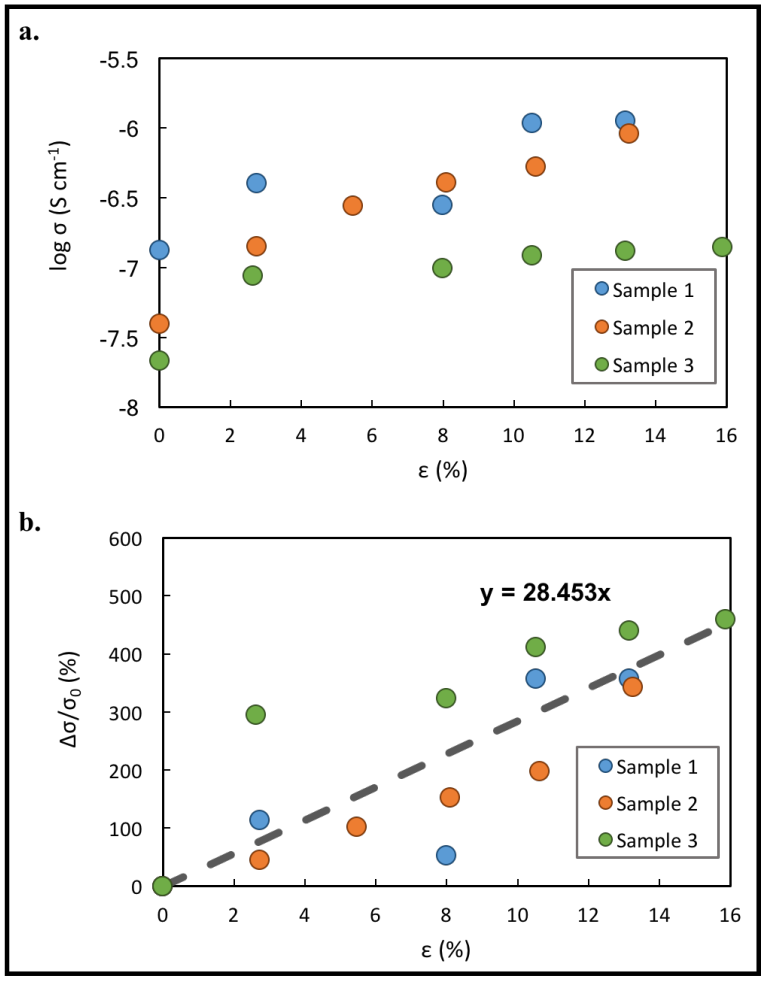

Figure 3.11 (a) logarithmic ion conductivity deformed 25% samples vs. tensile strain and (b) enhancement in ion conductivity vs. tensile strain

3.5 Conclusions

In summary, the mechanical and electrochemical behaviors of nanofilled and unfilled PEO molecular weight blended electrolytes, containing differential amounts of 100k and 600k PEO, were determined. The elastic modulus, yield strength, and ultimate tensile strength of the polymer blends steadily decreases with an increasing 100k PEO content. Adding 1%wt. GO nanoparticles enhances the mechanical strength of the polymer films, but also causes them to be brittle and negatively affects the elastic strain region of the electrolyte.

The ion conductivities of the filled and unfilled molecular weight blend electrolytes followed a linearly increasing trend with an increasing content of 100k Mw PEO. The effect of graphene oxide nanoparticles on ion conductivity enhancement is most pronounced in the pure 100k Mw PEO samples. This suggests that the ability to open up or disentangle chain conformations and enhance ease of ion transport across the electrolyte membrane is limited in high molecular weight polymer electrolytes. DSC data, including glass transition temperature and percent crystallinity, for all of the samples further confirmed the ion conductivity enhancement trends in the filled and unfilled PEO molecular weight blend electrolytes.

An *in situ* ion conductivity test was performed to observe the effect of strain on ion conductivity in the 25% electrolyte. The 25% unfilled sample was chosen for its balance of mechanical and electrochemical properties and its larger elastic strain region when compared to its 25% + 1% wt. GO counterpart. The *in situ* test results

reveal an increase in conductivity with strain and the material's CSDICE value is 28.453, which is similar to a previously reported value of 27.228 for a pure 600k PEO electrolyte film.

Chapter 4: Stretchable Lithium Ion Battery Displaying Enhanced Performance with Strain

4.1 Overview

Development of stretchable batteries is an emerging field in the energy storage space. A fully stretchable lithium ion battery, in which all components including the electrodes, electrolyte, and encapsulation are stretchable, has yet to be developed. Previous work has shown that solid polymer electrolytes are a viable stretchable battery electrolyte option. Kelly et al., demonstrated that ion conductivity of a PEO-based electrolyte increases linearly with tensile deformation. Here, solid polyethylene oxide is used to develop a stretchable lithium ion battery, using a sliding electrode design, and the effect of electrolyte strain on overall battery performance is investigated.

4.2 Introduction

There has been a heavy interest in using lithium ion batteries as energy storage devices for decades. This is because lithium ion batteries can achieve higher gravimetric energy densities compared to other commercially available battery chemistries, such as alkaline and nickel metal hydride. Being able to meet the mobile energy demands of electronic devices without requiring heavy and bulky batteries is critical for this day and age. Furthermore, the demand for flexible and

stretchable batteries will rise as technology becomes increasingly integrated into our daily lives.

The recent media coverage of Samsung battery fires due to thermal runaway have brought heavy attention to lithium ion battery safety for at least the fourth time in the past four years. Thermal runaway can be initiated through various mechanisms including external heating, mechanical trauma, and battery misuse. In many cases, shorting causes the battery temperature to rise until a critical temperature reached, at which the battery undergoes self-heating and ignites the flammable electrolyte. Further heating causes the conventional battery cathode (lithium cobalt oxide, LiCoO2) to ignite and catastrophic failure [28-35].

The inherent mechanical and thermal instability of organic liquid electrolytes make conventional lithium ion batteries an unsafe energy storage option for wearable, implantable, and deformable electronic devices. Methods for enhancing battery safety include liquid electrolyte additives or replacement. Recently, solid ceramic and polymer electrolytes have garnered great attention for their high thermal stability. Solid ceramics offer high ion conductivities, but are unsuitable for flexible and stretchable applications [31,32,41,59,148,149]. In contrast, solid polymer electrolytes pliable, but suffer from low ion conductivities.

Methods for enhancing the ion conductivity of solid polymer electrolytes include adding nanoparticles [3,29,34,56,62,81,142], polymer blending [40,57,60,95,96,115], and plasticization. All of these methods aim to enhance molecular chain mobility through creating more amorphicity within the polymer matrix. Unfortunately, the

best reported conductivity that was achieved is still two orders of magnitude less than the conductivity of liquid electrolytes. However, polymer electrolytes remain to be the best and safest electrolyte option for the next generation of flexible and stretchable lithium ion batteries.

While there is a substantial amount of work in developing flexible lithium ion batteries [9,49,81,89], work in stretchable batteries is an emerging field. In 2013, Xu et al., developed a stretchable battery consisting of individual cells electrically connected using spring-like wires [87]. The battery is capable of achieving strains upwards of 300%. Additionally, Xu et al., report a high initial area capacity of 1.1 mAh cm^{-2}. Unfortunately, the battery experiences rapid capacity fading over the first twenty cycles. In 2015, Song et al., created a kirigami inspired stretchable lithium ion battery [93]. Based on its folding design, the battery is able to stretch 150% and exhibits a stable capacity at both stretched and unstretched states up to 20 cycles. However, from cycles 20-100 at its fully stretched state, the battery experiences a 30% capacity drop.

The stretching mechanism of these batteries is based on design. The battery cells themselves are stationary while the electrical connections are free to deform. This study presents a fully stretchable lithium ion battery based on a sliding electrode design. The battery uses the 25%wt. 100k Mw PEO blend described in Chapter 3, containing a three to one ratio of 600k Mw to 100k Mw PEO, in and investigates the effect of tensile deformation on overall battery performance.

4.3 Methods

4.3.1 Stretchable Battery Fabrication

The battery is composed of two layered $LiFePO_4$ electrodes and two layered graphite electrodes separated by a thin film, PEO-based electrolyte, as seen in **Figure 4.1**. With this configuration, the electrodes slide, increasing the exposed electrode area, while the electrolyte stretches when the battery is strained. Each electrode measures 1cm in width and 2cm in length.

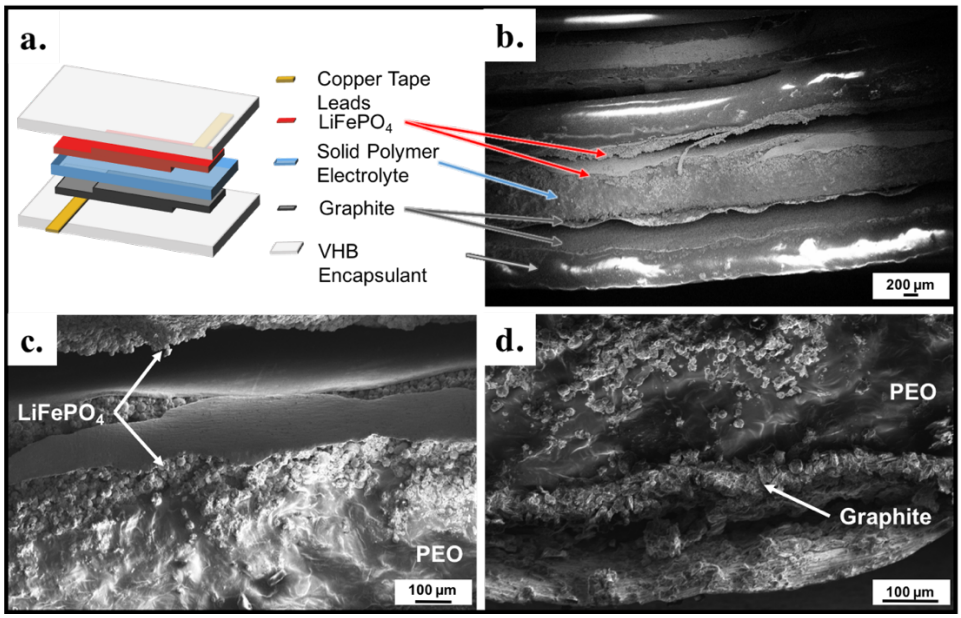

Figure 4.1 (a) Diagram of stretchable battery with (b, c, d) SEM images of the stretchable battery cross-section.

The battery contains a small amount of liquid electrolyte to enhance the electrode-electrolyte interface contact. The battery electrodes were soaked in liquid electrolyte and the amount of liquid absorbed made up 10% wt. of the battery electrolyte. The remaining liquid was removed from the electrode surfaces, making the electrodes appear dry.

Copper tape was used as electrical leads to connect the battery to the Autolab battery tester and the battery was encapsulated in a VHB double-sided adhesive manufactured by 3M. The encapsulated battery was then laminated twice using a standard a laminating machine. The heat and pressure applied during lamination further improves the electrode-electrolyte interface contact. Finally, the lamination plastic is removed from the battery and the battery is ready for use.

4.3.2 Battery Testing

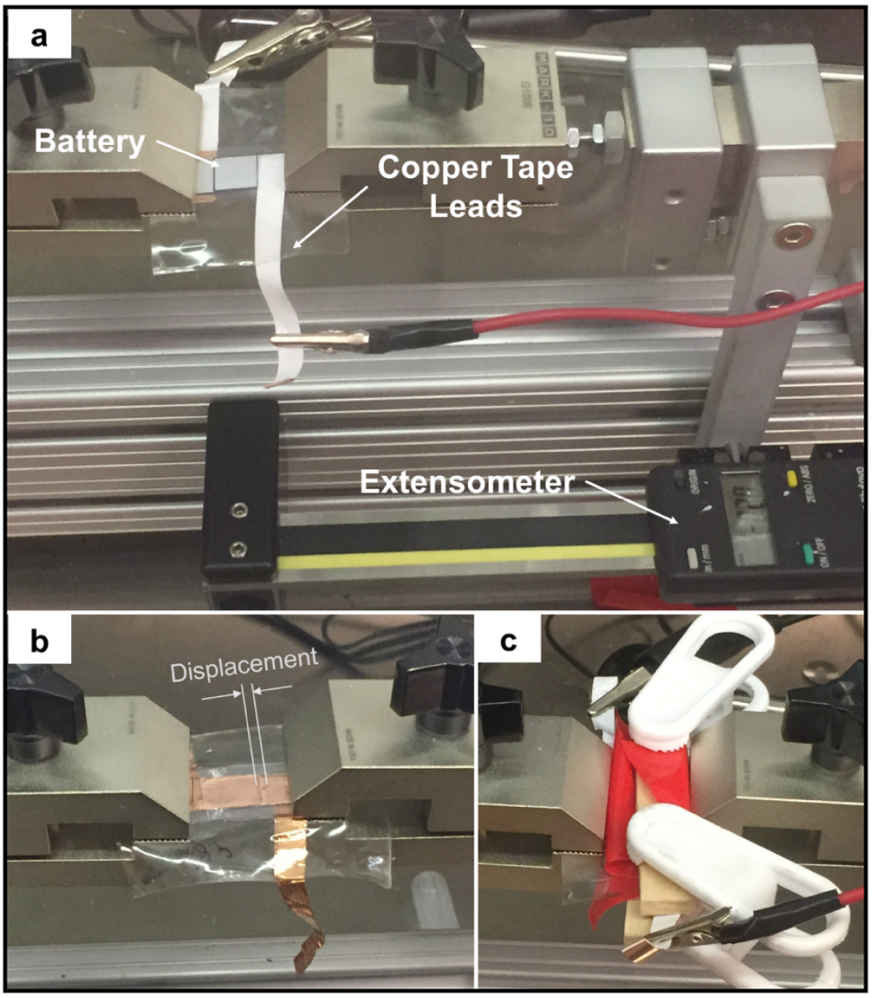

Figure 4.2 Pictures of (a) the stretchable battery experimental setup, (b) a battery under tensile strain, and (c) a pinned battery.

The encapsulated battery is placed in a manual, horizontal tensile test stand in an argon filled glove box (**Figure 4.2a**). Electrical wires connect the copper leads to the Autolab battery tester capable of conducting electrochemical impedance spectroscopy, cyclic voltammetry, and chronopotentiometry. The battery is strained in small increments, demonstrated in **Figure 4.2b**, and pinned to reduce the contact resistance between the battery electrodes and electrolyte, seen in **Figure 4.2c**. At each strain increment charge/discharge cycling data is obtained and at varying strain increments electrochemical impedance and cyclic voltammetry data are collected to further quantify electrochemical change with strain.

4.3.3 Mechanical Testing

The stretchable battery was loaded into a MARK-10 ESM301L motorized test stand in ambient room conditions and strained at 10 mm/min. The yield strength, ultimate tensile strength, Young's modulus, and % elongation of the battery were determined. Additionally, the elastic VHB encapsulation material was independently tested to determine its Young's modulus, ultimate tensile strength, % elongation. The adhesive strength of the VHB material was determined using a T-peel test.

4.4 Results and Discussion

4.4.1 VHB Encapsulation Material

The stretchable battery is composed of mechanically incompatible materials; the electrode substrates are foils, the electrolyte is a viscoelastic, semi-crystalline

polymer, and the encapsulation is an elastic adhesive. The mechanical behavior of the 25% 100k Mw PEO molecular weight blend polymer has been studied and reported in Chapter 3. It is important to also determine the mechanical properties of the VHB encapsulation material. The mechanical and adhesive strength of the VHB material was determined and a summary of the VHB mechanical properties can be found in **Figure 4.3**.

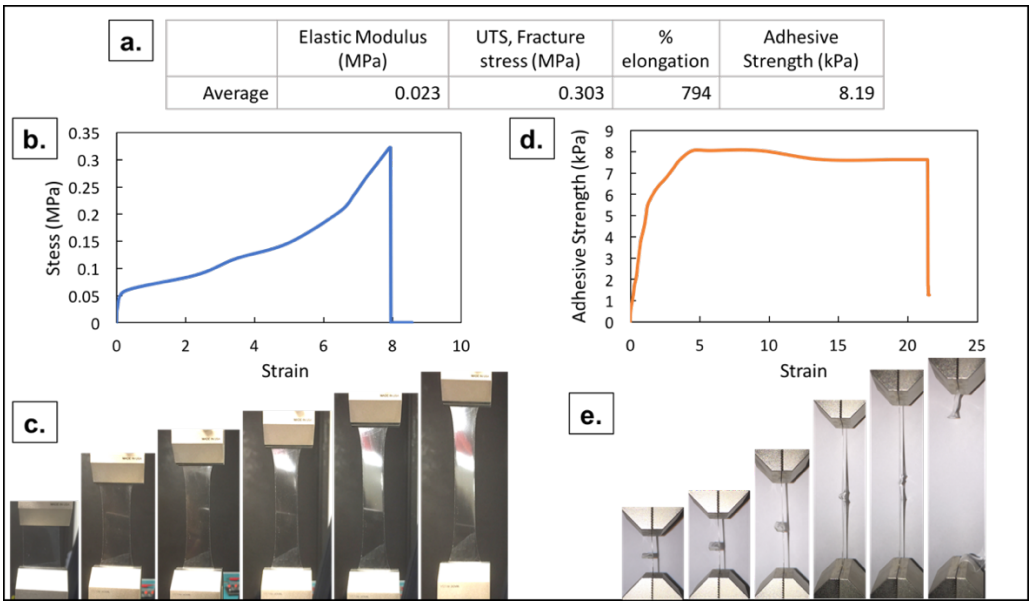

Figure 4.3 (a) Table of VHB mechanical properties, (b) VHB stress-strain curve, (c) photo images of VHB under tensile load, (d) adhesive strength-strain curve, and (e) photo images of the peeling test.

More important than its mechanical properties, the VHB's ability to provide a hermetic seal was investigated and the results are shown in **Figure 4.4** and **Figure 4.5**. An unstrained battery was charged/discharged at a constant current of 0.1mA outside of the glove box. The discharge capacity and Coulombic efficiency vs. cycle of the battery are provided in **Figure 4.4a** – **Figure 4.4b**, respectively. The battery experiences rapid capacity fading, suggesting oxidation. This is confirmed by the

battery's low and decreasing efficiency, which indicates ion trapping. Furthermore, **Figure 4.4c** captures the clear and progressive oxidation of the battery cathode with every charge/discharge cycle.

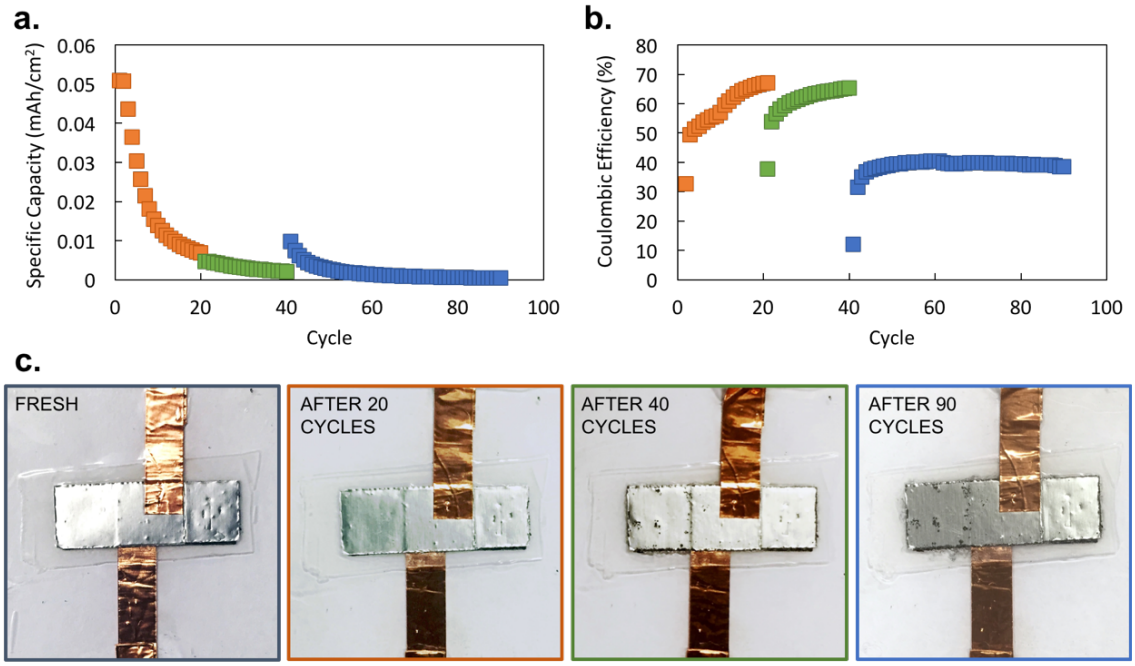

Figure 4.4 Plots of the (a) specific capacity and (b) coulombic efficiency vs. cycle of an unstrained battery tested outside of the glove box. (c) Corresponding images of battery degradation with cycle.

A second unstrained battery was charged and discharged in the room conditions for 20 cycles then charged and discharged for additional 80 cycles in an inert environment to see if the battery could stabilize and recover some of the capacity that was lost when outside of the glove box. **Figure 4.5a** and **Figure 4.5b** compare the cycling behavior of the battery depicted in **Figure 4.4** (orange) and the battery just described (blue). The second battery (blue) shows significant capacity loss in the first 20 cycles, but then stabilizes in the following cycles after being moved into the glove box. The Coulombic efficiency of the battery continues to

increase after the first 20 cycles indicating that there was no additional ion trapping when the battery was in the inert environment.

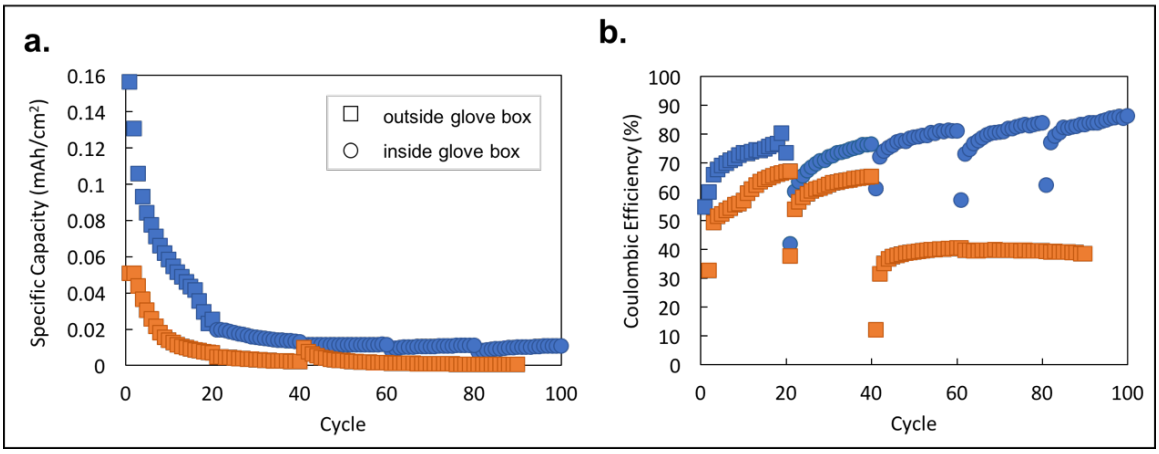

Figure 4.5 Plots comparing the (a) specific capacity vs. cycle and (b) coulombic efficiency vs. cycle of two batteries tested inside and outside of the glove box.

This data suggests that the VHB adhesive does not hermetically seal the battery and all further testing of the stretchable battery should be conducted in an inert environment. Although this is not ideal nor a realistic environment for commercial application, this study is a fundamental investigation of the effect of electrolyte strain on the electrochemical performance of a stretchable lithium ion battery.

4.4.2 Stretchable Battery Mechanical Analysis

Figure 4.6 depicts the mechanical testing and analysis of the stretchable battery. The plot in the upper left compares the stress-strain curves of the battery and the 25% 100k Mw PEO electrolyte and the table to the right summarizes and

compares the mechanical properties of the battery, PEO electrolyte, and VHB encapsulation.

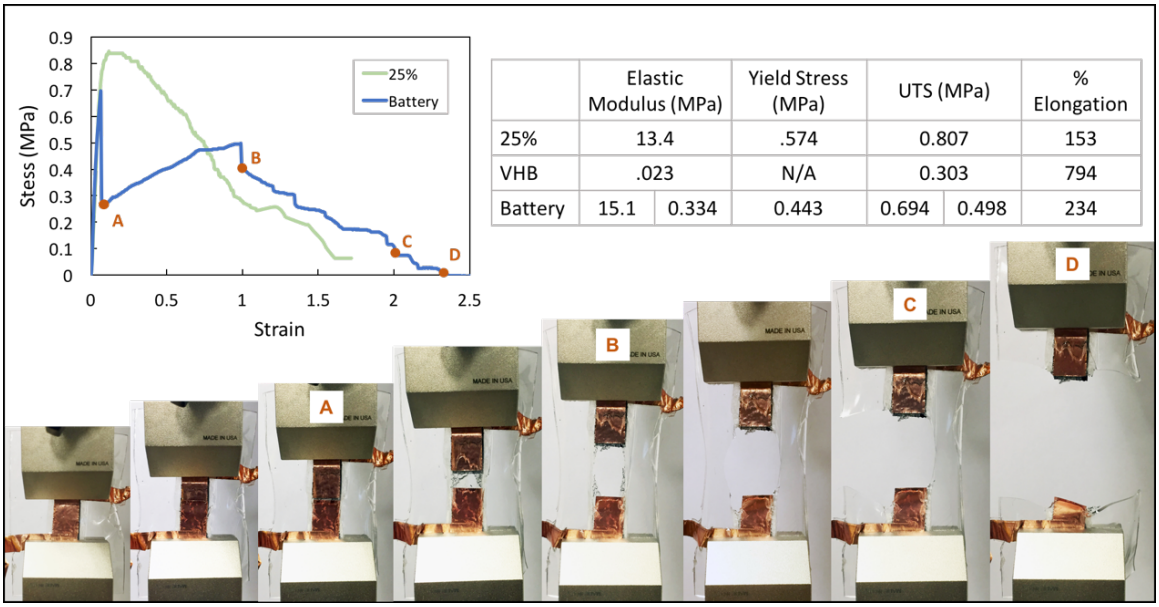

	Elastic Modulus (MPa)		Yield Stress (MPa)	UTS (MPa)		% Elongation
25%	13.4		.574	0.807		153
VHB	.023		N/A	0.303		794
Battery	15.1	0.334	0.443	0.694	0.498	234

Figure 4.6 Comparison of electrolyte and battery stress-strain curves, table of mechanical properties for the 25% 100k Mw PEO electrolyte, VHB, and battery, photo images of the battery under tensile loading

The mechanical behavior of the battery is mainly influenced by the mechanical properties of the electrodes, electrolyte, current collectors and encapsulation, and the design of the battery. The points on the battery stress-strain curve are paired with photo images of the tensile test. The points denote failure of the electrolyte (A), failure of the VHB (B,C), and failure of the battery (D). The first spike in the battery stress-strain produces an elastic modulus of 15.1 MPa, yield stress of .443 MPa, and an ultimate tensile strength of 0.694 MPa. These values are similar to those of the 25% 100k Mw PEO electrolyte, listing strength values of 13.4, 0.574, and 0.807, respectively, supporting that point A is the failure of the electrolyte. The battery then shows elastic deformation with an elastic modulus of 0.334 and an

ultimate tensile strength of 0.498, which is more similar to the property values of 0.023 MPa and 0.303 MPa, respectively, of the VHB material.

4.4.3 Electrochemical Analysis

The battery was charged and discharged at 0.1 mA for 20 cycles at each strain increment. In its unstretched state, the battery exhibits an initial capacity of 0.1 mAh cm^{-2}, which steadily rises to 0.18 mAh cm^{-2} during the first 20 charge-discharge cycles, seen in **Figure 4.7**. This initial cyclic capacity increase could be due to optimization of the electrode-electrolyte interface and increased availability of activation sites caused by the deformation and volume changes of the electrode materials as they are repeatedly lithiated and delithiated [150]. Subsequent battery testing occurred at 2%, 5%, and 10% strains. At a 10% strain, the battery underwent a total of 60 charge-discharge cycles to determine if capacity degradation would continue or stabilize.

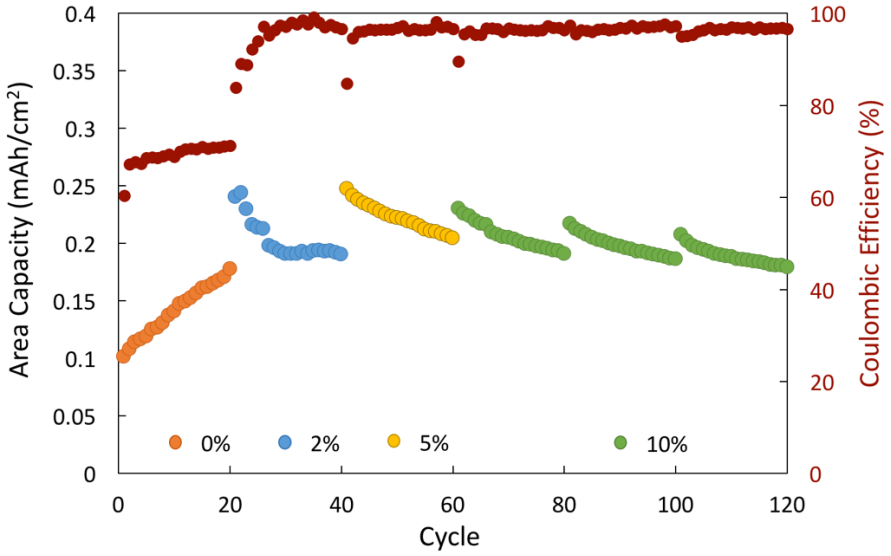

Figure 4.7 Area capacity vs. cycle and coulombic efficiency vs. cycle for each strain increment of the battery

Figure 4.7 clearly shows a notable increase in capacity with battery strain followed by steady capacity fading over the subsequent charge-discharge cycles. The initial rise in capacity with strain is likely due to a combination of factors:

1. Enhanced ion conduction through the strained polymer electrolyte
2. Increased electrode surface area and available activation sites
3. Solid-electrolyte interphase (SEI) destruction.

SEI is an ionically conducting passivation layer that forms over the anode surface, as seen in the SEM images comparing pristine and used graphite in **Figure 4.8a** and **Figure 4.8b**. SEI is composed of electrolyte degradation materials and is most commonly seen in batteries with liquid electrolytes. The SEI layer stabilizes chemical reactions occurring at the electrode surface by preventing further electrolyte degradation. The SEI layer stabilizes chemical reactions occurring at the electrode surface by preventing further electrolyte degradation. However, the SEI also slows ion transport at the anode surface, causing a drop in capacity. Stretching the battery disrupts this SEI layer and exposes more active materials to the battery electrolyte, thus enhancing the battery capacity. SEI formation is expected within the cell because this stretchable battery contains a 10% wt. content of liquid electrolyte.

On the other hand, SEI formation and accumulation is responsible for the continuous capacity fading at each strain increment, as seen in **Figure 4.7**. The stretchable battery achieves a Coulombic efficiency of approximately 96% to 97%,

meaning that ions, and ultimately capacity, are lost upon battery discharge. We hypothesize that ion trapping within the battery cell is a result of SEI accumulation. As previously mentioned, the SEI layer is disrupted with tensile deformation, but is rebuilt over the 20 charge-discharge cycles at each strain increment. The continuous cycle of SEI destruction and reformation causes SEI materials to accumulate within the battery and impede lithium ion transport to and from the electrodes.

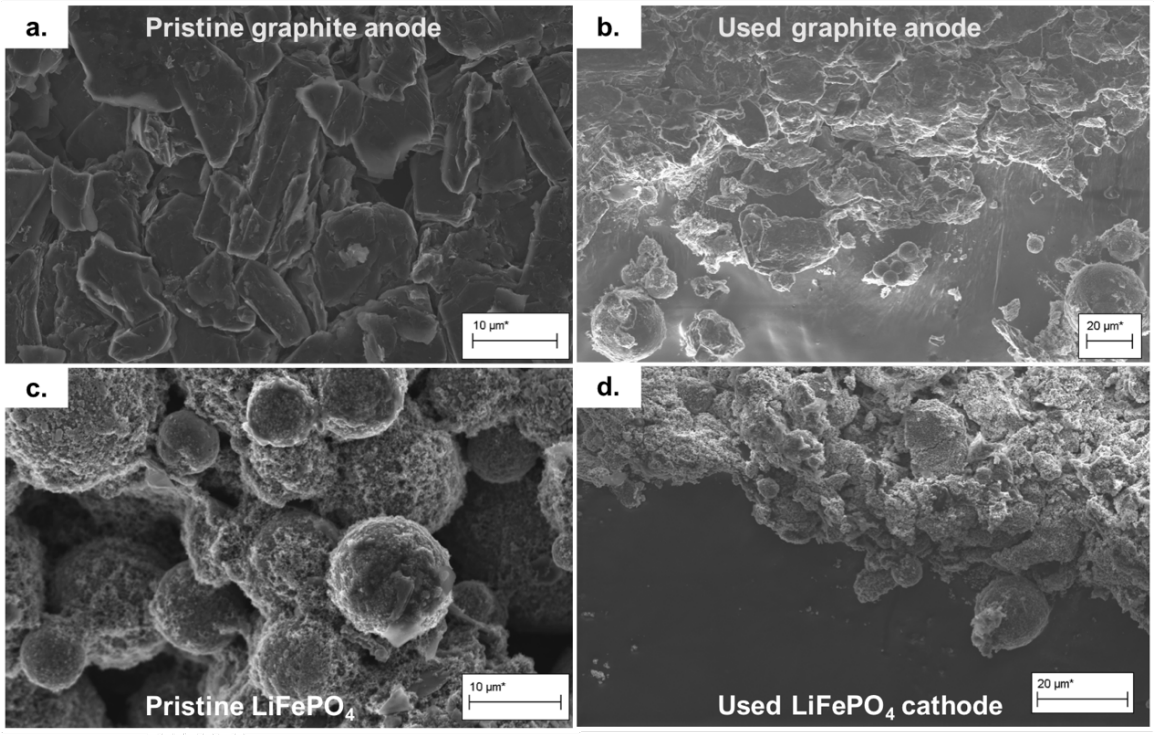

Figure 4.8 SEM images of pristine (a) graphite and (c) $LiFePO_4$ electrodes. SEM images of used (b) graphite and (d) $LiFePO_4$ electrodes.

The Nyquist plots and voltagramms in **Figures 4.9a** and **4.9b**, respectively, support this hypothesis of ion trapping due to SEI accumulation. The Nyquist plots show an increasing solid electrolyte interphase (SEI) resistance, depicted with the red arrows in **Figure 4.9a**, suggesting there is an increase in SEI materials within

the cell at each strain increment. Additionally, the Nyquist plots reveal an increasing SEI capacitance with strain, denoted by blue arrows in **Figure 4.9a**, which is supported by the decreasing reduction potential with strain, seen in **Figure 4.9b**. As SEI continues to accumulate within the cell, charge polarization at the electrode-SEI interface occurs more readily, due to the growing inability of the ions to intercalate to and from the battery electrodes.

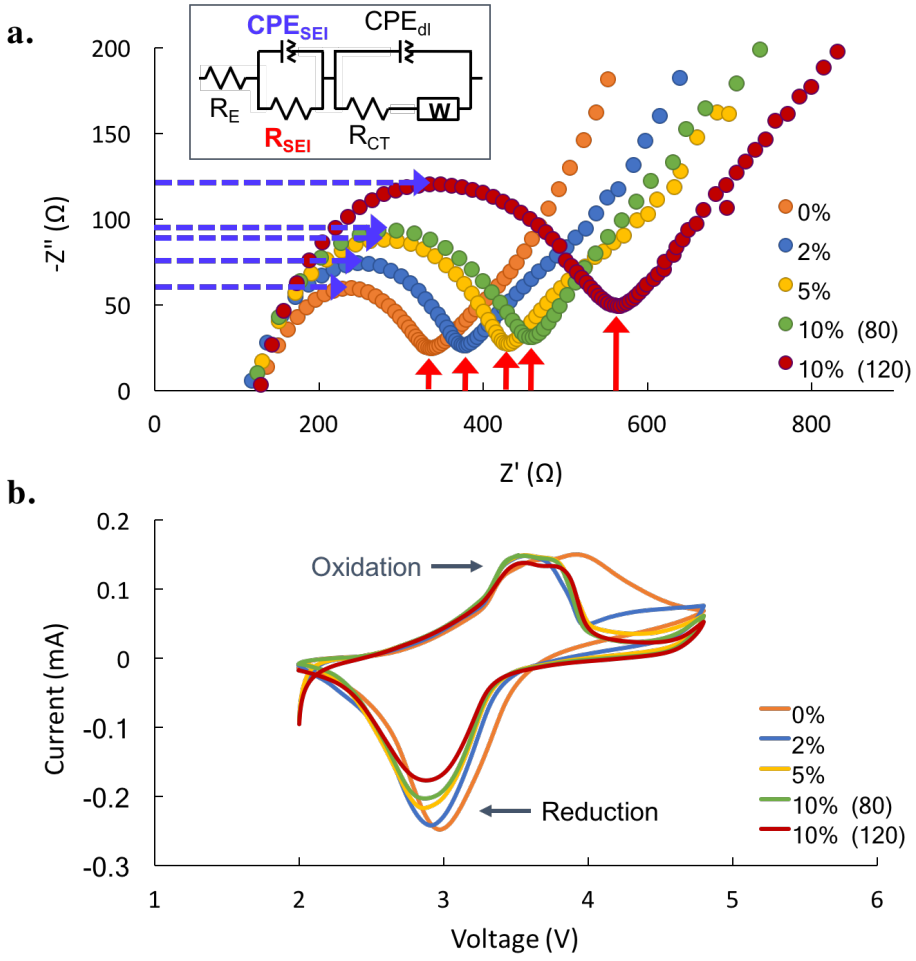

Figure 4.9 (a) Nyquist plots at 0%, 2%, 5%, and 10% strains with equivalent circuit inset and (b) voltagramm of the stretchable battery at the corresponding strain increments.

There is a clear and positive relationship between tensile strain and battery capacity, as demonstrated in **Figure 4.7**, but this strain-dependent capacity enhancement behavior is limited by the mechanical degradation of the strained battery electrolyte. When the polymer electrolyte is strained elastically to 2% and 5%, capacity improves by 33% and 32%, respectively. However, when the electrolyte is strained plastically to 10%, the battery capacity only grows by 15% and capacity fading occurs more rapidly during the subsequent cycles. This suggests that past yielding, the effect of the compromised mechanical stability of the stretched polymer electrolyte outweighs the strain-dependent ion conductivity enhancement behavior of PEO. Furthermore, extended cycling of the battery at a 10% strain reveals continued capacity fading (**Figure 4.7**), increased SEI resistance and capacitance (**Figure 4.8a**), and an additional oxidation reaction peak (**Figure 4.8b**) at cycle 120, implying that a secondary reaction is occurring within the cell. Therefore, thinning and continued mechanical degradation of the polymer electrolyte allows for some electrochemical instability within the battery.

4.5 Conclusions

A $LiFePO_4$/graphite stretchable lithium ion battery with a sliding electrode design was fabricated using the 25% 100k Mw PEO molecular weight blend electrolyte, chosen for its balance of mechanical and electrochemical properties. The stretchable battery was cycled at 0%, 2%, 5%, and 10% strain increments and exhibits a near 30% capacity enhancement with elastic strain. This capacity enhancement is due to the combination of greater electrode area exposure,

enhanced ion mobility of the strained polymer electrolyte, and disruption of the SEI layer. However, capacity fading is also observed over the 20 cycles following each strain increase as a result of ion trapping and SEI accumulation within the battery cell.

At a 10% strain, which is within the plastic deformation zone of PEO, the battery capacity cannot achieve the same 30% improvement as it did when strained elastically at 2% and 5%. Furthermore, the battery exhibits more rapid capacity fading in the following 20 cycles. This suggests that the effect of mechanical degradation in plastically deformed PEO outweighs the strain-dependent ion conductivity enhancement behavior of the electrolyte.

Although this battery is unable to achieve large tensile deformations, like the batteries reported by Xu et al. [87] and Song et al. [93], it is fully stretchable, does not require additional parts that add mass and volume to the battery, and shows capacity increase with elastic strain.

Chapter 5: Conclusions and Future Work

5.1 Conclusions

The demand for flexible and stretchable energy storage will rise as devices get smaller and more integrated into our daily lives. Lithium ion batteries have been a popular energy storage option for decades because of their ability to achieve high energy densities. However, the number of recent incidences of publicized battery fires has caused growing concerns with respect to the safety of these batteries.

Using conventional lithium ion batteries for flexible and stretchable electronics devices is not an option, especially when these batteries will likely be next to or on human beings. However, the development of safe lithium ion batteries is feasible by replacing the chemically and mechanically unstable organic liquid electrolyte with a solid polymer. Although solid polymer electrolytes are unable to achieve ion conductivities comparable to that of liquid electrolyte, they do offer the mechanical and thermal stability necessary for deformable batteries.

Development of stretchable lithium ion batteries is an emerging area of research. Being able to account for the dynamic interplay of mechanical stresses and chemical reactions while trying to build a battery that is reliable is a challenging task. Most of the previously published work on stretchable lithium ion batteries is based on the battery pack design. This dissertation is unique as it presents the feasibility of using solid polymer electrolytes to develop fully stretchable lithium ion batteries, in which all battery components are deformable.

The effect of tensile strain on PEO-based polymer electrolyte properties was first investigated to determine the practicality of developing a stretchable and lithium ion battery. An *in situ* ion conductivity experiment revealed that tensile deformation positively affects ion conductivity. It is hypothesized that the conductivity enhancement is the result of creating more amorphous regions within the polymer electrolyte through mechanical means. Amorphicity is important in semi-crystalline polymers because it is widely agreed upon that ion transport occurs through the chain segmental motions of the polymer host.

It has been determined that polyethylene oxide is a viable electrolyte option for stretchable lithium ion batteries. And although stretching enhances the electrolyte conductivity, the issue of low ion conductivity remains. Methods for increasing the ion conductivity of solid polymer electrolytes includes plasticization and the introduction of, both of which enhance the polymers' degree of amorphicity. However, plasticization, which is the act of softening the polymer through the addition of liquid electrolyte, compromises the mechanical stability and, ultimately, the safety of the polymer electrolyte. Although have shown promising results with regard to ion conductivity, they often cause the polymer electrolyte to become more brittle. Neither of these ion conductivity enhancement methods are practical for stretchable battery applications.

Instead, this dissertation presents an alternative method for optimizing the mechanical and electrochemical properties of PEO-based electrolytes through molecular weight blending. High molecular weight polymers often exhibit greater

mechanical stability and lower ion conductivity because of they are composed of long polymer chains. On the other hand, low molecular weight polymers consist of short molecular chains allowing for more free motion of the chains. This allows for enhanced ion conductivity for the cost of sacrificing mechanical strength. Polymer electrolytes consisting of high (600k) and low (100k) Mw PEO mixed in various ratios were subjected to mechanical testing and electrochemical impedance spectroscopy. As expected, the mechanical strength of the electrolyte films decreased and the ion conductivity increased with an increasing content of the low Mw PEO.

The polymer molecular weight blend containing a 25% 100k Mw PEO content (a three to one ratio of 600k to 100k Mw PEO) was used to develop a stretchable and lithium ion battery based on a sliding electrode design. The battery was subject to electrochemical testing while deformed at various strain increments. The battery maintained a high area capacity > 0.17 mAh cm^{-2} at each strain increment of 2%, 5%, and 10%. The battery was cycled twenty times at each strain and exhibited an initial spike in capacity followed by steady capacity fading. The capacity spike is the result of the combination of electrolyte deformation, a larger exposed electrode area and more activation sites, and SEI layer destruction. The subsequent capacity fade is the result of SEI formation and accumulation and a growing double-layer capacitance at the electrode-electrolyte interface with each strain.

Furthermore, although ion conductivity appears to increase with strain, the change in battery capacity with strain does not follow the same trend. Stretching may cause an increase in capacity, however the capacity increase of the battery deformed within its elastic region is larger than that of the battery deformed past yielding. This suggests that the effect of the compromised mechanical strength of the electrolyte past yielding plays a greater role in battery performance than the strain-dependent ion conductivity behavior of the electrolyte. Ultimately, this work has successfully demonstrated the possibility of developing safe and fully stretchable lithium ion batteries.

5.2 Future Work

5.2.1 Battery Development

The present work demonstrates proof of concept, but future work lies in improvement of the battery materials. First, PEO, and most polymers, have small elastic regions. Finding or developing a more elastic electrolyte material is vital in order for the battery to achieve larger elastic strains. Second, it is necessary to develop electrochemically and mechanically compatible stretchable electrodes. Ideally, the mechanical properties of the electrodes, and encapsulation for that matter, should be similar to those of the stretchable electrolyte in order to maximize the mechanical longevity of the battery. Third, finding a suitable encapsulation material is critical. Capacity fade due to the inability of hermetically sealing the battery in a soft and deformable encapsulant is a common problem seen across lithium ion battery research. Finding an appropriate encapsulation material is

necessary for commercial use. The encapsulation material should be soft enough to stretch, but stiff enough to keep the battery components in place and ensure adequate contact pressure between the battery components to reduce the electrode-electrolyte interface resistance.

5.2.2 Fundamental Studies

In addition to improving the battery materials and design, fundamental studies are necessary for better understanding the ion transport mechanisms in strained electrolytes. This work provides a mechanistic hypothesis for the strain-dependent ion conductivity enhancement behavior of solid PEO, but further investigation is needed to verify or disprove this postulation. Furthermore, it would be interesting to understand the effects of various polymer parameters, such as composition, molecular weight, salt content, polymer blending, etc., on this observed strain-dependent conductivity enhancement. Similarly, further investigation of the strain-dependent capacity enhancement mechanisms of the battery is needed and the effect of large electrolyte strains on battery performance should be explored.

Lastly, although this dissertation did not cover the specifics of certain testing procedures, understanding why these PEO-based batteries can be continually overcharged without signs of battery performance degradation needs to be researched. Overcharging lithium ion batteries can cause lithium plating, increasing the potential for an internal short resulting in thermal runaway. Additional work should focus on the electrode-electrolyte interface to determine if

the solid polymer electrolyte prevents lithium plating with continual overcharging as well as study the degradation of both electrode and electrolyte materials when overcharged.

The vision for this research is to develop fully stretchable lithium ion batteries as energy storage options for wearable, implantable, and stretchable electronic devices. There are many challenges that need to be resolved in order to develop a commercially viable stretchable lithium ion battery. The work presented in this dissertation lays out the necessary framework to overcome such challenges toward a successful stretchable battery development.

References

1 Bhatt, M. D. & O'Dwyer, C. Recent Progress in Theoretical and Computational Investigations of Li-Ion Battery Materials and Electrolytes. *Phys Chem Chem Phys* **17**, 4799-4844, doi:10.1039/c4cp05552g (2015).

2 Goodenough, J. B. & Park, K. S. The Li-ion rechargeable battery: a perspective. *J Am Chem Soc* **135**, 1167-1176, doi:10.1021/ja3091438 (2013).

3 Hassoun, Jusef & Scrosati, Bruno. Review—Advances in Anode and Electrolyte Materials for the Progress of Lithium-Ion and beyond Lithium-Ion Batteries. *Journal of The Electrochemical Society* **162**, A2582-A2588, doi:10.1149/2.0191514jes (2015).

4 Hu, Meng, Pang, Xiaoli & Zhou, Zhen. Recent progress in high-voltage lithium ion batteries. *Journal of Power Sources* **237**, 229-242, doi:10.1016/j.jpowsour.2013.03.024 (2013).

5 Zhu, Gaolong, Wen, Kechun, Lv, Weiqiang, Zhou, Xingzhi, Liang, Yachun, Yang, Fei, Chen, Zhilin, Zou, Minda, Li, Jinchao, Zhang, Yuqian & He, Weidong. Materials insights into low-temperature performances of lithium-ion batteries. *Journal of Power Sources* **300**, 29-40, doi:10.1016/j.jpowsour.2015.09.056 (2015).

6 Landi, Brian J., Ganter, Matthew J., Cress, Cory D., DiLeo, Roberta A. & Raffaelle, Ryne P. Carbon nanotubes for lithium ion batteries. *Energy & Environmental Science* **2**, 638, doi:10.1039/b904116h (2009).

7 Xie, K. & Wei, B. Materials and structures for stretchable energy storage and conversion devices. *Adv Mater* **26**, 3592-3617, doi:10.1002/adma.201305919 (2014).

8 Deoff, Marca, M. in *Batteries for Sustainability: Selected Entries from the Encyclopedia 5 of Sustainability Science and Technology* Ch. 2, (Springer Science+Business Media, 2013).

9 Gwon, Hyeokjo, Hong, Jihyun, Kim, Haegyeom, Seo, Dong-Hwa, Jeon, Seokwoo & Kang, Kisuk. Recent Progress on Flexible Lithium Rechargeable Batteries. *Energy Environ. Sci.* **7**, 538-551, doi:10.1039/c3ee42927j (2014).

10 Ramadass, P., Haran, Bala, White, Ralph & Popov, Branko N. Mathematical modeling of the capacity fade of Li-ion cells. *Journal of Power Sources* **123**, 230-240, doi:10.1016/s0378-7753(03)00531-7 (2003).

11 Tarascon, J.-M. & Armand, M. Issues and challenges facing rechargeable lithium batteries. *Nature* **414**, 9 (2001).

12 Pikul, James H., Liu, Jinyun, Braun, Paul V. & King, William P. Integration of high capacity materials into interdigitated mesostructured electrodes for high energy and high power density primary microbatteries. *Journal of Power Sources* **315**, 308-315, doi:10.1016/j.jpowsour.2016.03.034 (2016).

13 Liu, Jinyun, Kelly, Sean J., Epstein, Eric S., Pan, Zeng, Huang, Xingjiu, Liu, Jinhuai & Braun, Paul V. Three-dimensionally scaffolded Co3O4 nanosheet anodes with high rate performance. *Journal of Power Sources* **299**, 40-48, doi:10.1016/j.jpowsour.2015.08.078 (2015).

14 Zhang, H. & Braun, P. V. Three-Dimensional Metal Scaffold Supported Bicontinuous Silicon Battery Anodes. *Nano Lett* **12**, 2778-2783, doi:10.1021/nl204551m (2012).

15 Zhang, H., Shi, T., Wetzel, D. J., Nuzzo, R. G. & Braun, P. V. 3D Scaffolded Nickel-Tin Li-Ion Anodes with Enhanced Cyclability. *Adv Mater* **28**, 742-747, doi:10.1002/adma.201504780 (2016).

16 Choi, Jae-Yong, Lee, Dong Jin, Lee, Yong Min, Lee, Young-Gi, Kim, Kwang Man, Park, Jung-Ki & Cho, Kuk Young. Silicon Nanofibrils on a Flexible Current Collector for Bendable Lithium-Ion Battery Anodes. *Advanced Functional Materials* **23**, 2108-2114, doi:10.1002/adfm.201202458 (2013).

17 Song, T., Xia, J., Lee, J. H., Lee, D. H., Kwon, M. S., Choi, J. M., Wu, J., Doo, S. K., Chang, H., Park, W. I., Zang, D. S., Kim, H., Huang, Y., Hwang, K. C., Rogers, J. A. & Paik, U. Arrays of sealed silicon nanotubes as anodes for lithium ion batteries. *Nano Lett* **10**, 1710-1716, doi:10.1021/nl100086e (2010).

18 Baker, Daniel R., Verbrugge, Mark W. & Bower, Allan F. Swelling and Elastic Deformation of Lithium-Silicon Electrode Materials. *Journal of The Electrochemical Society* **163**, A624-A631, doi:10.1149/2.0211605jes (2016).

19 Wu, H., Chan, G., Choi, J. W., Ryu, I., Yao, Y., McDowell, M. T., Lee, S. W., Jackson, A., Yang, Y., Hu, L. & Cui, Y. Stable cycling of double-walled silicon nanotube battery anodes through solid-electrolyte interphase control. *Nat Nanotechnol* **7**, 310-315, doi:10.1038/nnano.2012.35 (2012).

20 Zhang, Xiangchun, Shyy, Wei & Marie Sastry, Ann. Numerical Simulation of Intercalation-Induced Stress in Li-Ion Battery Electrode Particles. *Journal of The Electrochemical Society* **154**, A910, doi:10.1149/1.2759840 (2007).

21 Zhao, Kejie, Pharr, Matt, Cai, Shengqiang, Vlassak, Joost J. & Suo, Zhigang. Large Plastic Deformation in High-Capacity Lithium-Ion Batteries Caused by Charge and

Discharge. *Journal of the American Ceramic Society* **94**, s226-s235, doi:10.1111/j.1551-2916.2011.04432.x (2011).

22 Zhao, Kejie, Pharr, Matt, Vlassak, Joost J. & Suo, Zhigang. Fracture of electrodes in lithium-ion batteries caused by fast charging. *Journal of Applied Physics* **108**, 073517, doi:10.1063/1.3492617 (2010).

23 Ellis, Brian L., Town, Kaitlin & Nazar, Linda F. New composite materials for lithium-ion batteries. *Electrochimica Acta* **84**, 145-154, doi:10.1016/j.electacta.2012.04.113 (2012).

24 Yang, Chenge, Zhang, Dawei, Zhao, Yongbin, Lu, Yuhao, Wang, Long & Goodenough, John B. Nickel foam supported Sn–Co alloy film as anode for lithium ion batteries. *Journal of Power Sources* **196**, 10673-10678, doi:10.1016/j.jpowsour.2011.08.089 (2011).

25 Chan, C. K., Peng, H., Liu, G., McIlwrath, K., Zhang, X. F., Huggins, R. A. & Cui, Y. High-Performance Lithium Battery Anodes Using Silicon Nanowires. *Nat Nanotechnol* **3**, 31-35, doi:10.1038/nnano.2007.411 (2008).

26 Mouawad, Jad & Drew, Christopher. in *The New York Times* (2013).

27 Walker, W. & Ardebili, H. Thermo-electrochemical analysis of lithium ion batteries for space applications using Thermal Desktop. *Journal of Power Sources* **269**, 486-497, doi:10.1016/j.jpowsour.2014.07.020 (2014).

28 Aurbach, Doron, Talyosef, Yosef, Markovsky, Boris, Markevich, Elena, Zinigrad, Ella, Asraf, Liraz, Gnanaraj, Joseph S. & Kim, Hyeong-Jin. Design of Electrolyte Solutions for Li and Li-Ion Batteries: A Review. *Electrochimica Acta* **50**, 247-254, doi:10.1016/j.electacta.2004.01.090 (2004).

29 Fu, Xiaotao, Yu, Danni, Zhou, Junwen, Li, Siwu, Gao, Xing, Han, Yuzhen, Qi, Pengfei, Feng, Xiao & Wang, Bo. Inorganic and organic hybrid solid electrolytes for lithium-ion batteries. *CrystEngComm* **18**, 4236-4258, doi:10.1039/c6ce00171h (2016).

30 Gomadam, Parthasarathy M., Weidner, John W., Dougal, Roger, A. & White, Ralph E. Mathematical Modeling of Lithium-Ion and Nickel Battery Systems. *Journal of Power Sources* **110**, 18 (2002).

31 Jung, Yun-Chae, Kim, Seul-Ki, Kim, Moon-Sung, Lee, Jeong-Hye, Han, Man-Seok, Kim, Duck-Hyun, Shin, Woo-Cheol, Ue, Makoto & Kim, Dong-Won. Ceramic separators based on Li+-conducting inorganic electrolyte for high-performance lithium-ion batteries with enhanced safety. *Journal of Power Sources* **293**, 675-683, doi:10.1016/j.jpowsour.2015.06.001 (2015).

32 Zhang, Sheng Shui. A review on the separators of liquid electrolyte Li-ion batteries. *Journal of Power Sources* **164**, 351-364, doi:10.1016/j.jpowsour.2006.10.065 (2007).

33 Marcinek, M., Syzdek, J., Marczewski, M., Piszcz, M., Niedzicki, L., Kalita, M., Plewa-Marczewska, A., Bitner, A., Wieczorek, P., Trzeciak, T., Kasprzyk, M., P.Łężak, Zukowska, Z., Zalewska, A. & Wieczorek, W. Electrolytes for Li-ion transport – Review. *Solid State Ionics* **276**, 107-126, doi:10.1016/j.ssi.2015.02.006 (2015).

34 Yuan, Mengying, Erdman, Jeremy, Tang, Changyu & Ardebili, Haleh. High performance solid polymer electrolyte with graphene oxide nanosheets. *RSC Adv.* **4**, 59637-59642, doi:10.1039/c4ra07919a (2014).

35 Wang, Qingsong, Ping, Ping, Zhao, Xuejuan, Chu, Guanquan, Sun, Jinhua & Chen, Chunhua. Thermal runaway caused fire and explosion of lithium ion battery. *Journal of Power Sources* **208**, 210-224, doi:10.1016/j.jpowsour.2012.02.038 (2012).

36 King, Hope. in *CNN Wire* (2015).

37 Song, J. Y., Wang, Y. Y. & Wan, C. C. Review of gel-type polymer electrolytes for lithium-ion batteries. *Journal of Power Sources* **77**, 15 (1999).

38 Burba, C. M., Woods, L., Millar, S. Y. & Pallie, J. Polymer Chain Organization in Tensile-Stretched Poly(Ethylene Oxide)-Based Polymer Electrolytes. *Electrochim Acta* **57**, 165-171, doi:10.1016/j.electacta.2011.06.025 (2011).

39 Matsui, S., Muranaga, T., Higobashi, H., Inoue, S. & Sakai, T. Liquid-free rechargeable Li polymer battery. *Journal of Power Sources* **97-98**, 3 (2000).

40 Xue, Zhigang, He, Dan & Xie, Xiaolin. Poly(ethylene oxide)-based electrolytes for lithium-ion batteries. *J. Mater. Chem. A* **3**, 19218-19253, doi:10.1039/c5ta03471j (2015).

41 Abe, Takeshi, Sagane, Fumihiro, Ohtsuka, Masahiro, Iriyama, Yasutoshi & Ogumi, Zempachi. Lithium-Ion Transfer at the Interface Between Lithium-Ion Conductive Ceramic Electrolyte and Liquid Electrolyte-A Key to Enhancing the Rate Capability of Lithium-Ion Batteries. *Journal of The Electrochemical Society* **152**, A2151, doi:10.1149/1.2042907 (2005).

42 Ciosek, M., Sannier, L., Siekierski, M., Golodnitsky, D., Peled, E., Scrosati, B., Głowinkowski, S. & Wieczorek, W. Ion Transport Phenomena in Polymeric

Electrolytes. *Electrochimica Acta* **53**, 1409-1416, doi:10.1016/j.electacta.2007.03.037 (2007).

43 Park, Myounggu, Zhang, Xiangchun, Chung, Myoungdo, Less, Gregory B. & Sastry, Ann Marie. A review of conduction phenomena in Li-ion batteries. *Journal of Power Sources* **195**, 7904-7929, doi:10.1016/j.jpowsour.2010.06.060 (2010).

44 Kondo, Kazutaka, Sano, Mitsuru, Hiwara, Akio, Omi, Takehiko, Fujita, Miho, Kuwae, Akio, Iida, Masayasu, Mogi, Koichi & Yokoyama, Haruhiko. Conductivity and Solvation of Li+ Ions of LiPF6 in Propylene Carbonate Solutions. *Journal of Physical Chemistry B* **104**, 5 (2000).

45 Stallworth, P. E., Fontanella, J. J., Wintersgill, M. C., Scheidler, Christopher D., Immel, Jeffrey J., Greenbaum, S. G. & Gozdz, A. S. NMR, DSC and high pressure electrical conductivity studies of liquid and hybrid electrolytes. *Journal of Power Sources* **81-82**, 9 (1999).

46 Alonso, Jose A., Sanz, Jesus, Santamaria, Jacobo, Leon, Carlos, Varez, Alejandro & Fernandez-Diaz, Maria T. On the Location of Li+ Cations in the Fast Li-Cation Conductor La0.5Li0.5TiO3 Perovskite. *Angew Chem Int Ed Engl* **39**, 3 (2000).

47 Knauth, Philippe. Inorganic solid Li ion conductors: An overview. *Solid State Ionics* **180**, 911-916, doi:10.1016/j.ssi.2009.03.022 (2009).

48 Evans, James, Vincent, Colin A. & Bruce, Peter G. Electrochemical Measuement of Transference Numbers in Polymer Electrolytes. *Polymer* **28**, 5, doi:0032-3861/87/132323-05$03.00 (1987).

49 Li, Lin, Wu, Zhong, Yuan, Shuang & Zhang, Xin-Bo. Advances and Challenges for Flexible Energy Storage and Conversion Devices and Systems. *Energy & Environmental Science* **7**, 2101, doi:10.1039/c4ee00318g (2014).

50 Livshits, E., Kovarsky, R., Lavie, N., Hayashi, Y., Golodnitsky, D. & Peled, E. New insights into structural and electrochemical properties of anisotropic polymer electrolytes. *Electrochimica Acta* **50**, 3805-3814, doi:10.1016/j.electacta.2005.02.047 (2005).

51 Manuel Stephan, A. & Nahm, K. S. Review on composite polymer electrolytes for lithium batteries. *Polymer* **47**, 5952-5964, doi:10.1016/j.polymer.2006.05.069 (2006).

52 Weber, Adam Z. & Newman, John. Transport in Polymer-Electrolyte Membranes. *Journal of The Electrochemical Society* **150**, A1008, doi:10.1149/1.1580822 (2003).

53 Cameron, G. G., Ingram, M. D. & Sorrie, G. A. Ionic Conductivity in Liquid Polymeric Electrolytes. *Journal of Electroanalytical Chemistry* **198**, 3 (1986).

54 Cheng, Chin-Shu, Liu, Wei-Ren & Wang, Fu-Ming. A Novel Ionic Host Solid Electrolyte Interface Formation on Reduced Graphene Oxide of Lithium Ion Battery. *Electrochimica Acta* **106**, 425-431, doi:10.1016/j.electacta.2013.06.018 (2013).

55 Cheng, Qiao, Cui, Zhenyu, Li, Jiangbo, Qin, Shuhao, Yan, Feng & Li, Jianxin. Preparation and Performance of Polymer Electrolyte Based on Poly(Vinylidene Fluoride)/Polysulfone Blend Membrane Via Thermally Induced Phase Separation

Process for Lithium Ion Battery. *Journal of Power Sources* **266**, 401-413, doi:10.1016/j.jpowsour.2014.05.056 (2014).

56 Choi, Bong Gill, Huh, Yun Suk, Park, Young Chul, Jung, Doo Hwan, Hong, Won Hi & Park, HoSeok. Enhanced transport properties in polymer electrolyte composite membranes with graphene oxide sheets. *Carbon* **50**, 5395-5402, doi:10.1016/j.carbon.2012.07.025 (2012).

57 Choi, Nam-Soon & Park, Jung-Ki. New polymer electrolytes based on PVC/PMMA blend for plastic lithium-ion batteries. *Electrochimica Acta* **46**, 7 (2001).

58 Croce, F., Appetecchi, G. B., Persi, L. & Scrosati, B. Nanocomposite Polymer Electrolytes for Lithium Batteries. *Letters to Nature* **394**, 4 (1998).

59 Fergus, Jeffrey W. Ceramic and polymeric solid electrolytes for lithium-ion batteries. *Journal of Power Sources* **195**, 4554-4569, doi:10.1016/j.jpowsour.2010.01.076 (2010).

60 Ji, Jianying, Li, Bin & Zhong, Wei-Hong. Simultaneously Enhancing Ionic Conductivity and Mechanical Properties of Solid Polymer Electrolytes Via a Copolymer Multi-Functional Filler. *Electrochimica Acta* **55**, 9075-9082, doi:10.1016/j.electacta.2010.08.036 (2010).

61 Kovarsky, R., Golodnitsky, D., Peled, E., Khatun, S., Stallworth, P. E., Greenbaum, S. & Greenbaum, A. Conductivity enhancement induced by casting of polymer electrolytes under a magnetic field. *Electrochimica Acta* **57**, 27-35, doi:10.1016/j.electacta.2011.04.016 (2011).

62 Li, Qin, Wood, Eric & Ardebili, Haleh. Elucidating the mechanisms of ion conductivity enhancement in polymer nanocomposite electrolytes for lithium ion batteries. *Applied Physics Letters* **102**, 243903, doi:10.1063/1.4809837 (2013).

63 Michael, M. S., Jacob, M. M. E., Prabaharan, S. R. S. & Radhakrishna, S. Enhanced Lithium Ion Transport in PEO-Based Solid Polymer Electrolytes Employing a Novel Class of Plasticizers. *Solid State Ionics* **98**, 8 (1997).

64 Moreno, Mabel, Quijada, Raúl, Santa Ana, María A., Benavente, Eglantina, Gomez-Romero, Pedro & González, Guillermo. Electrical and mechanical properties of poly(ethylene oxide)/intercalated clay polymer electrolyte. *Electrochimica Acta* **58**, 112-118, doi:10.1016/j.electacta.2011.08.096 (2011).

65 Prasanth, Raghavan, Shubha, Nageswaran, Hng, Huey Hoon & Srinivasan, Madhavi. Effect of poly(ethylene oxide) on ionic conductivity and electrochemical properties of poly(vinylidenefluoride) based polymer gel electrolytes prepared by electrospinning for lithium ion batteries. *Journal of Power Sources* **245**, 283-291, doi:10.1016/j.jpowsour.2013.05.178 (2014).

66 Quatarone, Eliana, Mustarelli, Piercarlo & Magistris, Aldo. PEO-based composite polymer electrolytes. *Solid State Ionics* **110**, 14 (1998).

67 Wang, Conghua, Liu, Qingguo, Cao, Qijuan, Meng, Qingan & Yang, Leiling. Investigation on the structure and conductivity of plasticized polymer electrolytes. *Solid State Ionics* **53-56**, 5 (1992).

68 Wen, Zhaoyin, Itoh, Takahito, Ichikawa, Yoshiaki, Kubo, Masataka & Yamamoto, Osamu. Blend-based polymer electrolytes of poly(ethylene oxide) and

hyperbranched poly[bis(triethylene glycol)benzoate] with terminal acetyl groups. *Solid State Ionics* **134**, 9 (2000).

69 Xu, Kang & von Cresce, Arthur. Interfacing electrolytes with electrodes in Li ion batteries. *Journal of Materials Chemistry* **21**, 9849, doi:10.1039/c0jm04309e (2011).

70 Chattoraj, J., Knappe, M. & Heuer, A. Dependence of Ion Dynamics on the Polymer Chain Length in Poly(ethylene oxide)-Based Polymer Electrolytes. *J Phys Chem B* **119**, 6786-6791, doi:10.1021/jp512734g (2015).

71 Diddens, D. & Heuer, A. Simulation study of the lithium ion transport mechanism in ternary polymer electrolytes: the critical role of the segmental mobility. *J Phys Chem B* **118**, 1113-1125, doi:10.1021/jp409800r (2014).

72 Gadjourova, Zlatka , Andreev, Yuri G. , Tunstall, David P. & Bruce, Peter G. . Ionic Conductivity in Crystalline Polymer Electrolytes. *Letters to Nature* **412**, 4 (2001).

73 Gitelman, L., Averbuch, A., Nathan, M., Schuss, Z. & Golodnitsky, D. Stochastic model of lithium ion conduction in poly(ethylene oxide). *Journal of Applied Physics* **107**, 064318, doi:10.1063/1.3357272 (2010).

74 Gitelman, L., Israeli, M., Averbuch, A., Nathan, M., Schuss, Z. & Golodnitsky, D. Modeling and simulation of Li-ion conduction in poly(ethylene oxide). *Journal of Computational Physics* **227**, 1162-1175, doi:10.1016/j.jcp.2007.08.033 (2007).

75 Gitelman, L., Israeli, M., Averbuch, A., Nathan, M., Schuss, Z. & Golodnitsky, D. Polymer geometry and Li+ conduction in poly(ethylene oxide). *Journal of Computational Physics* **227**, 8437-8447, doi:10.1016/j.jcp.2008.06.006 (2008).

76 Golodnitsky, D., Ardel, G. & Peled, E. Ion-transport phenomena in concentrated PEO-based composite polymer electrolytes. *Solid State Ionics* **147**, 15 (2002).

77 Li, Na, Chen, Zongping, Ren, Wencai, Li, Feng & Cheng, Hui-Ming. Flexible Graphene-Based Lithium Ion Batteries with Ultrafast Charge and Discharge Rates. *PNAS* **109**, 6 (2012).

78 Bamford, D., Reiche, A., Dlubek, G., Alloin, F., Sanchez, J. Y. & Alam, M. A. Ionic Conductivity, Glass Transition, and Local Free Volume in Poly(Ethylene Oxide) Electrolytes: Single and Mixed Ion Conductors. *The Journal of Chemical Physics* **118**, 9420, doi:10.1063/1.1567717 (2003).

79 Armand, Michael B., Bruce, Peter G., Forsyth, Maria, Scrosati, Bruno & Wieczorek, Wladyslaw. in *Energy Materials* Ch. 1, 31 (Wiley & Sons, 2011).

80 Kaltenbrunner, M., Kettlgruber, G., Siket, C., Schwodiauer, R. & Bauer, S. Arrays of Ultracompliant Electrochemical Dry Gel Cells for Stretchable Electronics. *Adv Mater* **22**, 2065-2067, doi:10.1002/adma.200904068 (2010).

81 Kammoun, M., Berg, S. & Ardebili, H. Flexible Thin-Film Battery Based on Graphene-Oxide Embedded in Solid Polymer Electrolyte. *Nanoscale* **7**, 7, doi:10.1039/x0xx00000x (2015).

82 Kil, E. H., Choi, K. H., Ha, H. J., Xu, S., Rogers, J. A., Kim, M. R., Lee, Y. G., Kim, K. M., Cho, K. Y. & Lee, S. Y. Imprintable, bendable, and shape-conformable polymer electrolytes for versatile-shaped lithium-ion batteries. *Adv Mater* **25**, 1395-1400, doi:10.1002/adma.201204182 (2013).

83 Li, Qin & Ardebili, Haleh. Flexible thin-film battery based on solid-like ionic liquid-polymer electrolyte. *Journal of Power Sources* **303**, 17-21, doi:10.1016/j.jpowsour.2015.10.099 (2016).

84 Ma, Xianguo, Huang, Xinglan, Gao, Jiandong, Zhang, Shu, Deng, Zhenghua & Suo, Jishuan. Compliant gel polymer electrolyte based on poly(methyl acrylate-co-acrylonitrile)/poly(vinyl alcohol) for flexible lithium-ion batteries. *Electrochimica Acta* **115**, 216-222, doi:10.1016/j.electacta.2013.10.169 (2014).

85 Zhang, Ruisi, Chen, Yuanfen & Montazami, Reza. Ionic Liquid-Doped Gel Polymer Electrolyte for Flexible Lithium-Ion Polymer Batteries. *Materials* **8**, 2735-2748, doi:10.3390/ma8052735 (2015).

86 Kelly, T., Ghadi, B. M., Berg, S. & Ardebili, H. In Situ Study of Strain-Dependent Ion Conductivity of Stretchable Polyethylene Oxide Electrolyte. *Scientific Reports* **6**, 20128, doi:10.1038/srep20128 (2016).

87 Xu, S., Zhang, Y., Cho, J., Lee, J., Huang, X., Jia, L., Fan, J. A., Su, Y., Su, J., Zhang, H., Cheng, H., Lu, B., Yu, C., Chuang, C., Kim, T. I., Song, T., Shigeta, K., Kang, S., Dagdeviren, C., Petrov, I., Braun, P. V., Huang, Y., Paik, U. & Rogers, J. A. Stretchable batteries with self-similar serpentine interconnects and integrated wireless recharging systems. *Nat Commun* **4**, 1543, doi:10.1038/ncomms2553 (2013).

88 Li, Shisheng, Luo, Yanhong, Lv, Wei, Yu, Wanjing, Wu, Sida, Hou, Pengxiang, Yang, Quanhong, Meng, Qingbo, Liu, Chang & Cheng, Hui-Ming. Vertically Aligned Carbon Nanotubes Grown on Graphene Paper as Electrodes in Lithium-

Ion Batteries and Dye-Sensitized Solar Cells. *Advanced Energy Materials* **1**, 486-490, doi:10.1002/aenm.201100001 (2011).

89 Zhou, Guangmin, Li, Feng & Cheng, Hui-Ming. Progress in flexible lithium batteries and future prospects. *Energy Environ. Sci.* **7**, 1307-1338, doi:10.1039/c3ee43182g (2014).

90 Gaikwad, A. M., Zamarayeva, A. M., Rousseau, J., Chu, H., Derin, I. & Steingart, D. A. Highly stretchable alkaline batteries based on an embedded conductive fabric. *Adv Mater* **24**, 5071-5076, doi:10.1002/adma.201201329 (2012).

91 Zhang, Y., Bai, W., Cheng, X., Ren, J., Weng, W., Chen, P., Fang, X., Zhang, Z. & Peng, H. Flexible and stretchable lithium-ion batteries and supercapacitors based on electrically conducting carbon nanotube fiber springs. *Angew Chem Int Ed Engl* **53**, 14564-14568, doi:10.1002/anie.201409366 (2014).

92 Kettlgruber, Gerald, Kaltenbrunner, Martin, Siket, Christian M., Moser, Richard, Graz, Ingrid M., Schwödiauer, Reinhard & Bauer, Siegfried. Intrinsically Stretchable and Rechargeable Batteries for Self-Powered Stretchable Electronics. *Journal of Materials Chemistry A* **1**, 5505, doi:10.1039/c3ta00019b (2013).

93 Song, Z., Wang, X., Lv, C., An, Y., Liang, M., Ma, T., He, D., Zheng, Y. J., Huang, S. Q., Yu, H. & Jiang, H. Kirigami-based stretchable lithium-ion batteries. *Sci Rep* **5**, 10988, doi:10.1038/srep10988 (2015).

94 Chun, K. Y., Kim, S. H., Shin, M. K., Kim, Y. T., Spinks, G. M., Aliev, A. E., Baughman, R. H. & Kim, S. J. Free-standing nanocomposites with high conductivity and extensibility. *Nanotechnology* **24**, 165401, doi:10.1088/0957-4484/24/16/165401 (2013).

95 Kim, Sung-Kon, Kim, Ki-Hyun, Park, Jung Ock, Kim, Kihyun, Ko, Taeyun, Choi, Seong-Woo, Pak, Chanho, Chang, Hyuk & Lee, Jong-Chan. Highly durable polymer electrolyte membranes at elevated temperature: Cross-linked copolymer structure consisting of poly(benzoxazine) and poly(benzimidazole). *Journal of Power Sources* **226**, 346-353, doi:10.1016/j.jpowsour.2012.11.019 (2013).

96 Rajeswari, Natarajan, Selvasekarapandian, Subramanian, Prabu, Moni, Karthikeyan, Shunmugavel & Sanjeeviraja, C. Lithium ion conducting solid polymer blend electrolyte based on bio-degradable polymers. *Bulletin of Materials Science* **36**, 7 (2013).

97 Rolland, J., Brassinne, J., Bourgeois, J. P., Poggi, E., Vlad, A. & Gohy, J. F. Chemically anchored liquid-PEO based block copolymer electrolytes for solid-state lithium-ion batteries. *Journal of Materials Chemistry A* **2**, 11839, doi:10.1039/c4ta02327g (2014).

98 Ghelichi, Mahdi, Qazvini, Nader Taheri, Jafari, Seyed Hassan, Khonakdar, Hossein Ali, Farajollahi, Yaser & Scheffler, Christina. Conformational, thermal, and ionic conductivity behavior of PEO in PEO/PMMA miscible blend: Investigating the effect of lithium salt. *Journal of Applied Polymer Science* **129**, 1868-1874, doi:10.1002/app.38897 (2013).

99 Golodnitsky, D., Livshits, E., Kovarsky, R., Peled, E., Chung, S. H., Suarez, S. & Greenbaum, S. New Generation of Ordered Polymer Electrolytes for Lithium Ion Batteries. *Electrochemical and Solid-State Letters* **11**, 4 (2004).

100 Golodnitsky, D., Livshits, E., Rosenberg, Yu., Lapides, I. & Peled, E. Stretching-Induced Changes in Ion-Polymer Interactions in Semicrystalline LiI-P(EO)n Polymer Electrolytes. *Solid State Ionics* **147**, 9 (2002).

101 Golodnitsky, D., Livshits, E., Ulus, A., Barkay, Z., Peled, E., Chung, S. H. & Greenbaum, S. Fast Ion Transport Phenomena in Oriented Semicrystalline LiI-(PEO)n-Based Polymer Electrolytes. *Journal of Physical Chemistry A* **105**, 9 (2001).

102 Golodnitsky, D., Livshits, E., Ulus, A. & Peled, E. Highly Conductive, Oriented polymer Electrolytes for Lithium Batteries. *Polymers for Advanced Technologies* **13**, 683-689, doi:10.1002/pat.266 (2002).

103 Golodnitsky, D. & Peled, E. Stretching-Induced Conductivity Enhancement of LiI-(PEO)-Polymer Electrolyte. *Electrochimica Acta* **45**, 6 (2000).

104 Cooper, Kevin R. Progress Toward Accurate Through-Plane Ion Transport Resistance Measurement of Thin Solid Electrolytes. *Journal of The Electrochemical Society* **157**, B1731, doi:10.1149/1.3481561 (2010).

105 Soboleva, Tatyana, Xie, Zhong, Shi, Zhiqing, Tsang, Emily, Navessin, Titichai & Holdcroft, Steven. Investigation of the through-plane impedance technique for evaluation of anisotropy of proton conducting polymer membranes. *Journal of Electroanalytical Chemistry* **622**, 145-152, doi:10.1016/j.jelechem.2008.05.017 (2008).

106 Hong, K., Rastogi, A. & Strobi, G. A Model Treating Tensile Deformation of Semicrystalline Polymers: Quasi-Static Stress-Strain Relationship and Viscous Stress Determined for a Sample of Polyethylene. *Macromolecules* **37**, 9 (2004).

107 Fleck, N. A., Hutchinson, J. W. & Tvergaard, J. W. Softening by Void Nucleation and Growth in Tension and Shear. *Journal of the Mechanics and Physics of Solids* **37**, 26 (1989).

108 Drozdov, A. D. Mullins' Fffect in Semicrystalline Polymers. *International Journal of Solids and Structures* **46**, 3336-3345, doi:10.1016/j.ijsolstr.2009.05.001 (2009).

109 Drozdov, A. D., Klitkou, R. & Christiansen, J. deC. Multi-cycle deformation of semicrystalline polymers: Observations and constitutive modeling. *Mechanics Research Communications* **48**, 70-75, doi:10.1016/j.mechrescom.2013.01.001 (2013).

110 Drozdov, A. D., Klitkou, R. & Christiansen, J. deC. Cyclic viscoplasticity of semicrystalline polymers with finite deformations. *Mechanics of Materials* **56**, 53-64, doi:10.1016/j.mechmat.2012.09.005 (2013).

111 Hu, Dehong , Yu, Ji, Wong, Kim , Bagchi, Biman , Rossky, Peter J. & Barbara, Paul F. . Collapse of Stiff Conjugated Polymers with Chemical Defects into Ordered, Cylindrical Conformations. *Letters to Nature* **405**, 4 (2000).

112 Drozdov, A. D. & Dusunceli, N. Modeling of multi-cycle deformation of polymers with various deformation programs. *Multidiscipline Modeling in Materials and Structures* **9**, 4-22, doi:10.1108/15736101311329133 (2013).

113 Appetecchi, G. B., Croce, F., Hassoun, J., Scrosati, B., Salomon, Mark & Cassel, Frank. Hot-Pressed, Dry, Composite, PEO-Based Electrolyte Membranes. *Journal of Power Sources* **114**, 105-112, doi:10.1016/s0378-7753(02)00543-8 (2003).

114 Choudhary, Shobhna & Sengwa, R. J. Effects of Preparation Methods on Structure, Ionic Conductvity and Dielectric Relaxation of Solid Polymeric Electrolytes.

Materials Chemistry and Physics **142**, 172-181, doi:10.1016/j.matchemphys.2013.06.053 (2013).

115 Gwee, Liang, Choi, Jae-Hong, Winey, Karen I. & Elabd, Yossef A. Block copolymer/ionic liquid films: The effect of ionic liquid composition on morphology and ion conduction. *Polymer* **51**, 5516-5524, doi:10.1016/j.polymer.2010.09.026 (2010).

116 Drozdov, A. D. & Christiansen, J. deC. Model for the Viscoelastic and Viscoplastic Responses of Semicrystalline Polymers. *Journal of Applied Polymer Science* **88**, 13 (2002).

117 Argon, A. S., Galeski, A. & Kazmierczak, T. Rate Mechanisms of Plasticity in Semi-Crystalline Polyethylene. *Polymer* **46**, 11798-11805, doi:10.1016/j.polymer.2005.06.126 (2005).

118 Corté, Laurent, Beaume, François & Leibler, Ludwik. Crystalline Organization and Toughening: Example of Polyamide-12. *Polymer* **46**, 2748-2757, doi:10.1016/j.polymer.2005.01.040 (2005).

119 Detrez, F., Cantournet, S. & Seguela, R. Plasticity/damage coupling in semi-crystalline polymers prior to yielding: Micromechanisms and damage law identification. *Polymer* **52**, 1998-2008, doi:10.1016/j.polymer.2011.03.012 (2011).

120 Pawlak, Andrzej & Galeski, Andrzej. Cavitation during tensile drawing of annealed high density polyethylene. *Polymer* **51**, 5771-5779, doi:10.1016/j.polymer.2010.10.003 (2010).

121 Pawlak, Andrzej, Galeski, Andrzej & Rozanski, Artur. Cavitation during deformation of semicrystalline polymers. *Progress in Polymer Science* **39**, 921-958, doi:10.1016/j.progpolymsci.2013.10.007 (2014).

122 Sing, Charles E. & Alexander-Katz, Alfredo. Globule−Stretch Transitions of Collapsed Polymers in Elongational Flow Fields. *Macromolecules* **43**, 3532-3541, doi:10.1021/ma9028008 (2010).

123 Ward, I. M. & Sweeney, J. *Mechanical Properties of Solid Polymers*. 3 edn, (John Wiley & Sons Ltd., 2013).

124 Hansen, Eric F. , Derrick, Michele R., Schilling, Michael R. & Garcia, Raphael. The Effects of Solution Application on Some Mechanical and Physical Properties of Thermoplastic Amorphous Polymers Used in Conservation: Poly(Vinyl Acetate)s. *Journal of the American Institute for Conservation* **30**, 11 (1991).

125 Abrams, C. F. , Lee, N.-K. & Obukhov, S. P. . Collape Dynamics of a Polymer Chain: Theory and Simulation. *Europhysics Letters* **59**, 87 (2002).

126 Wu, Haiyan, Li, Xiaoxi, Wang, Yonghong, Wu, Jun, Huang, Ting & Wang, Yong. Fracture behaviors of isotactic polypropylene/poly(ethylene oxide) blends: Effect of annealing. *Materials Science and Engineering: A* **528**, 8013-8020, doi:10.1016/j.msea.2011.07.007 (2011).

127 Berg, Sean. *Development of Analytical Models for Evaluating the Mechanical and Electrochemical Response of Flexible and Stretchable Lithium Ion Battery Materials* Materials Science and Engineering, Ph.D. thesis, University of Houston, (2016).

128 Bower, A. F., Guduru, P. R. & Sethuraman, V. A. A Finite Strain Model of Stress, Diffusion, Plastic Flow, and Electrochemical Reactions in a Lithium-Ion Half-Cell. *Journal of the Mechanics and Physics of Solids* **59**, 804-828, doi:10.1016/j.jmps.2011.01.003 (2011).

129 Ferreira, J. A., Grassi, M., Gudiño, E. & de Oliveira, P. A new look to non-Fickian diffusion. *Applied Mathematical Modelling* **39**, 194-204, doi:10.1016/j.apm.2014.05.030 (2015).

130 Zhang, Chao, Santhanagopalan, Shriram, Sprague, Michael A. & Pesaran, Ahmad A. A representative-sandwich model for simultaneously coupled mechanical-electrical-thermal simulation of a lithium-ion cell under quasi-static indentation tests. *Journal of Power Sources* **298**, 309-321, doi:10.1016/j.jpowsour.2015.08.049 (2015).

131 Baker, Daniel R., Verbrugge, Mark W. & Bower, Allan F. Thermodynamics, Stress, and Stefan-Maxwell Diffusion in Solids: Application to Small-Strain Materials Used in Commercial Lithium-Ion Batteries. *Journal of Solid State Electrochemistry* **20**, 163-181, doi:10.1007/s10008-015-3012-7 (2015).

132 Monge, M. A., Diaz, J. A. & Pareja, R. Strain-Induced Changes of Free Volume Measured by Positron Lifetime Spectroscopy in Ultrahigh Molecular Weight Polyethylene. *Macromolecules* **37**, 8 (2004).

133 Termonia, Yves & Smith, Paul. Kinetic Model for Tensile Deformation of Polymers. 2. Effect of Entanglement Spacing. *Macromolecules* **21**, 6 (1988).

134 Hu, Liangbing, Wu, Hui, La Mantia, Fabio, Yang, Yuan & Cui, Yi. Thin, Flexible Secondary Li-Ion Paper Batteries. *Nano* **4**, 6 (2010).

135 Koo, M., Park, K. I., Lee, S. H., Suh, M., Jeon, D. Y., Choi, J. W., Kang, K. & Lee, K. J. Bendable Inorganic Thin-Film Battery for Fully Flexible Electronic Systems. *Nano Lett* **12**, 4810-4816, doi:10.1021/nl302254v (2012).

136 Lee, Keun Young, Gupta, Manoj Kumar & Kim, Sang-Woo. Transparent Flexible Stretchable Piezoelectric and Triboelectric Nanogenerators for Powering Portable Electronics. *Nano Energy* **14**, 139-160, doi:10.1016/j.nanoen.2014.11.009 (2015).

137 Liang, Hai-Wei, Guan, Qing-Fang, Zhu, Zhu, Song, Lu-Ting, Yao, Hong-Bin, Lei, Xuan & Yu, Shu-Hong. Highly conductive and stretchable conductors fabricated from bacterial cellulose. *NPG Asia Materials* **4**, e19, doi:10.1038/am.2012.34 (2012).

138 Liu, S., Wang, Z., Yu, C., Wu, H. B., Wang, G., Dong, Q., Qiu, J., Eychmuller, A. & David Lou, X. W. A flexible TiO(2)(B)-based battery electrode with superior power rate and ultralong cycle life. *Adv Mater* **25**, 3462-3467, doi:10.1002/adma.201300953 (2013).

139 Lu, Xihong, Yu, Minghao, Wang, Gongming, Tong, Yexiang & Li, Yat. Flexible solid-state supercapacitors: design, fabrication and applications. *Energy & Environmental Science* **7**, 2160, doi:10.1039/c4ee00960f (2014).

140 Pushparaj, Victor L. , Shaijumon, Manikoth M. , Kumar, Ashavani , Murugesan, Saravanababu , Ci, Lijie , Vajtai, Robert , Linhardt, Robert J. , Nalamasu, Omkaram & Ajayan, Pulickel M. . Flexible energy storage devices based on nanocomposite paper. *PNAS* **104**, 4 (2007).

141 Wang, C., Zheng, W., Yue, Z., Too, C. O. & Wallace, G. G. Buckled, stretchable polypyrrole electrodes for battery applications. *Adv Mater* **23**, 3580-3584, doi:10.1002/adma.201101067 (2011).

142 Barroso-Bujans, Fabienne, Alegría, Angel, Pomposo, Jose A. & Colmenero, Juan. Thermal Stability of Polymers Confined in Graphite Oxide. *Macromolecules* **46**, 1890-1898, doi:10.1021/ma302407v (2013).

143 Prasanth, Raghavan, Aravindan, Vanchiappan & Srinivasan, Madhavi. Novel polymer electrolyte based on cob-web electrospun multi component polymer blend of polyacrylonitrile/poly(methyl methacrylate)/polystyrene for lithium ion batteries—Preparation and electrochemical characterization. *Journal of Power Sources* **202**, 299-307, doi:10.1016/j.jpowsour.2011.11.057 (2012).

144 Apicella, A., Cappello, B., Del Nobile, M. A., La Rotonda, M. I., Mensitieri, G. & Nicolais, L. Poly(Ethylene Oxide) (PEO) and Different Molecular Weight PEO Blends Monolithic Devices for Drug Release. *Biomaterials* **14** (1993).

145 Maggi, L., Segale, L., Torre, M. L., Ochoa Machiste, E. & Conte, U. Dissolution behaviour of hydrophilic matrix tablets containing two different polyethylene oxides (PEOs) for the controlled release of a water-soluble drug Dimensionality study. *Biomaterials* **23**, 7 (2002).

146 Biswas, Nupur & Datta, Alokmay. Polymer Entanglement – A Barrier to Nanoparticles Aggregation. *Chemical Physics Letters* **531**, 177-182, doi:10.1016/j.cplett.2012.02.029 (2012).

147 He, Ruixuan, Echeverri, Mauricio, Ward, Daniel, Zhu, Yu & Kyu, Thein. Highly Conductive Solvent-Free Polymer Electrolyte Membrane for Lithium-Ion Natteries:

Effect of Prepolymer Molecular Weight. *Journal of Membrane Science* **498**, 208-217, doi:10.1016/j.memsci.2015.10.008 (2016).

148 Amiki, Yuichi, Sagane, Fumihiro, Yamamoto, Kazuo, Hirayama, Tsukasa, Sudoh, Masao, Motoyama, Munekazu & Iriyama, Yasutoshi. Electrochemical Properties of an All-Solid-State Lithium-Ion Battery with an In-Situ Formed Electrode Material Grown From a Lithium Conductive Glass Ceramics Sheet. *Journal of Power Sources* **241**, 583-588, doi:10.1016/j.jpowsour.2013.05.006 (2013).

149 Sagane, F., Abe, T. & Ogumi, Z. Electrochemical Analysis of Lithium-Ion Transfer Reaction through the Interface between Ceramic Electrolyte and Ionic Liquids. *Journal of The Electrochemical Society* **159**, A1766-A1769, doi:10.1149/2.027211jes (2012).

150 Shin, Joon-Ho, Henderson, Wesley A. & Passerini, Stefano. PEO-Based Polymer Electrolytes with Ionic Liquids and Their Use in Lithium Metal-Polymer Electrolyte Batteries. *Journal of The Electrochemical Society* **152**, A978, doi:10.1149/1.1890701 (2005).